Electrical Properties of Amorphous/Crystalline Semiconductor Heterojunctions and Determination of Gap-state Distributions in Amorphous Semiconductors

January 1994

Hideharu Matsuura

Kyoto University, Japan

To my wife

CONTENTS

ABSTRACT

This thesis describes the electrical properties of hydrogenated amorphous silicon-based alloy/crystalline silicon heterojunctions and development of new methods for getting information on midgap states in undoped hydrogenated amorphous silicon-based alloys. In order to investigate the heterojunctions in metal/amorphous/crystalline diodes, the property (Ohmic or rectifying) of each contact has been studied first. Then, characteristics of their current-voltage (I-V), capacitance-voltage (C-V) and transient capacitance have been measured and discussed. From the above fundamental studies, methods for determining a midgap-state density and its profile in highly resistive amorphous semiconductors, such as undoped hydrogenated amorphous silicon (a-Si:H), undoped hydrogenated amorphous silicon germanium alloys ($a\text{-}Si_{1-x}Ge_x:H$) and undoped hydrogenated amorphous silicon carbon alloys ($a\text{-}Si_{1-x}C_x:H$), have been developed. Furthermore, the nature of midgap states in them has been researched.

First of all, it has investigated the I-V characteristics of metal/undoped a-Si:H/n^+ (or p^+) crystalline silicon (c-Si) structures using Mg, Au, Pt and Al as a metal. Although Al has been thought to form an Ohmic contact with not only P-doped but also undoped a-Si:H, Al as well as Au and Pt is found to form a Schottky barrier junction with them. On the other hand, Mg is found to form a good Ohmic contact not only with P-doped a-Si:H but also with undoped a-Si:H. This contact does not exhibit the thermal degradation at least up to 100 ℃. Next, investigated are the I-V characteristics of metal(Au,Mg)/B-doped a-Si:H/c-Si(n^+,p^+) diodes for various doping levels of B in a-Si:H. The junction studies determine the conduction type of B-doped a-Si:H on the basis of "dominant" carrier concentration, and find that the p-n transition occurs at $B_2H_6/SiH_4 \sim 10^{-6}$ although the conductivity minimum appears at $B_2H_6/SiH_4 \sim 10^{-4}$.

From the study of the C-V characteristics of undoped a-Si:H/p c-Si heterojunctions under high frequency ($\geq$ 100 kHz), a

midgap-state density (N_I) of a-Si:H and an electron affinity (χ_2) of a-Si:H are obtained. This method is called a steady-state heterojunction-monitored capacitance (HMC) method. The analytical approach is that the capacitance in the a-Si:H side becomes equal to the geometric capacitance of the a-Si:H film due to its longer dielectric relaxation time, while that in the c-Si side is associated with the depletion width in c-Si which reflects the space charge of the depletion region in a-Si:H by a dc bias. In order to understand the physical background of N_I which is experimentally obtained from the steady-state HMC method, a model for simulating high-frequency C-V characteristics of highly resistive amorphous/lowly resistive crystalline semiconductor heterojunctions has been developed. In the reasonable case that its interface-state density is less than 10^{11} cm^{-2}, the results experimentally obtained from the steady-state HMC method are found to be valid.

It has also measured the temperature dependence of the I-V characteristics of undoped a-Si:H heterojunctions on p c-Si with different resistivities. The forward current of all the junctions studied shows voltage- and temperature-dependencies expressed as $\exp(-\Delta E_{af}/kT)\exp(AV)$, where ΔE_{af} and A are constants independent of an applied voltage (V) and a measuring temperature (T), being successfully explained by a multistep-tunneling capture-emission (MTCE) model proposed here. The reverse current is proportional to $(V_B-V)^{1/2}$, where V_B is the built-in potential. This current is probably limited by a generation process in the depletion regions.

A novel technique (transient HMC method) has been proposed for determining a midgap-state profile in highly resistive amorphous semiconductors from the study of the transient capacitance of highly resistive amorphous/lowly resistive crystalline semiconductor heterojunctions. The transient HMC method has been applied to undoped a-Si:H, undoped a-$Si_{1-x}Ge_x$:H and undoped a-$Si_{1-x}C_x$:H. These midgap states are found to correspond to singly-occupied dangling bonds (D^0). The density of the midgap states increases slowly with the Ge content in the film, while it increases rapidly with the C content. The peak of

the midgap-state profile appears clearly in a-Si:H and $a\text{-}Si_{1-x}Ge_x:H$, but it does not appear clearly in $a\text{-}Si_{1-x}C_x:H$. Next, changes of the midgap-state profile of light-soaked undoped a-Si:H have been measured in the process of a 150-℃ annealing by the transient HMC method. Monomolecular annealing kinetics are found to be suitable for explaining the results, and the thermal activation energy for annealing decreases with an increase in the energy position measured from the conduction-band edge. Finally, midgap-state profiles in undoped a-Si:H have been measured after light soaking, rapid cooling, and thermal annealing using the HMC method. After short-time ($\leq$ 4-h) light soaking under AM1 with 100 mW/cm^2 at room temperature, the increase in midgap states which are assigned to D^0 in as-deposited films are observed. The attempt-to-escape frequency (ν_n) for electrons of those states is $7x10^{11}$ s^{-1}. Successive long-time ($\geq$ 75-h) light soaking, however, mainly produces another midgap states with ν_n of $2x10^{13}$ s^{-1}. Both light-induced metastable states with two kinds of ν_n are located at around 0.85 eV below the conduction-band edge. After annealing those samples up to 200 ℃ for 2 h, both states are completely recovered, but recovering behavior is quite different from one with a small ν_n to the other with a large ν_n. On the other hand, the states produced by rapid cooling from 300 ℃ are similar to those induced by the short-time light soaking in their ν_n as well as in recovering behavior by the annealing.

ACKNOWLEDGMENTS

The author wishes to express his sincere gratitude to Professor Hiroyuki Matsunami for his kind guidance and hearty encouragement. He is grateful to Professor Akio Sasaki for his useful suggestions and constructive criticism of the manuscript. He also acknowledges Professor Sigeo Fujita for a critical reading of the manuscript and valuable comments.

This work has been done at the Non-Equilibrium Materials Section of the Materials Science Division in Electrotechnical Laboratory (ETL), and has been supported by the Sunshine project under the Agency of Industrial Science and Technology, Ministry of International Trade and Industry.

The author would like to express his deep gratitude to Dr. Kazunobu Tanaka, chief senior researcher of the National Institute for Advanced Interdisciplinary Research for his guidance and encouragement. He wishes to acknowledge his gratitude to Dr. Akihisa Matsuda, chief of the Non-Equilibrium Materials Section in ETL for his valuable insights and advice specially on the deposition of amorphous materials. He wishes to express his thanks to Dr. Hideyo Okushi, chief of the Material Fundamentals Section in ETL for his fruitful discussions and comments. He also wishes to thank Dr. Hidetoshi Oheda, Dr. Satoshi Yamasaki, Dr. Nobuhiro Hata, and other members of the Non-Equilibrium Materials Section in ETL for their valuable insights and comments. He would like to thank Mr. Tetsuhiro Okuno from Sharp Corporation for co-work of his early research. He would like to express his gratitude to Dr. Z E. Smith in Xerox Palo Alto Research Center for his fruitful discussion and also for carrying out CPM measurements. He is grateful to Mr. Seiichiro Yokoyama for measurements of ESR and to Mr. Mitsuhiro Tanaka and Mr. Masashi Ueda for helping with sample preparations.

The author would like to thank to Associate Professor Takashi Fuyuki, Dr. Masahiro Yoshimoto, Dr. Tsunenobu Kimoto, and the other members of Matsunami's Laboratory in Kyoto University for helping with drafting the manuscript.

CHAPTER I INTRODUCTION

Crystalline/crystalline semiconductor heterojunctions have been studied extensively over the years,[1-7] and their applications to devices such as heterojunction-bipolar transistors (HBT) with a wide band-gap emitter, laser diodes, and solar cells are well known. From the viewpoints of understanding the fundamental device physics, Anderson,[2] Rediker et al.,[3] Hampshire et al.,[4] Riben et al.,[5,6] Donnelly et al.,[7] and other groups reported the electrical properties of heterojunctions of crystalline materials. Anderson has initially proposed an energy-band diagram assuming no interface states and extremely abrupt change from one material to the other. Rediker et al.,[3] Hampshire et al.,[4] and Riben et al.[5] reported the experimental evidences for supporting the abrupt heterojunction model (i.e., Anderson's model) through their capacitance-voltage (C-V) measurements. With regard to the current-transport mechanism of the heterojunctions, Anderson[2] and Perlman et al.[8] have put the basis of their calculations on a Shockley diffusion model[9] and a Schottky emission model,[10] respectively, while Riben et al.,[5,6] Donnelly et al.,[7] and Rediker et al.[3] have independently published tunneling models to explain their own data.

On selecting the combination of crystalline materials in crystalline/crystalline semiconductor heterojunctions, it is always necessary to consider lattice matching between two crystalline materials, which greatly affects the properties of the heterojunctions. In the case of amorphous/crystalline semiconductor heterojunctions, on the other hand, it is not always necessary to consider the combination. Moreover, it is much easier to fabricate the heterojunctions than to do crystalline ones, for example, good amorphous films can easily be deposited onto crystalline semiconductors at such a low temperature of 250 ℃. Grigorovici[11] was the first to report the properties of amorphous germanium/crystalline germanium heterojunctions. Stourac[12] later reported that

chalcogenide/crystalline semiconductor heterojunctions could be essentially approximated by abrupt heterojunctions, and reported that the current-transport mechanism could be based on space-charge-limited currents (SCLC) in the amorphous material (chalcogenide). However, those amorphous materials were not appropriate for most of device applications. This is because the electrical properties of those amorphous materials were poor, i.e., it was quite difficult to make p-n control in these films.

In amorphous semiconductors, doping experiments intending to control the Fermi level from the conduction-band edge to the valence-band edge were not successful before 1975. In 1975, Spear and LeComber[13] achieved the initial success of p-n control in hydrogenated amorphous silicon (a-Si:H) using a glow-discharge technique, which was followed by the announcement of a-Si:H solar cells by the RCA group (Carlson and Wronski) in the following year.[14] This was recognized as real break through, because some pessimistic suggestions had been made by Mott[15] and Gubanov,[16] independently, against the capability of p-n control in disordered structures before 1975. The incorporation of hydrogen into amorphous silicon reduced the number of electrically active gap states, and thereby enabled p- or n-type doping via the incorporation of group Ⅲ or group Ⅴ element, respectively. Since then, a great number of experiments have been done in the area of a-Si:H from the viewpoints not only of the physics of amorphous semiconductors but also of their applications to a variety of electronic devices such as thin-film solar cells, xerographies, direct-contact line sensors, and thin-film transistor arrays.

Amorphous/amorphous semiconductor heterojunctions have been used for most of device applications, and for instance, hydrogenated amorphous silicon-carbon alloy ($a\text{-}Si_{1-x}C_x:H$)/a-Si:H solar cells have shown a great potentiality.[17] However, the physics of amorphous/amorphous semiconductor heterojunctions is clearly far from being understood; even the amorphous homojunctions being not yet completely understood.[18] The study of amorphous/crystalline semiconductor heterojunctions can thus be a first step towards understanding amorphous/amorphous

semiconductor junctions. From the investigation of amorphous/crystalline semiconductor heterojunctions, moreover, important information on amorphous semiconductors has been found to be obtained.[19] And this study has been important to take advantage of both the good properties of amorphous and crystalline materials in one device.[20]

In the early 1980's, it started to study hydrogenated amorphous silicon-based alloy/crystalline silicon (c-Si) heterojunctions. Sasaki et al.[21] have investigated the diodes with Al/undoped a-Si:H/n c-Si structures, and from the high-frequency C-V characteristics of them density-of-state (DOS) distributions [g(E)] in a-Si:H were estimated. From the reasons of similarity of high-frequency C-V characteristics between those heterojunctions and a metal-oxide-semiconductor (MOS) diode as well as of similarity of very high resistivity between the undoped a-Si:H film and the oxide film, it was natural to discuss their high-frequency C-V characteristics using a MOS-type analysis.

We have studied the diodes with Mg/undoped a-Si:H/p c-Si structures,[22] where the conduction type of undoped a-Si:H is n-type[23] and Mg forms a good Ohmic contact with undoped a-Si:H.[24] These diodes exhibited good rectifying properties and the current-voltage (I-V) characteristics of those diodes were found to originate from a p-n junction of the undoped a-Si:H/p c-Si heterojunction, which means that the depletion regions are formed in both sides of a-Si:H and c-Si and are changed by a dc applied voltage. Although the high-frequency C-V characteristics were somewhat similar to those of MOS diodes, they were discussed using a p-n junction-type analysis, which could estimate a midgap-state density (N_I) in undoped a-Si:H and conduction-band discontinuity (ΔE_C) between a-Si:H and c-Si. This method is referred to as a steady-state heterojunction-monitored capacitance (HMC) method.

Smid et al.[25] have also surveyed the undoped a-Si:H/p c-Si heterojunctions and concluded on the analogy of the study of chalcogenide/crystalline semiconductor heterojunctions that the currents in them were SCLC (i.e., bulk-limited currents), not

junction-limited currents which we have proposed. Moreover, the g(E) above the Fermi level in a-Si:H was estimated using an SCLC-type analysis.

As is clear from the above descriptions, two kinds of analyses have been proposed in order to explain those C-V characteristics;

1) a MOS-type analysis,

2) a p-n junction-type analysis.

Moreover, two sorts of current-transport mechanisms have been proposed in order to explain those I-V characteristics;

1) a bulk-limited current-transport mechanism,

2) a junction-limited current-transport mechanism.

Since those were reported, many researchers have been interested in those heterojunctions.

From a lot of studies in this field, the a-Si:H/c-Si heterojunction has been found to have junction properties suitable for a variety of device applications,[20] such as

(a) a high forward-to-reverse current ratio;

(b) a small dark current even at a large reverse bias condition;

(c) wide depletion regions in both a-Si:H and c-Si;

(d) large valence-band discontinuity (ΔE_V) and small conduction-band discontinuity (ΔE_C) between a-Si:H and c-Si.

Okuda et al.[26] have reported a-Si:H/poly-crystalline silicon stacked solar cells. Rahman and Furukawa[27] have reported the electrical properties of p^+ a-$Si_{1-x}C_x$:H/n c-Si heterojunctions, and applied those heterojunctions to solar cells which showed the open-circuit voltage of 0.50 V, the short-circuit current of 30 mA/cm^2, and the efficiency of 11.38 % under AM1 light (100 mW/cm^2). Also Furukawa's group[28] has studied an HBT with a wide band-gap emitter made of hydrogenated amorphous silicon-based alloys. Ghannam et al.[29] have investigated the similar HBTs. Mimura and Hatanaka[30] have studied vidicon targets without a p-n diode array, whose main junction is a B-doped a-Si:H/n c-Si heterojunction. Yabe et al.[31] reported a gamma-ray detector with an undoped a-Si:H/p c-Si heterojunction. Vidicon targets

and gamma-ray detectors make good uses of junction properties (b) and (c), solar cells take advantage of (a) and (c), and n-p-n HBTs make good uses of (a) and (d). Another big advantage of these heterojunctions is a low-temperature fabrication process.

There have been some disputes about those experimental results. For example, we have obtained that the average value for ΔE_C between a-Si:H and c-Si is 0.20 eV,[22] indicating that the main band discontinuity occurs in the valence band ($\Delta E_V \sim 0.44$ eV). On the other hand, Cuniot and Marfaing[32] have insisted that ΔE_V is close to zero using an internal photoemission technique, while Mimura and Hatanaka[33] have obtained the results similar to ours using the same internal photoemission technique as Cuniot and Marfaing used. Essick and Cohen[34] reported that ΔE_C was nearly zero (~ 0.05 eV) using the temperature dependence of capacitance in undoped a-Si:H/n c-Si heterojunctions. Another problem is concerned with their current-transport mechanism. We have proposed a multistep-tunneling capture-emission (MTCE) current for a forward bias condition and a generation current in the depletion regions for a reverse bias condition.[20,22] Xu et al.[35] and Symons et al.[36] have supported the MTCE model, and Mimura and Hatanaka[37] successfully applied the MTCE model to B-doped a-Si:H/n c-Si and B-doped a-Si:H/n-type crystalline gallium arsenide (n c-GaAs) heterojunctions. However, Mimura and Hatanaka[38] have insisted that in the case of B-doped a-Si:H the reverse current is a generation current at the interface, not in the depletion regions.

As for the theoretical approach of amorphous/crystalline semiconductor heterojunctions, Rubinelli et al.[39] first simulated their C-V characteristics at 0 Hz. The theory of the C-V characteristics of Schottky barrier junctions with amorphous semiconductors as well as amorphous/crystalline heterojunctions has not been well developed. There are two main problems when one tries to simulate the C-V characteristics: One is how to deal with energetically distributed gap states, and the other is how to treat the frequency dependence of capacitance, which is related to the dielectric relaxation time of the highly resistive

amorphous film as well as to the trapping/detrapping time of carriers between gap states and the extended states. Because of the latter problem, almost all the models can accurately simulate only zero-frequency C-V characteristics which cannot experimentally be measured. However, it has been found that the simulation of the high-frequency C-V characteristics in highly resistive amorphous/lowly resistive crystalline heterojunctions can easily solve the latter problem as follows. Since the frequency is high enough to be able to neglect the dielectric relaxation process as well as the trapping/detrapping process in the amorphous film, one only requires the thickness of the amorphous film and the width of the depletion region in the crystalline semiconductor produced by a dc reverse bias in order to calculate the capacitance, indicating that it is able to simulate accurately the high-frequency C-V characteristics of those amorphous/crystalline semiconductor heterojunctions.

Another big subject has been how to estimate g(E) in the mobility gap of amorphous materials, as shown in Fig. 1.1, because the optoelectronic properties of a-Si:H films are critically linked with the g(E) in a-Si:H. In order to enhance the performance of a-Si:H-based devices such as solar cells and thin-film transistors where undoped a-Si:H layers play the most important role, a low g(E) in undoped a-Si:H is essential. Measurement of the g(E) and understanding of the nature of gap states are, therefore, very important. The problem has received considerable attention, and many techniques have been developed to determine the g(E). These include both optical and electrical methods. Photoacoustic spectroscopy (PAS),[40] photothermal deflection spectroscopy (PDS),[41] and constant photocurrent measurements (CPM)[42] give the variation of the optical absorption coefficient (α) versus the photon energy ($h\nu$) in the material. The number of defects is related to the absorption. However, the optical absorption coefficient is associated with a joint density of the initial and final states. Therefore, in general, it is rather difficult to distinguish one from the other. The main results obtained by PAS, PDS, and CPM are considered to show information on the valence-band tail in the

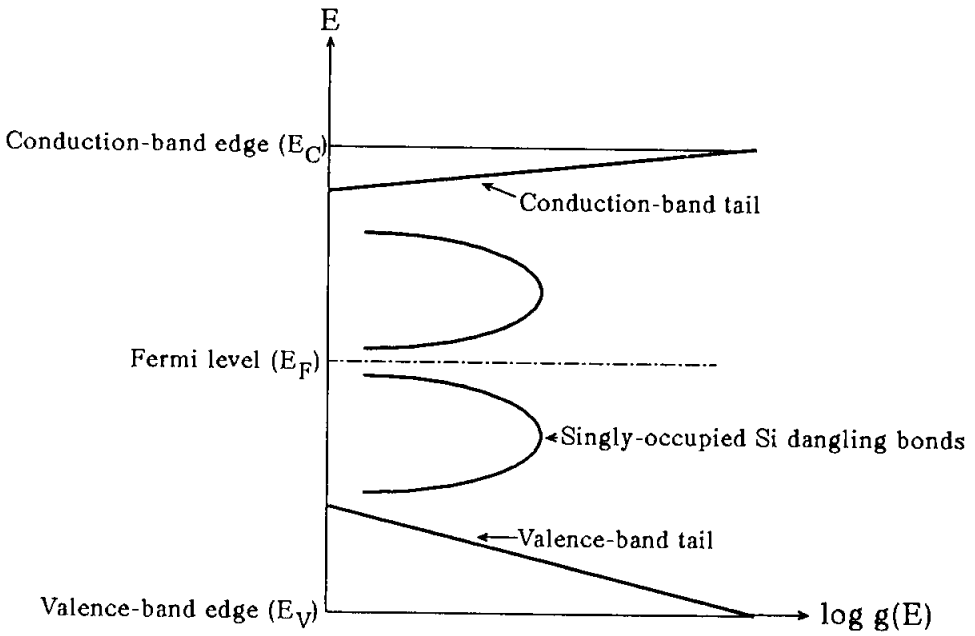

Fig.1.1. Schematic sketch of density-of-state distribution [g(E)] in undoped a-Si:H.

case of hydrogenated amorphous silicon-based alloys. While modulated photocurrent (MPC) methods[43] give information on the peak position of g(E) above the Fermi level for highly resistive (e.g., undoped) a-Si:H, estimation of the actual density of gap states is impossible. SCLC measurements[44] do give quantitative estimation of the g(E), but only above the Fermi level. However, the determination of the g(E) below the Fermi level for undoped films is important, because gap states located below the Fermi level include singly-occupied Si dangling bonds which are considered to be main midgap states. Moreover, those midgap states would determine the optoelectronic properties of the film and would, therefore, affect the performance of devices based on these films. Transient capacitance methods like deep-level transient spectroscopy (DLTS)[45] and isothermal capacitance transient spectroscopy (ICTS),[46] which usually make use of a Schottky barrier junction, are tested techniques for determining the g(E) below the Fermi level. However, these methods are limited in their application to doped samples of low resistivity. For high resistivity materials, such as undoped or compensated a-Si:H films, the dielectric relaxation times are too long for the measurement of the capacitance which can reflect the depletion width in the junction. That is why we have tried to determine the g(E) below the Fermi level in undoped hydrogenated amorphous silicon-based alloys. Since the steady-state HMC method could determine the density of the midgap states, transient capacitance of the undoped a-Si:H/p c-Si heterojunction must include information on the g(E) below the Fermi level in a-Si:H.[19,22] Actually, the study of the transient HMC has made it possible to determine the g(E) below the Fermi level in highly resistive amorphous semiconductors.[19]

A great problem, which has been directly associated with the degradation of the efficiency of a-Si:H solar cells, was reported in 1977, that is, Staebler and Wronski[47] discovered photo-induced metastable changes in the dark conductivity and photoconductivity of undoped a-Si:H. They found that both conductivities decrease after expose to prolonged band-gap illumination, and are restored to their original state by

subsequent thermal annealing at 150-200 ℃. Since then, much work has been done to elucidate the mechanism of this light-induced phenomenon, commonly called the Staebler-Wronski (S-W) effect, because it is directly associated with the stability of amorphous silicon-based photosensitive devices. Stutzmann et al.[48] have proposed the following mechanism; the rate of increase in dangling bond density (N_s) determined by electron spin resonance (ESR) measurements is given by the relation that dN_s/dt is proportional to $\Delta n \Delta p$, where Δn and Δp are the free electron and hole concentrations, respectively, under light exposure. Each concentration is proportional to G/N_s, where G is the carrier generation rate by light exposure. They have concluded that $N_s(t)$ is proportional to $G^{2/3}t^{1/3}$, where t is the time of light exposure. Once N_s has been increased by light exposure, the kinetics of its thermal annealing can be explored. Stutzmann et al.[49] have proposed a monomolecular annealing process with a distribution of activation energies (E_a), while Lee et al.[50] have proposed a bimolecular annealing process with constant E_a. Smith and Wagner[51] expanded the Stutzmann's model into a more general model which can explain the reason why N_s cannot be reduced to the value below 10^{15} cm^{-3} for undoped a-Si:H. Since the transient HMC method enables us to carry out the real-time measurements of the g(E) in the process of a 150-℃ annealing,[52] the annealing kinetics can be investigated and E_a at each energy position of midgap states can be directly determined from the method, where the g(E) can be obtained in a short time (e.g., several seconds). As is described above, both the nature and creation models of metastable midgap states have intensively been investigated.

The contribution of this thesis to a-Si:H solar cells is mentioned. As shown in Fig. 1.2, an n^+-p diode is suitable for a crystalline semiconductor solar cell while a p-i-n diode is desirable for an amorphous semiconductor solar cell, which results from the difference between minority carrier diffusion lengths in crystalline and amorphous semiconductors. In the crystalline semiconductor, electrons of electron-hole pairs produced by light exposure in the bulk region of the p-layer are

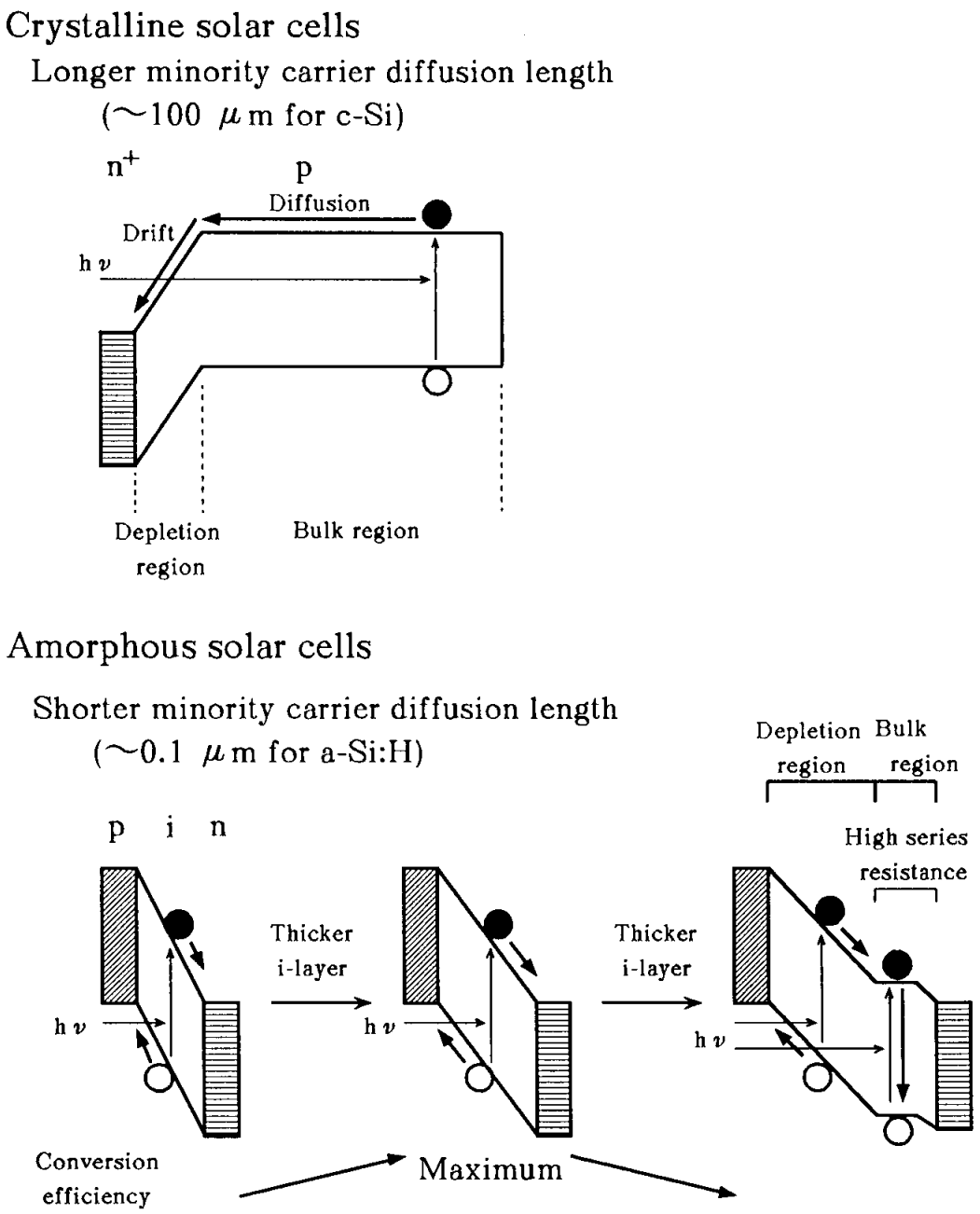

Fig.1.2. Schematic sketches of energy-band diagrams in crystalline and amorphous solar cells. The conversion efficiency of amorphous p-i-n solar cells depends on the i-layer thickness. The symbols of ○ and ● represent a hole and an electron, respectively.

diffused into the depletion region and are separated by the internal field in the depletion region, as shown in Fig. 1.2. In the amorphous semiconductor, however, electron-hole pairs cannot be separated due to its much shorter diffusion length. That is why the internal field is necessary in the place where electron-hole pairs are produced by light exposure, suggesting that the most suitable structure for the amorphous semiconductor is a p-i-n diode structure, where the i-layer is usually an undoped a-Si:H layer. Since light absorption in the i-layer contributes to a photocurrent of the a-Si:H solar cell, the thicker the i-layer becomes, the higher its conversion efficiency might be considered to be. However, a thicker i-layer is divided into the depletion region and the bulk region shown in Fig. 1.2, and the latter region does not contribute to the photocurrent at all. To make matters worse, the bulk region acts as high series resistance in the circuit, which means that the efficiency drops down. The thickest i-layer which is completely depleted, therefore, is desirable. A space-charge density (N_I) in the i-layer, which determines the depletion width in the i-layer, is necessary in order to know the desirable i-layer thickness. That is why a method for determining the value of N_I is discussed in this thesis. As mentioned before, origin of the photodegradation in a-Si:H solar cells has extremely been investigated. Even if an a-Si:H solar cell is designed to deplete the whole i-layer, after light exposure the bulk region appears in the i-layer, which makes the efficiency worse. This is because N_I in the i-layer increases by light exposure from a macroscopic point of view and because the singly-occupied Si dangling bonds are produced by light exposure from a microscopic standpoint. Since the singly-occupied Si dangling bonds are correlated with the g(E) under the Fermi level as shown in Fig. 1.1, a method for determining the g(E) under the Fermi level in the i-layer (e.g., undoped a-Si:H layer) is discussed in this thesis. Figure 1.3 shows the relationship between the contents of this thesis and problems in a-Si:H solar cells.

This thesis describes the electrical properties of a-Si:H/c-Si heterojunctions and applies these properties to estimating

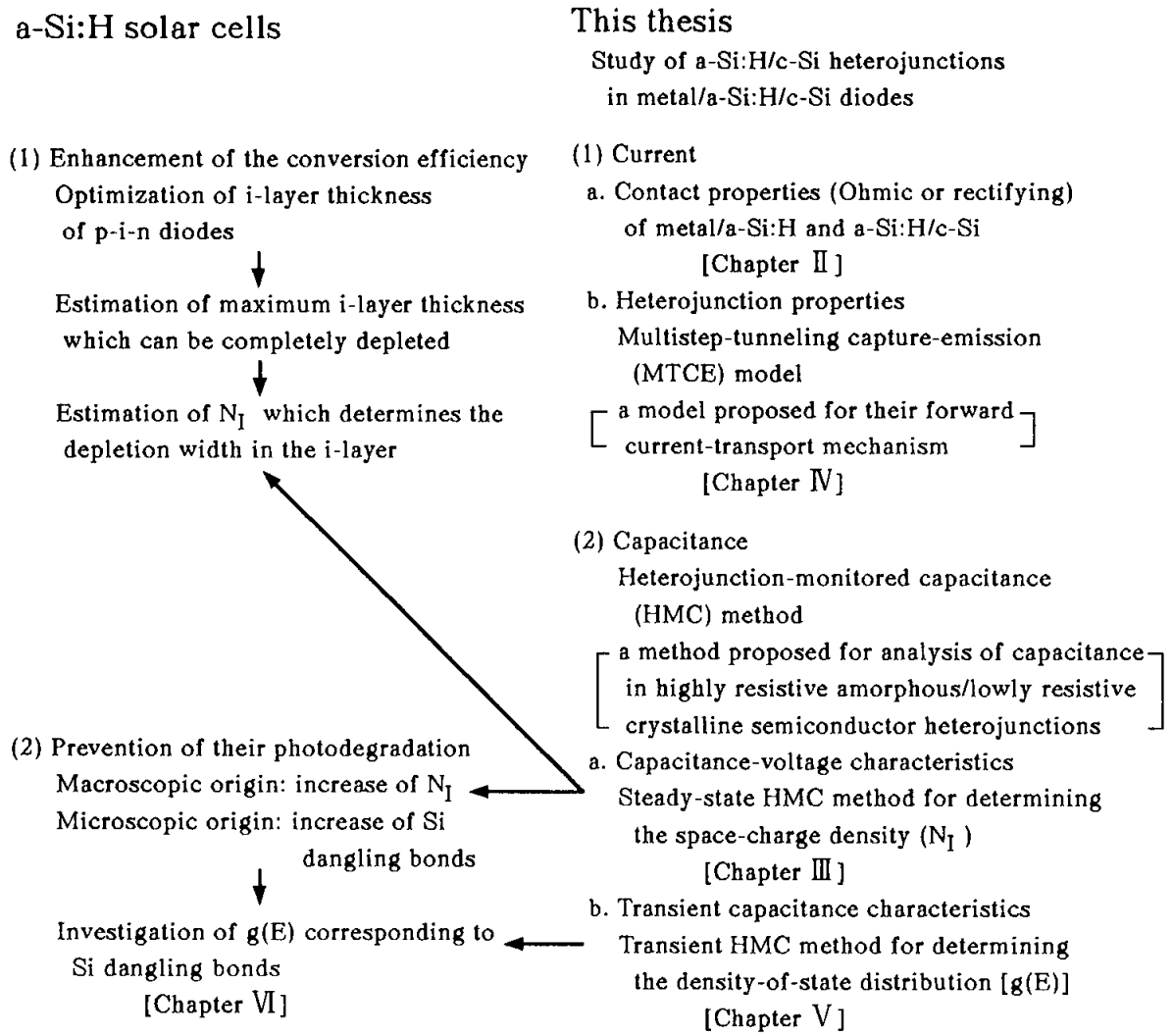

Fig.1.3. Relationship between the contents of this thesis and problems in a-SiH solar cells.

some important properties of undoped hydrogenated amorphous silicon-based alloys. Then it discusses changes of the g(E) in undoped a-Si:H by light soaking, rapid cooling, and thermal annealing.

Chapter II presents systematic experimental results of contact properties (Ohmic or rectifying) on metal/a-Si:H contacts and c-Si/a-Si:H heterojunctions. Since this study enables us to understand where a current is limited (i.e., in a junction or in the bulk) in a device and also whose contact exhibits a rectifying property, the investigation of metal/amorphous/crystalline diodes mentioned in the following chapters can be easily done.

Chapter III describes the high-frequency C-V characteristics of highly resistive amorphous/lowly resistive crystalline semiconductor heterojunctions experimentally as well as theoretically. From the study, a new method for estimating both the density of midgap states and band discontinuity between amorphous and crystalline semiconductors is developed.

Chapter IV presents the I-V characteristics of undoped a-Si:H/p c-Si heterojunctions with various resistivities of c-Si. A model for explaining the experimental results is discussed.

Chapter V develops a new method for determining the g(E) below the Fermi level in highly resistive semiconductors using the transient capacitance of these heterojunctions at various temperatures under high frequency.

Chapter VI describes the g(E) below the Fermi level in undoped a-Si:H, undoped a-$Si_{1-x}Ge_x$:H, and undoped a-$Si_{1-x}C_x$:H. Then, it discusses changes of the g(E) in undoped a-Si:H by light soaking, rapid cooling, and thermal annealing.

Finally, conclusions of the present study are made in Chapter VII.

References

1) S. M. Sze, Physics of Semiconductor Devices(Wiley-Interscience, New York, 1969), p.140.
2) R. L. Anderson, Solid-State Electron. 5(1962)341.
3) R. H. Rediker, S. Stopek, and J. H. R. Ward, Solid-State Electron. **7**(1964)621.
4) M. J. Hampshire and G. T. Wright, Br. J. Appl. Phys. **15**(1964)1331.
5) A. R. Riben and D. L. Feucht, Solid-State Electron. **9**(1966)1055.
6) A. R. Riben and D. L. Feucht, Int. J. Electron. **20**(1966)583.
7) J. P. Donnelly and A. G. Milnes, Proc. IEEE **113**(1966)1468.
8) S. S. Perlman and D. L. Feucht, J. Electron. **18**(1965)159.
9) W. Shockley, Electrons and Holes in Semiconductors(Van Nostrand, Princeton, 1950), p.309.
10) E. Spenke, Electronic Semiconductors(McGraw-Hill, New York, 1958), p.81.
11) R. Grigorovici, N. Croitoru, A. Devenyi, and E. Teleman, Proc. Int. Conf. Semiconductors, Paris 1964(Academic Press, New York, 1964), p.423.
12) L. Stourac, Proc. Int. Conf. Amorphous Semiconductors, edited by R. Grigorovici and M. Ciurea, Bucharest 1982(Central Institute of Physics, Bucharest, 1982), p.104.
13) W. E. Spear and P. G. LeComber, Solid-State Commun. **17**(1975)1193.
14) D. E. Carlson and C. R. Wronski, Appl. Phys. Lett. **28**(1976)671.
15) N. F. Mott, Phil. Mag. **19**(1969)835.
16) A. I. Gubanov, Sov. Phys. Solid State **3**(1962)1694.
17) Y. Tawada, M. Kondo, H. Okamoto, and Y. Hamakawa, Proc. 15th IEEE Photovoltaic Specialists Conf., Florida(1981), p.245.
18) H. Matsuura, A. Matsuda, H. Okushi, and K. Tanaka, J. Appl. Phys. **58**(1985)1578.
19) H. Matsuura, J. Appl. Phys. **64**(1988)1964.
20) H. Matsuura, IEEE Trans. **ED-36**(1989)2908.

21) G. Sasaki, S. Fujita, and A. Sasaki, J. Appl. Phys. **53**(1982)1013.
22) H. Matsuura, T. Okuno, H. Okushi, and K. Tanaka, J. Appl. Phys. **55**(1984)1012.
23) H. Matsuura, A. Matsuda, H. Okushi, T. Okuno, and K. Tanaka, Appl. Phys. Lett. **45**(1984)433.
24) H. Matsuura, T. Okuno, H. Okushi, S. Yamasaki, A. Matsuda, N. Hata, H. Oheda, K. Tanaka, Jpn, J. Appl. Phys. **22**(1983)L197.
25) V. Smid, J. J. Mares, L. Stourac, and J. Kristofik, in Tetrahedrally-Bonded Amorphous Semiconductors, edited by D. Adler and H. Fritzsche(Plenum, New York, 1985), p. 483.
26) K. Okuda, H. Okamoto, and Y. Hamakawa, Jpn. J. Appl. Phys. **22**(1983)L605.
27) M. M. Rahman and S. Furukawa, Tech. Dig. Int. PVSEC 1(Kobe, Japan, 1984), p. 171.
28) K. Sasaki, S. Furukawa, and M. M. Rahman, IEDM Tech. Dig., 1985, p.294.
29) M. Ghannam, J. Nijs, R. Mertens, and R. Dekeersmaecker, IEDM Tech. Dig.,1984, p.746.
30) H. Mimura and Y. Hatanaka, J. Appl. Phys. **61**(1987)2575.
31) M. Yabe, N. Sato, and Y. Seki, Proc. 4th Sensor Symp.(Tsukuba, Japan, 1984), p.105.
32) M. Cuniot and Y. Marfaing, Phil. Mag. **B57**(1988)291.
33) H. Mimura and Y. Hatanaka, Appl. Phys. Lett. **50**(1987)326.
34) J. M. Essick and J. D. Cohen, Mater. Res. Soc. Symp. Vol. 118, 1988, p.549.
35) Z. Y. Xu, W. Chen, B. F. Zhao, C. A. Wang, F. A. Zhang, and J. Y. Wang, J. Non-Cryst. Solids **97&98**(1987)983.
36) J. Symons, J. Nijs, and R. Mertens, Int. Topical Conf. Hydrogenated Amorphous Silicon Devices and Technology, Yorktown Height, 1988, p.159; IEEE Trans. **ED-36**(1989)2889.
37) H. Mimura and Y. Hatanaka, Jpn. J. Appl. Phys. **24**(1985)L355.
38) H. Mimura and Y. Hatanaka, Jpn. J. Appl. Phys. **26**(1987)60.
39) F. A. Rubinelli, M. R. Battioni, and R. H. Buitrago, J. Appl. Phys. **61**(1987)650.
40) S. Yamasaki, Phil. Mag. **B56**(1987)79.
41) N. M. Amer and W. B. Jackson, in Semiconductors and

Semimetals, edited by J. I. Pankove(Academic, Orlando, FL, 1984), Vol. 21, part B, p.83.

42) M. Vanecek, J. Kocka, J. Stuchlik, Z. Kozisek, O. Stika, and A. Triska, Solar Energy Mater. **8**(1983)411.

43) H. Oheda, S, Yamasaki, T. Yoshida, A. Matsuda, H. Okushi, and K. Tanaka, Jpn. J. Appl. Phys. **21**(1982)L440.

44) K. D. Mackenzie, P. G. LeComber, and W. E. Spear, Phil. Mag. **B46**(1982)377.

45) J. D. Cohen and D. V. Lang, Phys. Rev. **B25**(1982)5321.

46) H. Okushi, Phil. Mag. **B52**(1985)33.

47) D. L. Staebler and C. R. Wronski, Appl. Phys. Lett. **31**(1977)292.

48) M. Stutzmann, W. B. Jackson, and C. C. Tsai, Appl. Phys. Lett. **45**(1984)1075.

49) M. Stutzmann, W. B. Jackson, and C. C. Tsai, Phys. Rev. **B34**(1986)63.

50) C. Lee, W. D. Ohlsen, P. C. Taylor, H. S. Ullal, and G. P. Ceasar, Phys. Rev. **B31**(1985)100.

51) Z E. Smith and S. Wagner, Phys. Rev. **B32**(1985)5510.

52) H. Matsuura, Appl. Phys. Lett. **54**(1989)344.

CHAPTER II PROPERTIES OF CONTACTS BETWEEN HYDROGENATED AMORPHOUS SILICON AND OTHER MATERIALS

2-1. Introduction

Studies of metal/semiconductor junctions and heterojunctions are helpful for understanding fundamental device physics as well as for realizing applications to various devices. In other words, it is necessary to recognize whether each contact in a device shows Ohmic behavior or rectifying behavior.

This thesis has investigated the electrical properties of a rectifying junction between an undoped hydrogenated amorphous silicon-based alloy and crystalline silicon (c-Si) in a metal/amorphous/crystalline diode. So, it is necessary to make only one rectifying heterojunction and the other good Ohmic contacts in the diode. In order to get Ohmic contacts with undoped hydrogenated amorphous silicon-based alloys, however, the use of heavily doped hydrogenated amorphous silicon (a-Si:H) should be avoided because of keeping the dopant of heavily doped a-Si:H from contaminating the undoped hydrogenated amorphous silicon-based alloy. This is because the properties of undoped hydrogenated amorphous silicon-based alloys have been investigated by the study of those heterojunctions. Therefore, metal is preferable to an Ohmic-contact material for undoped hydrogenated amorphous silicon-based alloys as long as metal is evaporated onto amorphous films at room temperature.

This chapter has investigated electrical properties of metal(Au,Pt,Al,Mg)/a-Si:H/c-Si(n^+,p^+) diodes and has described the property (Ohmic or rectifying) of each contact. Furthermore, the conduction type of P-doped, undoped, and B-doped a-Si:H has been classified into three categories such as n-type, intrinsic, and p-type from the study of junction properties.

2-2. Contact Properties for Undoped and P-doped a-Si:H

CHAPTER II PROPERTIES OF CONTACTS

Undoped a-Si:H films, ~ 1 μm in thickness, were deposited on n^+ and p^+ c-Si heated to 250 ℃ by the rf glow-discharge decomposition of pure SiH_4. A flow rate of 5 sccm and a gas pressure of 50 mTorr were maintained during the deposition. The dark conductivity at 297 K and its activation energy were $5x10^{-9}$ S/cm and 0.72 eV, respectively. After depositing a-Si:H films, four different kinds of metals (Mg,Al,Au,Pt) were subsequently evaporated onto different positions of identical a-Si:H films. Current-voltage (I-V) measurements have been performed on those metal/undoped a-Si:H/c-Si structures.

P-doped a-Si:H films were deposited on n^+ c-Si heated to 300 ℃ from PH_3/SiH_4 gas mixture under the gaseous impurity ratios of $3x10^{-4}$ and $3x10^{-3}$, where a total gas-flow rate of 5 sccm and a gas pressure of 50 mTorr were kept constant. Similar measurements have also been done on metal/P-doped a-Si:H/n^+ c-Si specimens.

Figure 2.1 shows the I-V characteristics of the metal/undoped a-Si:H/n^+ c-Si specimens for four different kinds of metals. The essential features of the characteristics of the Au, Pt, and Al specimens are almost the same, while the I-V characteristics of the Mg specimen are quite different from the others.

As is shown in Fig. 2.1, the magnitudes of the currents in the Mg/undoped a-Si:H/n^+ c-Si diode at bias voltages of ± 0.1 V are equal to or larger than $5x10^{-8}$ A/mm^2 which is simply calculated from the dark conductivity ($5x10^{-9}$ S/cm) and thickness (about 1 μm) of the a-Si:H film, indicating that the current in the Mg specimen must be a bulk-limited current like an Ohmic current or a space-charge-limited current (SCLC). Therefore, both the contacts of Mg/undoped a-Si:H and n^+ c-Si/undoped a-Si:H must behave as an Ohmic contact. This results in an energy-band diagram of Fig. 2.2(b). Although this diode shows a little rectifying property, the Mg/undoped a-Si:H contact could not affect the electrical properties of undoped a-Si:H/p c-Si heterojunctions in Mg/undoped a-Si:H/p c-Si diodes mentioned in the following chapters because the current level studied there is much lower than the Ohmic current level.

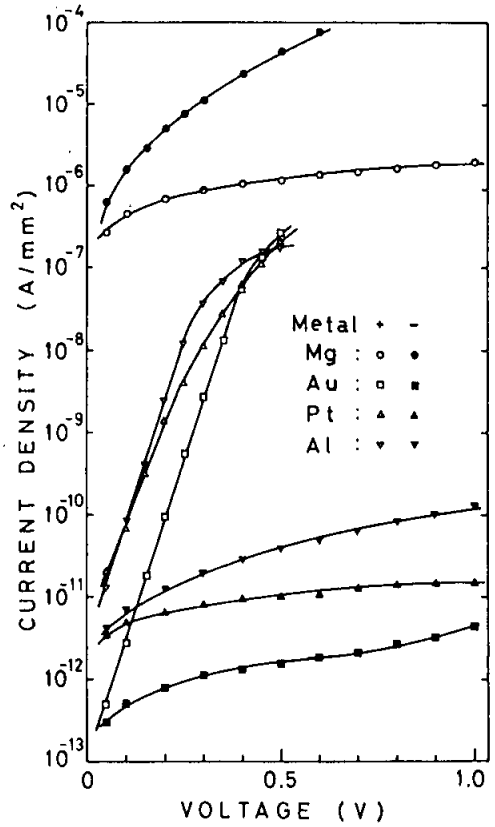

Fig.2.1. I-V characteristics of metal/undoped a-Si:H/n^+ c-Si structures.

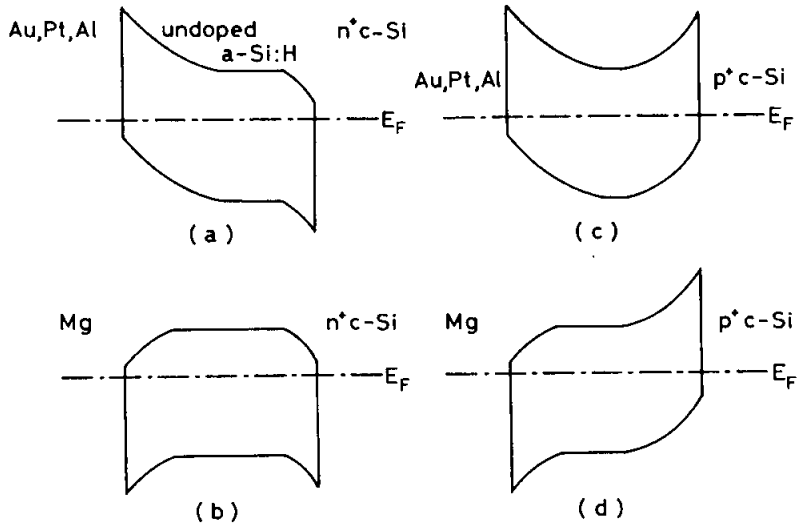

Fig.2.2. Energy-band diagrams of undoped a-Si:H: (a) metal(Au,Pt,Al)/undoped a-Si:H/n^+ c-Si; (b) Mg/undoped a-Si:H/n^+ c-Si; (c) metal(Au,Pt,Al)/undoped a-Si:H/p^+ c-Si; (d) Mg/undoped a-Si/p^+ c-Si.

CHAPTER II PROPERTIES OF CONTACTS

In contrast to the Mg specimen, the I-V characteristics of the Au, Pt and Al specimens are mainly limited by Schottky barrier junctions formed by metal/undoped a-Si:H contacts, because the n^+ c-Si/undoped a-Si:H contact is found to be Ohmic. Actually, considering the I-V characteristics shown in Fig. 2.1, it is quite reasonable to present an energy-band diagram of undoped a-Si:H for Al, Pt and Au contacts, as is sketched in Fig. 2.2(a). A positive bias voltage on the metal electrodes induces forward currents.

Figure 2.3 shows the I-V characteristics of the metal/undoped a-Si:H/p^+ c-Si specimens. It is considered that the currents of metal(Au,Pt,Al)/undoped a-Si:H/p^+ c-Si specimens for a negative bias on the metals are limited by the reverse-biased metal/undoped a-Si:H contacts, since the magnitudes are of the same order as those of the reverse currents of the corresponding metal(Au,Pt,Al)/undoped a-Si:H/n^+ c-Si specimens shown in Fig. 2.1. On the other hand, the current flowing through each specimen, on applying a positive bias voltage to the metals, is determined by the reverse-biased p^+ c-Si/undoped a-Si:H contact, which is evident from the fact that each value coincides with every other independent of metal electrodes within a small statistical scatter. Consequently, the I-V characteristics of the metal(Au,Pt,Al)/undoped a-Si:H/p^+ c-Si structures are considered to be those of back-to-back diodes with an energy-band diagram shown in Fig. 2.2(c).

Only when a negative bias voltage is applied to the Mg electrode, does the specimen show forward I-V characteristics originating from the property of the p^+ c-Si/undoped a-Si:H contact, since the current level is considerably lower than that of the Mg/undoped a-Si:H contact shown in Fig. 2.1. An energy-band diagram of Fig. 2.2(d) can thus be obtained for the Mg/undoped a-Si:H/p^+ c-Si structure.

From the above experimental results, it is clear that Mg makes a good Ohmic contact with undoped a-Si:H. These experimental results could be discussed in terms of the difference in work functions between metal (ϕ_m) and a-Si:H (ϕ_s). According to the conventional metal/semiconductor

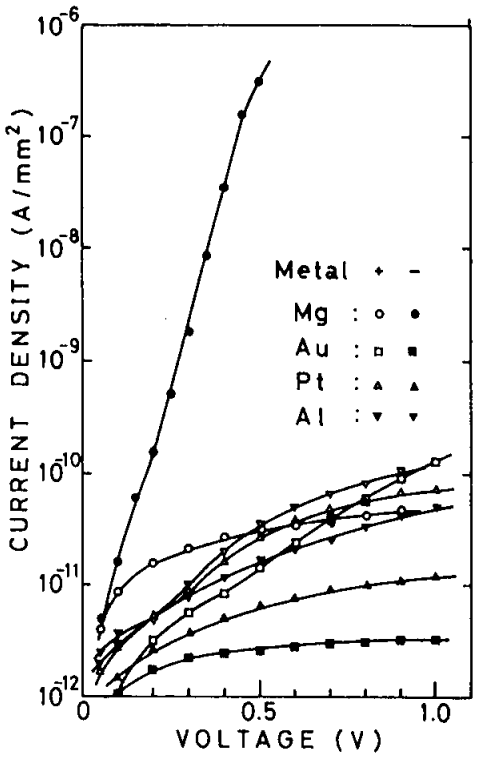

Fig.2.3. I-V characteristics of metal/undoped a-Si:H/p^+ c-Si structures.

junction theory,[1] the relation

$$\phi_m \leqq \phi_s \qquad (2\text{-}1)$$

should be satisfied for making an Ohmic contact when majority carriers are electrons, as long as its interface states are assumed to be absent.

The work function of each metal used in the present study is 3.46, 4.20, 4.70 and 5.48 eV for Mg, Al, Au and Pt, respectively.[2] On the other hand, the electron affinity of the a-Si:H (χ_2) can be tentatively estimated from the photoemission data of Yamamoto et al.[3] on SiO_2/a-Si:H structure, because the electron affinity of SiO_2 [$\chi(SiO_2)$] is independently given as 0.90 eV. Then χ_2 is calculated as

$$\chi_2 = \phi + \chi(SiO_2) = 3.93 \text{ eV} \quad , \qquad (2\text{-}2)$$

where ϕ represents the barrier height at SiO_2/a-Si:H and was estimated to be 3.03 eV.[3] As will be discussed in Chapter Ⅲ, the study of the high-frequency capacitance-voltage (C-V) characteristics of undoped a-Si:H/p c-Si heterojunctions will make it possible to estimate χ_2. Since 0.72 eV is the activation energy (δ_2) of the dark conductivity of the present undoped a-Si:H as mentioned above, ϕ_s becomes 4.65 eV because $\phi_s = \chi_2 + \delta_2$.

From the above discussion, both Mg and Al satisfy the condition represented by Eq. (2-1), while the present study indicates that only Mg forms an Ohmic contact with undoped a-Si:H. The observed non-Ohmic property of Al/undoped a-Si:H contacts might be caused by the presence of the interface states.[4] Namely, ϕ_m of Al is not low enough to make the Al/undoped a-Si:H contact Ohmic.

The metal(Mg,Al)/P-doped a-Si:H contacts for different doping levels of P have also been investigated, as shown in Fig. 2.4. As is clearly indicated, Mg forms better Ohmic contacts than Al regardless of doping levels of P in P-doped a-Si:H. It is likely that Mg is a desirable Ohmic-contact material, superior

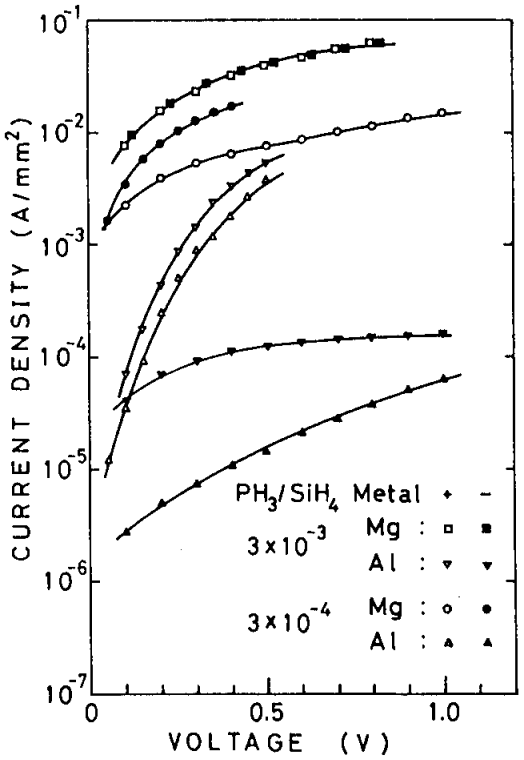

Fig.2.4. I-V characteristics of metal/P-doped a-Si:H/n^+ c-Si structures.

to Al, even for n^+ a-Si:H which is usually introduced into a-Si:H devices as an intermediate layer between Al and undoped a-Si:H for getting Ohmic contacts.

In order to check the stability of the Mg/a-Si:H contact, a thermal annealing experiment at 374 K under N_2 atmosphere for 6 hours was performed. The I-V characteristics of the specimens showed no change before and after the thermal annealing.

On discussing the C-V and I-V characteristics of Mg/undoped a-Si:H/p c-Si diodes in Chapters III and IV, it is worthy of note that a dc applied voltage can form the depletion regions in not only p c-Si but also undoped a-Si:H of undoped a-Si:H/p c-Si heterojunctions, which is quite different from the case of chalcogenide/c-Si heterojunctions[5] and amorphous germanium/crystalline germanium heterojunctions.[6] Its reason is as follows. Since the contacts between metal(Pt,Au,Al) and undoped a-Si:H exhibit rectifying properties which originate from a Schottky barrier junction, the depletion region must be formed in the a-Si:H. Its another evidence was reported that at low frequency the diodes with those metal/a-Si:H contacts showed the C-V characteristics originating from the Schottky barrier junctions.[7] Therefore, the quality of these undoped a-Si:H is good enough to form the depletion region in a-Si:H.

2-3. Contact Properties for B-doped a-Si:H

Junction properties of metal(Au,Mg)/B-doped a-Si:H/c-Si(n^+,p^+) structures as a function of B-doping level are studied, and the conduction type of each B-doped specimen in terms of carrier concentration is discussed. Crystalline Si wafers were soaked in a solution of HF to remove SiO_2 on c-Si, then rinsed in distilled water. B-doped as well as undoped a-Si:H films, $\sim$ 1.5 μm in thickness, were deposited on both n^+ and p^+ c-Si heated to 300 ℃ by means of the rf glow-discharge decomposition of B_2H_6/SiH_4 gas mixtures; the B_2H_6-to-silane ratios were between 0 and 1.1×10^{-2}. A flow rate of 5 sccm, a gas pressure of 50 mTorr, and an rf power of 5 W were maintained during the deposition.

The dark conductivity of a-Si:H deposited in this way was measured in a coplanar electrode geometry on Corning 7059 glass substrate, and the lowest dark conductivity was around 10^{-12} S/cm at $B_2H_6/SiH_4 \sim 10^{-4}$. After depositing a-Si:H films, Au and Mg patterns were evaporated onto the virginal surface of each a-Si:H film to produce four different types of diodes; type-1(Au/a-Si:H/n^+ c-Si), type-2(Au/a-Si:H/p^+ c-Si), type-3(Mg/a-Si:H/n^+ c-Si), and type-4(Mg/a-Si:H/p^+ c-Si). The I-V measurements have been performed for these diodes at room temperature. In these diodes the depth profile of B concentration in the a-Si:H layer is found to be flat by secondary ion mass spectroscopy (SIMS). That is why c-Si is used as a substrate instead of heavily P- or B-doped a-Si:H, thereby avoiding "cross contamination" of the two a-Si:H layers.

Figure 2.5 shows the I-V characteristics of diodes (types 1-4) with the a-Si:H films deposited at five different doping levels;(a) B_2H_6/SiH_4=0, (b) 3.0×10^{-6}, (c) 1.5×10^{-5}, (d) 2.7×10^{-3}, and (e) 8.0×10^{-3}.

For the case of undoped a-Si:H, shown in Fig. 2.5(a), the type-3 diode shows Ohmic behavior and the current is limited by the resistance of the a-Si:H film, which means that the junctions of Mg/a-Si:H and n^+ c-Si/a-Si:H are Ohmic. The currents of type-2 and type-4 diodes, for a positive bias on both metals, are of the same order of magnitude, indicating that those currents are limited by the reverse-biased p^+ c-Si/a-Si:H junction in both diodes. Likewise, the similar I-V characteristics of type-1 and type-2 diodes for a negative bias on the metal(Au) imply that the currents are limited by the reverse-biased Au/a-Si:H junction. The properties of the junctions involved in each diode for B_2H_6/SiH_4=0 can then be classified qualitatively into "R" (rectifying) or "O" (Ohmic), and can be summarized in the first column of Table 2-1.

When diodes of B-doped a-Si:H with B_2H_6/SiH_4 ratio of 1.5×10^{-5} shown in Fig. 2.5(c) are compared with the diodes of undoped a-Si:H shown in Fig. 2.5(a), the type-2 diode in Fig. 2.5(c) shows the behavior similar to the type-3 diode in Fig. 2.5(a), indicating that the junctions of Au/a-Si:H and p^+ c-Si/a-

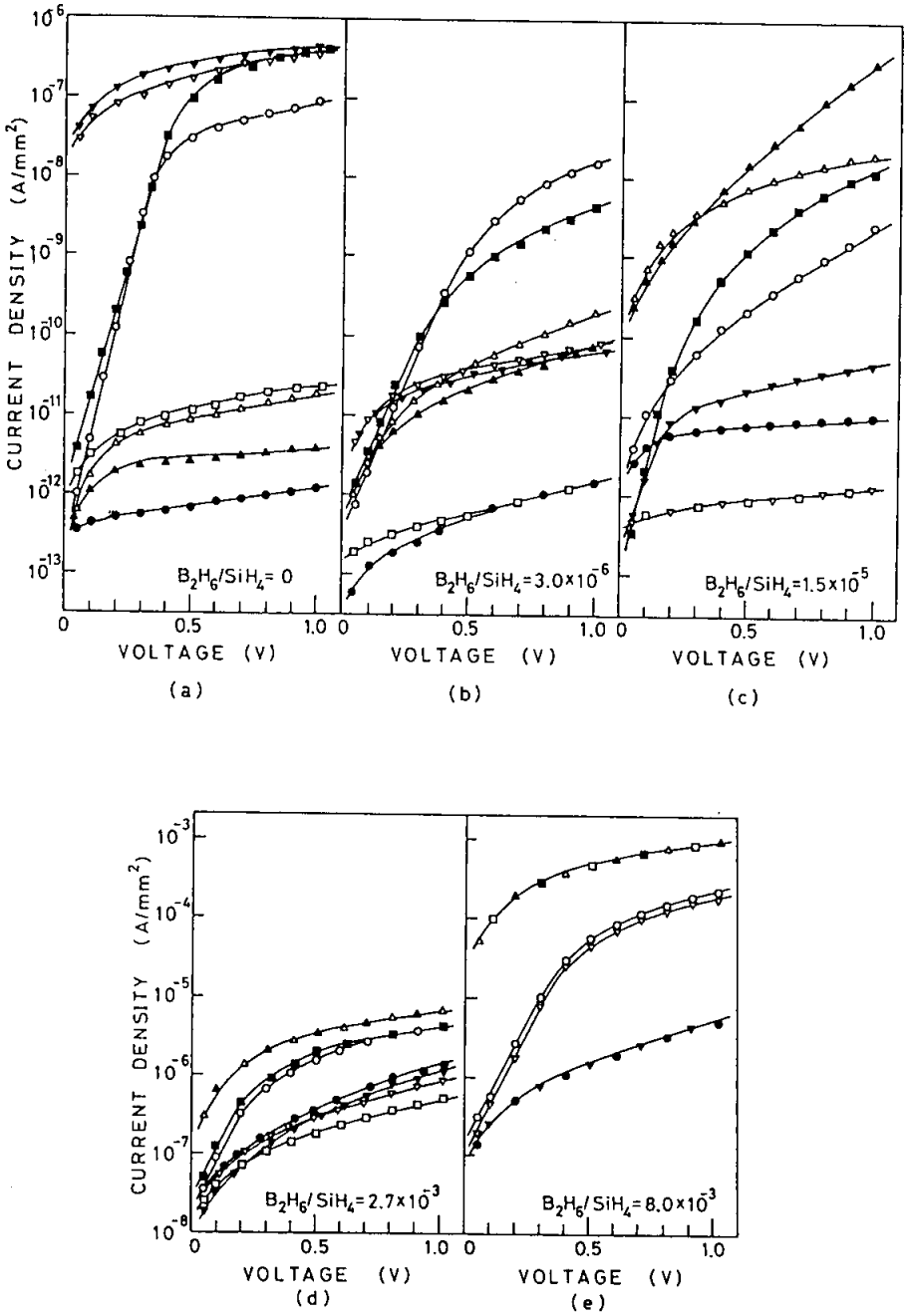

Fig. 2.5. I-V characteristics of four different types of diodes: ○,●, type-1 (Au/a-Si:H/n^+ c-Si); △,▲, type-2(Au/a-Si:H/p^+ c-Si); ▽,▼, type-3(Mg/a-Si:H/n^+ c-Si); and □,■, type-4(Mg/a-Si/p^+ c-Si). B_2H_6/SiH_4 ratios are (a) 0, (b) $3.0x10^{-6}$, (c) $1.5x10^{-5}$, (d) $2.7x10^{-3}$, and (e) $8.0x10^{-3}$. Open and solid marks represent data points for a positive bias and a negative bias voltage on metal, respectively.

TABLE 2-1. Properties of metal/semiconductor junctions and heterojunctions with various B-doped a-Si:H.

B_2H_6/SiH_4	Au/a-Si:H	p^+c-Si/a-Si:H	Mg/a-Si:H	n^+c-Si/a-Si:H	Conduction type[b]
0	R	R	O	O	n
$7.0x10^{-7}$ $1.5x10^{-6}$ $3.0x10^{-6}$	R	R	R	R	intrinsic
$1.5x10^{-5}$ $2.7x10^{-3}$	O	O	R	R	p
$4.0x10^{-3}$ $8.0x10^{-3}$ $1.1x10^{-2}$	O	O	O	R	p

[a] R:rectifying property, O:Ohmic property.
[b] Judging from junction properties.

Si:H are Ohmic for $B_2H_6/SiH_4=1.5x10^{-5}$. The currents of type-3 and type-4 diodes, for a positive bias on Mg, are of the same order of magnitude, supporting that those currents are limited by the reverse-biased Mg/a-Si:H junction in both diodes. Likewise, the similar I-V characteristics of type-1 and type-3 diodes for a negative bias on both metals imply that the currents are limited by the reverse-biased n^+ c-Si/a-Si:H junction. The behavior of the diodes with $B_2H_6/SiH_4=2.7x10^{-3}$, shown in Fig. 2.5(d), is similar to that with $B_2H_6/SiH_4=1.5x10^{-5}$. Therefore, the properties of the junctions involved in each diodes for the gas ratios of $1.5x10^{-5}$ and $2.7x10^{-3}$ can be summarized in the third column of Table 2-1.

Diodes of B-doped a-Si:H with B_2H_6/SiH_4 ratios of $4.0x10^{-3}$, $8.0x10^{-3}$, and $1.1x10^{-2}$ exhibit similar characteristics, as shown in Fig. 2.5(e). The currents of type-2 and type-4, which is quite different from those shown in Fig 2.5(c) and (d), are of the same order of the magnitude, indicating that the Mg/a-Si:H junction changes from rectifying into Ohmic when the B_2H_6/SiH_4 ratio increases from $2.7x10^{-3}$ to $4.0x10^{-3}$. On the other hand, the behavior of type-1 and type-3 results from that of the n^+ c-Si/a-Si:H junction. Then the properties of those junctions are classified, as shown in the fourth column of Table 2-1.

Diodes of B-doped a-Si:H with the gas ratios of $7.0x10^{-7}$, $1.5x10^{-6}$, and $3.0x10^{-6}$ exhibit similar characteristics, as shown in Fig. 2.5(b). The forward-biased currents of type-1 and type-4 diodes at higher voltages are limited by the resistance of the B-doped a-Si:H films. Since the currents of type-2 and type-3 diodes are substantially lower than the forward-biased currents of type-1 and type-4 diodes at higher voltages, it is reasonable to consider type-2 and type-3 diodes as back-to-back diodes. Then all junctions here are rectifying, as seen in the second column of Table 2-1.

The above results can be discussed in more detail using energy-band diagrams for the diodes of types 1-4 shown in Fig. 2.2. The energy-band diagrams were obtained on the basis of undoped a-Si:H films, as described in Section 2-2. But the essential features should be similar qualitatively for the diodes

of B-doped a-Si:H. Since the junction properties of undoped a-Si:H are similar to those of P-doped a-Si:H as described in Section 2-2, the conduction type of undoped a-Si:H is n-type, i.e., the majority carriers in undoped a-Si:H are electrons. Therefore, junctions of Au/a-Si:H and p^+ c-Si/a-Si:H behave as a rectifying contact and agree with the experimental results summarized in Table 2-1.

For $B_2H_6/SiH_4 \geqq 1.5\times10^{-5}$, on the other hand, junctions of Mg/B-doped a-Si:H and n^+ c-Si/B-doped a-Si:H exhibit rectification, indicating that the conduction type of those B-doped a-Si:H in the above doping range is p-type, i.e., the majority carriers are holes. The junction of Mg/B-doped a-Si:H switches from rectifying to Ohmic when B_2H_6/SiH_4 exceeds 4.0×10^{-3}, which is due to tunneling of holes through the very thin Schottky barrier which results from the heavy doping of B.

In B-doped a-Si:H for doping ratios between 7.0×10^{-7} and 3.0×10^{-6}, all junctions exhibit rectification which means that both electrons and holes probably affect the junction properties; the concentration (p) of holes is nearly equal to that (n) of electrons.

From junction properties, the conduction type of a-Si:H deposited at $B_2H_6/SiH_4 \geqq 1.5\times10^{-5}$ is found to be p-type, while the minimum conductivity occurred at $B_2H_6/SiH_4 \sim 10^{-4}$, similar to the case of Spear and LeComber.[8] The conductivity is given by $q(\mu_p p + \mu_n n)$, where μ_p and μ_n are the drift mobilities of holes and electrons, respectively, and q the magnitude of electronic charge. Although p exceeds n at $B_2H_6/SiH_4=1.5\times10^{-5}$, $\mu_p p$ is still smaller than $\mu_n n$ because μ_p is much smaller than μ_n.[9-11] Therefore, the value of $\mu_p p$ is close to that of $\mu_n n$ at $B_2H_6/SiH_4 \sim 10^{-4}$.

Although it is general to determine the conduction type (p- or n-type) of semiconductor by means of Hall measurements, it is quite difficult to do in the case of a-Si:H because its low conductivity makes a Hall voltage immeasurably small. Spear and LeComber[8] have reported on the basis of the activation energy of film conductivity that a transition from n- to p-type conduction in a-Si:H occurs at $B_2H_6/SiH_4 \sim 10^{-4}$ since the activation energy

shows the maximum at that doping ratio. In contrast, in the present work which is based on the junction properties we have successfully characterized B-doped a-Si:H into three categories of conduction type in terms of "dominant" carrier concentration; n-type for $B_2H_6/SiH_4<10^{-7}$, intrinsic for $B_2H_6/SiH_4\sim 10^{-6}$, and p-type for $B_2H_6/SiH_4>10^{-5}$.

On discussing the C-V characteristics of undoped a-Si:H/p c-Si heterojunctions, it is noteworthy that near the interface between undoped a-Si:H and p c-Si the energy band of undoped a-Si:H shows an upward bending, while the energy band of p c-Si shows a downward bending. This is because the conduction type of undoped a-Si:H is found to be n-type.

2-4. Summary

(1) The electrical properties of undoped a-Si:H/p c-Si heterojunctions can be investigated in Mg/a-Si:H/p c-Si diodes, because the Mg/undoped a-Si:H contacts are found to be Ohmic.

(2) In the undoped a-Si:H/p c-Si heterojunctions, the depletion regions are formed in both sides of a-Si:H and p c-Si, and these heterojunctions behave like a p-n junction because the conduction type of undoped a-Si:H is n-type.

(3) P-doped and undoped a-Si:H films make a rectifying contact with Au, Pt, Al, and p^+ c-Si, but those form an Ohmic contact with Mg and n^+ c-Si, indicating that majority carriers in those films are electrons.

(4) B-doped a-Si:H films, which are deposited in the range of $7\times10^{-7}\leq B_2H_6/SiH_4\leq 3\times10^{-6}$, form a rectifying contact with all of the metals(Au,Mg) and c-Si(n^+,p^+), suggesting that the films should be intrinsic.

(5) B-doped a-Si:H films for $B_2H_6/SiH_4\geq 1.5\times10^{-5}$ make a rectifying contact with Mg and n^+ c-Si, while those films form an Ohmic contact with Au and p^+ c-Si, indicating that majority carriers in those films are holes.

(6) Although the conduction type of B-doped a-Si:H changes from n-type to p-type at $B_2H_6/SiH_4\sim 10^{-6}$ from the study of the

junction properties, the minimum conductivity appears at $B_2H_6/SiH_4 \sim 10^{-4}$. This is simply because the value of $\mu_p p$ becomes nearly equal to that of $\mu_n n$ at the gas ratio of 10^{-4}.

(7) Al does not form an Ohmic contact with undoped and n^+ a-Si:H.

References

1) R. H. Bube, Photoconductivity of Solids(John Wiley and Sons, New York, 1960) p.112.
2) A. G. Melnes and D. L. Feucht, Heterojunctions and Metal-Semiconductor Junctions(Academic Press, New York, 1972) p. 158.
3) T. Yamamoto, Y. Mishima, M. Hirose, and Y. Osaka, Proc. 2nd Photovoltaic Science & Engineering Conf. Japan, Tokyo, 1980; Jpn. J. Appl. Phys. **20**(1981) Suppl. 20-2, p. 185.
4) C. R. Wronski and D. E. Carlson, Solid State Commun. **23**(1977)421.
5) L. Stourac, Proc. Int. Conf. Amorphous Semiconductors, edited by R. Grigorovici and M. Ciurea, Bucharest 1982(Central Institute of Physics, Bucharest, 1982), p. 104.
6) R. Grigorovici, N. Croitoru, A. Devenyi, and E. Teleman, Proc. Int. Conf. Semiconductors, Paris 1964(Academic Press, New York, 1964), p. 423.
7) H. Matsuura and H. Okushi, J. Appl. Phys. **62**(1987)2871.
8) W. E. Spear and P. G. LeComber, Phil. Mag. **33**(1976)935.
9) A. R. Moore, Appl. Phys. Lett. **31**(1977)762.
10) D. Allan, Phil. Mag. **B38**(1978)381.
11) T. Tiedje, B. Abeles, D. L. Morel, T. D. Moustakas, and C. R. Wronski, Appl. Phys. Lett. **36**(1980)695.

CHAPTER Ⅲ CAPACITANCE-VOLTAGE CHARACTERISTICS OF UNDOPED a-Si:H/p c-Si HETEROJUNCTIONS

3-1. Introduction

Hydrogenated amorphous silicon (a-Si:H) has been a highly important material for device applications. In order to take advantage of both the good properties of a-Si:H and crystalline silicon (c-Si), electric properties of a-Si:H/c-Si heterojunctions have been intensively studied.[1,2] Moreover, the study of these heterojunctions helps to obtain a midgap-state (i.e., space-charge) density (N_I) of undoped a-Si:H, with which the electronic properties of a-Si:H-based devices are critically linked.

In the case of lowly resistive semiconductor (e.g., c-Si and P-doped a-Si:H), it is easy to estimate the value of its space-charge density which determines the depletion width in it using Schottky barrier junctions and p-n junctions. In the case of highly resistive semiconductor (e.g., undoped a-Si:H), however, it is quite difficult to do using those junctions. Figure 3.1 shows the schematic energy-band diagram and the equivalent circuit of a Schottky barrier junction, where C_D is the capacitance determined by the depletion width (W_2), which is expressed as $C_D = \varepsilon_{s2}/W_2$, C_g is the capacitance due to the trapping/detrapping processes of electrons between gap states and the conduction band, C_B is the capacitance determined by the width in the bulk region [i.e., $C_B = \varepsilon_{s2}/(L-W_2)$], and G_B is the conductance in the bulk region. Here, L is the thickness of undoped a-Si:H. The influence of admittance in the bulk region on the measuring capacitance (C) changes with the measuring frequency. The frequency, which corresponds to a dielectric relaxation time in the film, is considered;

$$f_{de} = G_B/2\pi C_B$$

$$= 1/2\pi \varepsilon_{s2}\rho_2 \quad ,$$

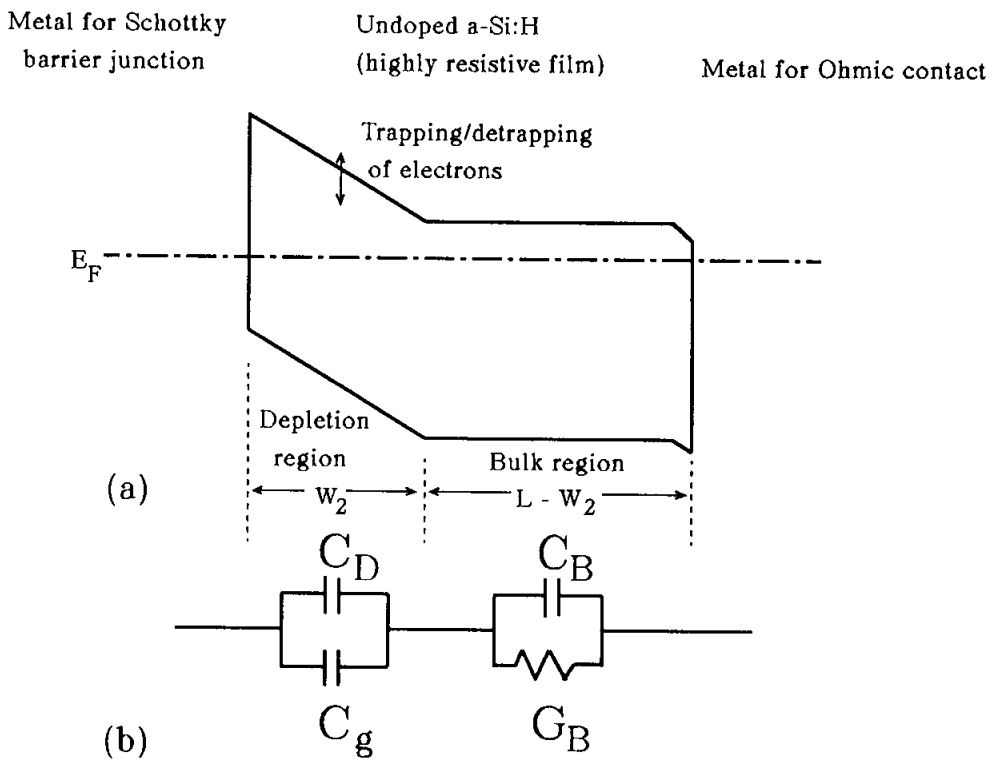

Fig.3.1. Schematic sketches of (a) energy-band diagram in Schottky barrier junction and (b) equivalent circuit.

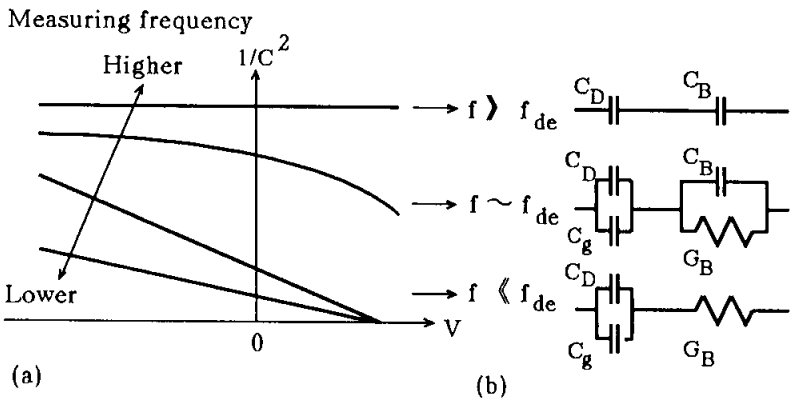

Fig.3.2. Frequency dependencies of (a) $1/C^2$-V characteristics and (b) equivalent circuits.

where ε_{s2} and ρ_2 are the semiconductor permittivity and the resistivity of highly resistive amorphous semiconductor, respectively, and $\varepsilon_{s2}\rho_2$ is referred to as a dielectric relaxation time. In the case of undoped a-Si:H ($\varepsilon_{s2} \sim 12\varepsilon_0$, and $\rho_2 \sim 10^9$ Ω cm),

$$f_{de} \sim 160 \text{ Hz}$$

and

$$\varepsilon_{s2}\rho_2 \sim 10^{-3} \text{ s} \quad .$$

Figure 3.2 shows the schematic $1/C^2$-V characteristics and the equivalent circuits corresponding to different measuring frequencies. At a frequency much higher than 160 Hz, C becomes constant and is given by the thickness of the undoped a-Si:H film as $C=\varepsilon_{s2}/L$. At a frequency much lower than 160 Hz, however, C becomes the value of C_D+C_g and $1/C^2$ is empirically proportional to V. The space-charge density can be estimated from the reciprocal of this slope, but it is strongly dependent on the measuring frequency because of frequency dependence of C_g. In order to estimate N_I which determines the depletion width, the value of C_D should be measured because of $C_D=\varepsilon_{s2}/W_2$.

The main discussion in this chapter is derived from the study of undoped a-Si:H/p-type crystalline silicon (p c-Si) heterojunctions. As is clear from Chapter Ⅱ, a Mg/undoped a-Si:H/p c-Si diode enables us to investigate the undoped (i.e., slightly n-type) a-Si:H/p c-Si heterojunction. These heterojunctions, moreover, are found to behave like a p-n junction. On other words, the depletion regions are formed in both sides of a-Si:H and c-Si, and vary with a dc applied voltage, resulting from the evidences that the current in the diode is limited by the undoped a-Si:H/p c-Si heterojunction as well as that the heterojunction exhibits a good rectifying property.

The high-frequency C-V characteristics of those heterojunctions have experimentally been studied, from which N_I

and conduction-band discontinuity (ΔE_C) between a-Si:H and c-Si are discussed. Moreover, in order to make the above discussion clearer, a model for simulating high-frequency C-V characteristics of highly resistive amorphous/lowly resistive crystalline semiconductor heterojunctions has been developed, where the high frequency indicates a frequency higher than f_{de}.

3-2. Experimental High-frequency C-V Characteristics

3-2-1. C-V characteristics

In the case of undoped a-Si:H the thermal emission rate of electrons from a gap state to the conduction band is usually much lower than the capture rate of electrons from the conduction band into the gap state, indicating that the capacitance should be measured from a higher to a lower reverse bias. In order to get the steady-state condition, moreover, the voltage sweep rate (dV/dt) should be small, for example, the C-V characteristics in this study were measured at dV/dt smaller than 0.004 V/s, and the heterojunction at the highest reverse bias (starting bias for the C-V measurements) was kept for a few minutes. Figure 3.3 shows typical high-frequency C-V characteristics of an undoped a-Si:H/p c-Si heterojunction with the acceptor density (N_A) in p c-Si of 1.0×10^{16} cm^{-3}. When p c-Si is replaced by p^+ c-Si, having the resistivity of $\leqq 0.01$ Ω cm, the capacitance was found to be independent of the applied voltage. The value of this capacitance is found to be determined by the film thickness of the undoped a-Si:H layer, and it is the same as that of the saturated capacitance (C_2) in the positive bias region in Fig. 3.3, indicating that the dc applied bias forms the wide depletion region in a-Si:H but the negligible depletion region in p^+ c-Si. This suggests that the capacitance in Fig. 3.3 is a series of the capacitance determined by the width (W_1) of the depletion region in c-Si and the capacitance determined by the thickness (L) of the a-Si:H film.

In order to explain the high-frequency C-V characteristics, two kinds of models have been proposed;

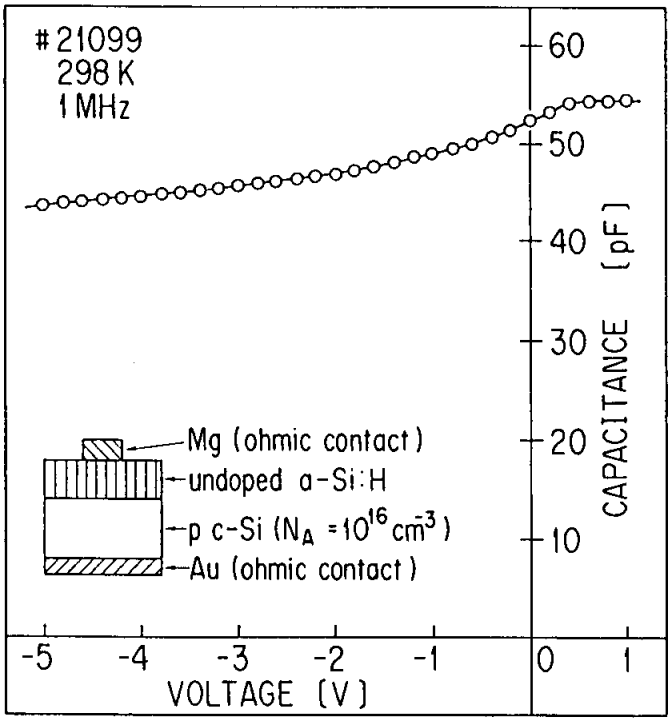

Fig.3.3. C-V characteristics of undoped a-Si:H/p c-Si heterojunction.

CHAPTER Ⅲ C-V CHARACTERISTICS

1. a metal-oxide-semiconductor (MOS)-type model, where a-Si:H is considered to behave as an oxide layer (i.e., insulator);[3-5]
2. a p-n junction-type model.[6,7]

In the MOS-type analysis, the electric field produced by the dc applied bias should be constant over a-Si:H. Furthermore, the quasi-Fermi level for electrons is assumed to coincide with the quasi-Fermi level for holes in the depletion region, which means that at any applied bias the Fermi level can be defined in the depletion region. In the p-n junction-type analysis, on the other hand, the electric field produced by the dc applied bias should not be constant in a-Si:H at all and exists only in the depletion region. Moreover, when the dc bias is applied across the junction, the quasi-Fermi level for electrons is separated from the quasi-Fermi level for holes in the depletion region. As is clear from Fig. 2.3, the undoped a-Si:H/p^+ c-Si heterojunction, where the depletion region formed by the dc bias is negligible in p^+ c-Si, exhibits a good rectifying property, suggesting that the current should be controlled by the change of the depletion width in a-Si:H. In the case of the undoped a-Si:H/p c-Si heterojunctions which will be investigated here, therefore, the C-V characteristics should be analyzed by using the p-n junction-type analysis. Another evidence is also presented as follows.

The frequency dependence of the C-V characteristics for the a-Si:H/p c-Si heterojunction at 298 K is shown in Fig. 3.4. The frequency of 1 kHz remains higher than the reciprocal of the dielectric relaxation time given by $1/2\pi\varepsilon_{s2}\rho_2$ (about 160 Hz), where ε_{s2} is the semiconductor permittivity of undoped a-Si:H and ρ_2 is the resistivity of undoped a-Si:H. The C-V characteristics measured at 100 Hz were much different from those given in Fig. 3.4. The saturated capacitance (C_2) observed at a high forward bias for 1-MHz curve did not appear at the frequency lower than 100 Hz, because the capacitance in a-Si:H is no longer determined by the thickness of the a-Si:H film. On other words, the capacitance in principle approaches a series of the capacitance determined by the depletion width (W_1) in c-Si and

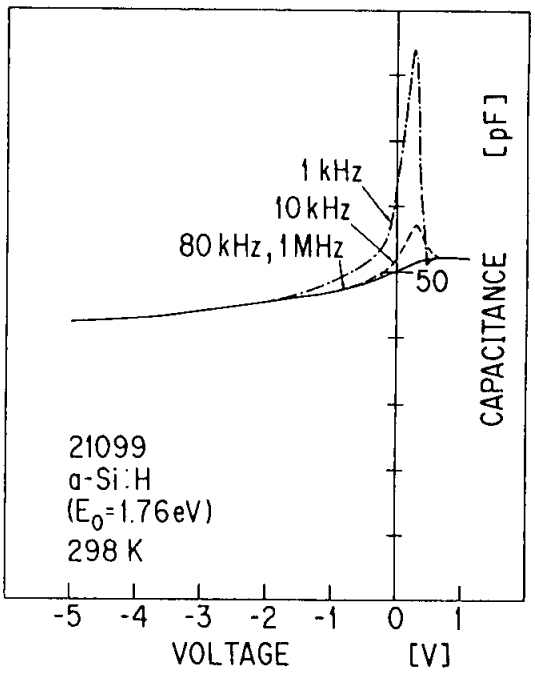

Fig.3.4. Set of four C-V characteristics at 298 K corresponding to different measuring frequencies for undoped a-Si:H/p c-Si (N_A=1.0x10^{16} cm^{-3}) heterojunction.

the capacitance determined by the depletion width (W_2) in a-Si:H instead of the thickness (L) of a-Si:H, as the measuring frequency decreases from 160 Hz, as long as the capacitance due to the trapping/detrapping processes is neglected. That is why the p-n junction analysis should be applied to discussing those C-V characteristics as will be described in the next section. In the figure, the capacitance measured at $V \leqq -2$ V is independent of the frequency, while the capacitance at $V \geqq -2$ V depends on the frequency, indicating that the information obtained in the range of $V \leqq -2$ V is unaffected by capacitances (e.g., diffusion capacitance) which results from the current flow across the heterojunction due to an ac voltage.

The low-frequency (<160-Hz) C-V characteristics are affected not only by the dielectric relaxation process but also by the trapping/detrapping process of electrons and holes between gap states and the extended states, indicating that the midgap-state density obtained from those low-frequency C-V characteristics depends on the measuring frequency. Furthermore, the simulation of their low-frequency C-V characteristics has been so difficult that the physical background of the apparent midgap-state density could not be understood clearly, as is similar to the case of Schottky barrier junctions. Although the zero-frequency C-V characteristics have been simulated because it is not necessary to consider the dielectric relaxation process and the trapping/detrapping process, those cannot experimentally be measured in fact. Since the high frequency enables us to neglect the dielectric relaxation process as well as the trapping/detrapping process, the simulation of the high-frequency C-V characteristics must be possible. Therefore, the C-V characteristics under a frequency much higher than 160 Hz have been measured and discussed in this chapter.

3-2-2. Steady-state heterojunction-monitored capacitance method

In order to understand the above results more clearly, a systematic study of undoped a-Si:H/p c-Si heterojunctions has been performed. Undoped a-Si:H films were deposited by the rf glow-discharge decomposition of pure SiH_4 on four kinds of p c-Si

(0.005-0.01, 0.1-0.15, 1-2, and 5-10 Ω cm) substrates heated to 250 ℃. Prior to a-Si:H deposition, silicon wafers were soaked in a solution of HF to remove SiO_2 and then rinsed in distilled water. A flow rate of 5 sccm and a gas pressure of 50 mTorr were maintained during the deposition. Mg was subsequently evaporated on the a-Si:H films in a vacuum of $7x10^{-7}$ Torr at room temperature. Table 3-1 summarizes Mg/undoped a-Si:H/p c-Si diodes used in the present work, where a film thickness (L) of a-Si:H, the resistivity (ρ_1) in p c-Si and the density (N_A) of acceptor impurities in p c-Si are listed. The value of N_A was determined by C-V measurements on Mg/p c-Si Schottky barrier diodes.

The C-V characteristics of these diodes have been measured at 100 kHz at room temperature. This frequency is high enough to be able to neglect the dielectric relaxation process in undoped a-Si:H (around 10^9 Ω cm in resistivity). Therefore, one can get information on the width of the depletion region extending in the p c-Si side regardless of that of the a-Si:H side. In fact, the capacitance of the diode (sample 5) using p^+ c-Si (0.005-0.01 Ω cm) measured at 100 kHz showed a constant value independent of the dc applied voltage, coinciding with that of the capacitance determined only by the film dimension of a-Si:H, i.e.,

$$C_2 = \varepsilon_{s2}/L \quad , \tag{3-1}$$

where ε_{s2} is the dielectric permittivity of a-Si:H and L is the thickness of a-Si:H measured by Talystep. It clearly indicates that the measuring frequency is higher than the reciprocal of the dielectric relaxation time of undoped a-Si:H, and besides, the depletion region is negligibly thin in the side of p^+ c-Si (0.005-0.01 Ω cm).

Figure 3.5 shows the $1/C^2$-V characteristics of sample 7 (1-2 Ω cm). The capacitance level of the diode replaced by p^+ c-Si of 0.005-0.01 Ω cm (sample 5) is also indicated in the figure by a broken line. Different from the conventional C-V theory, as is shown in the figure, $1/C^2$ is not proportional to the applied voltage.

TABLE 3-1. Various data of materials and diodes used in the present work. Experimental results obtained from C-V characteristics are also listed.

	p c-Si			undoped a-Si:H						
Sample number	ρ_1 (Ω cm)	N_A ($\times 10^{15}$ cm^{-3})	δ_1[a] (eV)	L (μm)	δ_2 (eV)	b	V_B (V)	N_I ($\times 10^{15}$ cm^{-3})	ΔE_C (eV)	χ_2[c] (eV)
2	5-10	2.0	0.22	1.16	0.72	C	0.31	6.2	0.13	3.92
3	1-2	9.0	0.18	0.80	0.76	C	0.51	3.6	0.33	3.72
4	1-2	9.0	0.18	2.19	0.72	C	0.37	2.8	0.15	3.90
5	0.005-0.01	——	0	1.02	0.72	C	——	——	——	——
6	0.1-0.15	180	0.10	1.02	0.72	C	——	——	——	——
7	1-2	9.0	0.18	1.02	0.72	C	0.42	3.9	0.20	3.85
8	5-10	2.0	0.22	1.02	0.72	C	0.38	4.0	0.20	3.85
9	1-2	9.0	0.18	1.77	0.84	I	0.37	1.6	0.27	3.78
10	5-10	2.0	0.22	1.77	0.84	I	0.20	1.8	0.14	3.91

[a] $\delta_1 = kT\ln(N_V/N_A)$, $N_V = 1.02\times10^{19}$ cm^{-3}.

[b] C:capacitively-coupled glow-discharge reaction chamber, I:inductively-coupled glow-discharge reaction chamber.

[c] χ_1 of 4.05 eV and E_{g1} of 1.12 eV are used to obtain χ_2.

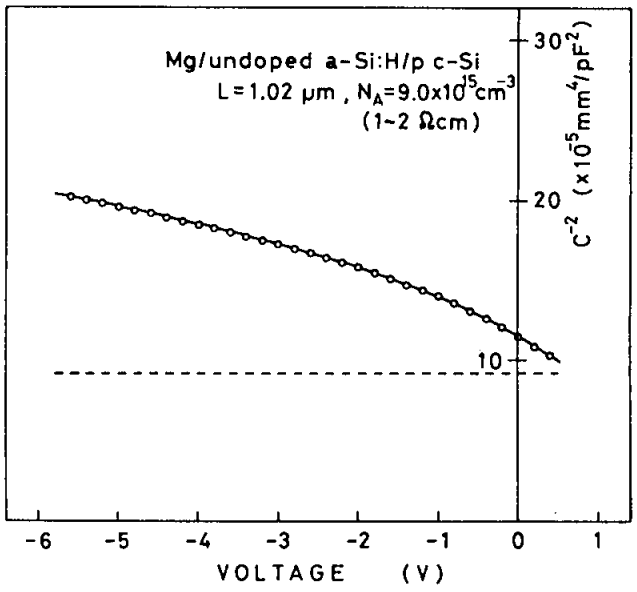

Fig.3.5. $1/C^2$-V characteristics of sample 7. The broken line is those of sample 5.

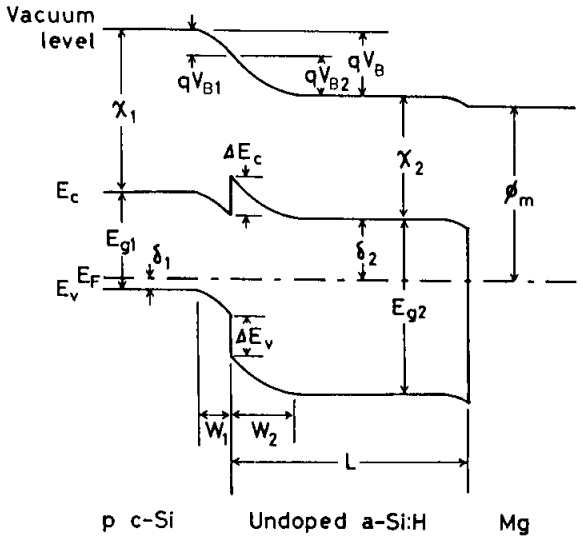

Fig.3.6. Energy-band diagram of p c-Si/undoped a-Si:H/Mg structure at equilibrium.

(A) p c-Si

(a) energy-band diagram

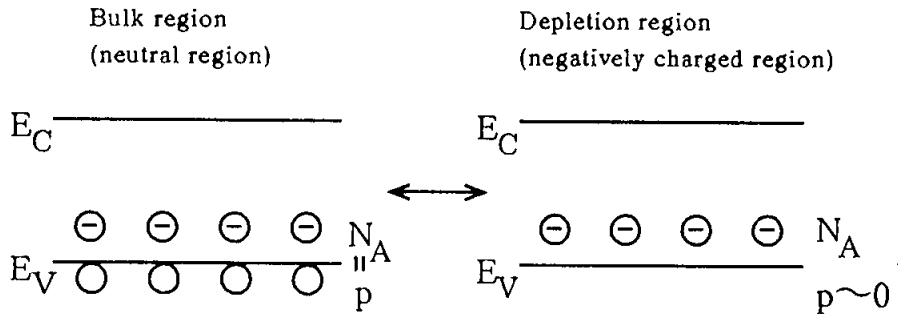

(B) undoped a-Si:H

(a) energy-band diagram

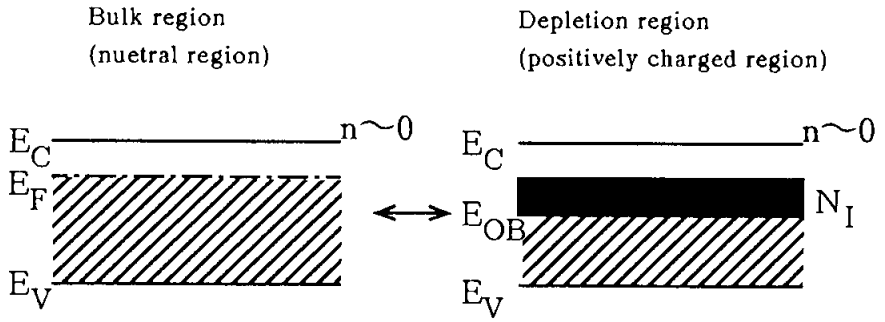

(b) density-of-state distribution [g(E)]

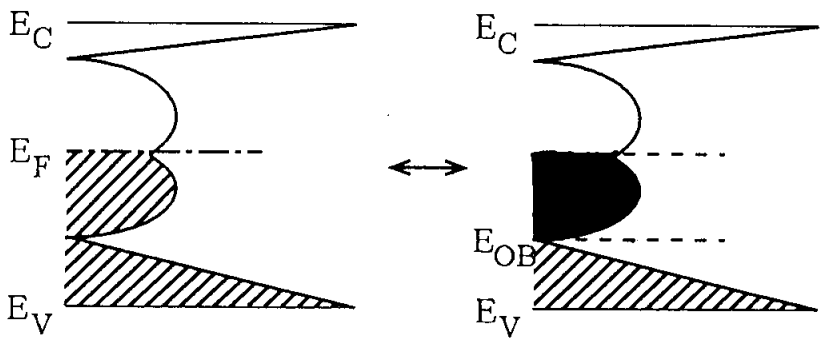

Fig.3.7. Changes of charged carriers and charged gap states between bulk and depletion regions in (a) energy-band diagrams and (b) density-of-state distributions for the cases of (A) p c-Si and (B) undoped a-Si:H. The symbols of ⊖ and ○ represent a negatively charged acceptor and a hole, respectively. The value of N_I is the amount of thermally emitted electrons per unit volume in the black area, which corresponds to the integration value of g(E) from E_{OB} to E_F. The gap states indicated by hatched areas are full of electrons.

The C-V characteristics in the figure is reasonably interpreted by assuming an ideal abrupt heterojunction without interface states. According to the abrupt heterojunction model, the present undoped (i.e., slightly n-type) a-Si/p c-Si heterojunction can be approximated by the energy-band diagram as is shown in Fig. 3.6, where χ is the electron affinity, V_B the built-in potential, δ the distance in energy from the Fermi level to the nearest band edge, E_g the energy-band gap of the semiconductor, W the width of the depletion region, L the thickness of a-Si:H, ΔE the different in energy between band edges of the two semiconductors, and ϕ_m the work function of Mg. The subscripts 1 and 2 refer to p c-Si and undoped a-Si:H, respectively, and the subscripts C and V refer to the conduction band and the valence band, respectively.

The depletion regions formed by the undoped a-Si:H/p c-Si heterojunction are considered. When a reverse bias voltage (V) is applied, it makes the space-charge regions both in a-Si:H and c-Si wider. Under the assumption that this p c-Si has only shallow acceptors, the space charge in p c-Si is formed by negatively charged acceptors and the space-charge density in p c-Si becomes N_A, as shown in Fig. 3.7(A). However, the amorphous component possesses gap states. Origin of the space charge in a-Si:H is schematically discussed using Fig. 3.7(B). In the bulk region, all the gap states below the Fermi level (E_F) are approximately considered to be occupied by electrons, while in the depletion region the states above E_{OB} indicated by the black area are approximately considered to be vacant of electrons, where E_{OB} is determined by thermal-emission rates for electrons and holes from gap states to the extended states and is given by (See Appendix)

$$E_{OB} = E_V + E_{g2}/2 + (kT/2)\ln(\nu_p/\nu_n) \quad . \qquad (3\text{-}2)$$

Here, ν_p and ν_n are the attempt-to-escape frequencies for holes and electrons, respectively. Since the difference between the bulk region and the depletion region is based on the change of electron occupation in the black area in the figure, the gap

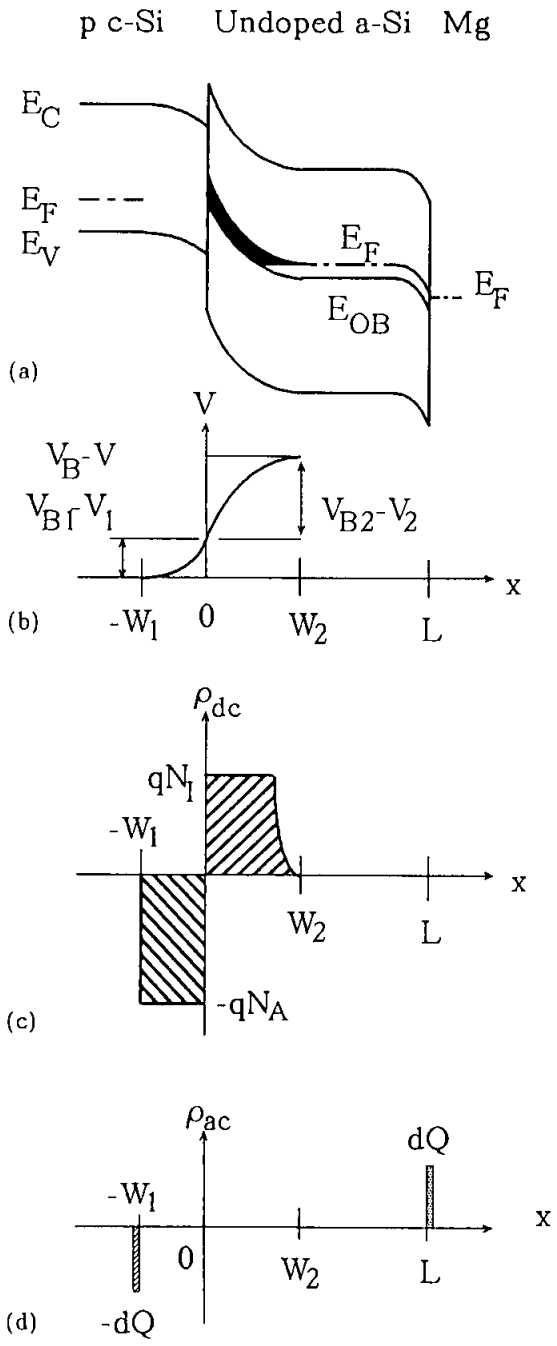

Fig.3.8. Schematic sketches of heterojunction: (a) energy-band diagram; (b) potential variation; (c) space-charge density for a reverse dc voltage; (d) charge in response to a small 100-kHz ac voltage to measure capacitance. The gap states indicated by the black area of (a) behave as positively charged states.

states in the black area behave like positively charged states, referred to as donorlike states, and N_I represents the density of the donorlike states. Therefore, the space-charge density is equal to the midgap-state density [i.e., the integration value of g(E) from E_{OB} to E_F]. So, N_I is referred to as a space-charge density as well as a midgap-state density in these undoped films.

Figure 3.8 shows schematic sketches of the heterojunction. The gap states in the black area in Fig. 3.8(a) behave like positively charged states. Figure 3.8(b) shows the potential variation with distance where V_B is the built-in potential. The depletion width (W_1) in p c-Si is given by[8)]

$$W_1 = [2\varepsilon_{s1}(V_{B1} - V_1)/qN_A]^{1/2} \tag{3-3}$$

and the depletion width (W_2) in a-Si:H is expressed as

$$W_2 \fallingdotseq [2\varepsilon_{s2}(V_{B2} - V_2)/qN_I]^{1/2} \tag{3-4}$$

and the charge neutrality in the heterojunction is described by

$$qN_AW_1 \fallingdotseq qN_IW_2 \quad . \tag{3-5}$$

The capacitance is measured using a small ac voltage of 100 kHz. The resistivity (ρ_1) of p c-Si used in this study is lower than 10 Ω cm so that the dielectric relaxation time ($\varepsilon_{s1}\rho_1$) becomes 10^{-11} s, indicating that the redistribution of holes (majority carriers in p c-Si) can respond to the 100-kHz ac voltage. The capacitance (C_1) in c-Si, therefore, is given by

$$C_1 = \varepsilon_{s1}/W_1 \quad . \tag{3-6}$$

On the other hand, the value of resistivity (ρ_2) for undoped a-Si:H is about 10^9 Ω cm. Then, the dielectric relaxation time becomes 10^{-3} s, suggesting that the redistribution of electrons (majority carriers in undoped a-Si:H) cannot respond to the ac voltage higher than 160 Hz. Thus, the undoped a-Si:H is considered as a dielectric material in its behavior in the case

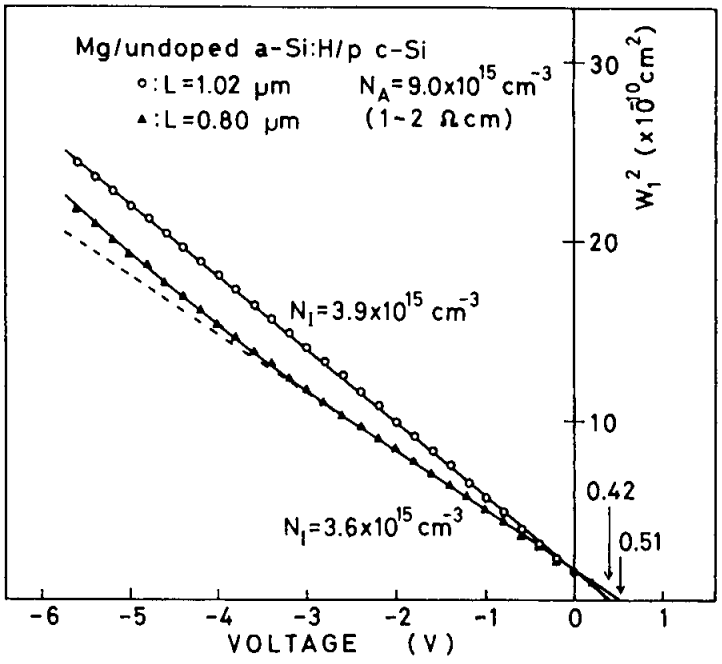

Fig.3.9. Width (W_1) of depletion region in c-Si as a function of voltage for sample 3 (L=0.80 μm) and 7 (L=1.02 μm).

of the 100-kHz ac voltage, indicating that the capacitance (C_2) in a-Si:H should be expressed by

$$C_2 = \varepsilon_{s2}/L \quad . \tag{3-7}$$

The measured capacitance (C) at 100 kHz is from a series of C_1 and C_2, and is given as

$$1/C = 1/C_1 + 1/C_2 \quad , \tag{3-8}$$

because spatially the redistribution of charged carriers can respond to the 100-kHz ac voltage at W_1 and L, as shown in Fig. 3.8(d). From Eqs. (3-3)-(3-5), the following relation is derived;

$$(V_{B1} - V_1)/(V_{B2} - V_2) \fallingdotseq N_I \varepsilon_{s2}/N_A \varepsilon_{s1} \quad . \tag{3-9}$$

The final equation is obtained as

$$W_1^2 = \varepsilon_{s1}^2(1/C - 1/C_2)^2 \tag{3-10}$$

$$\fallingdotseq 2\varepsilon_{s1}\varepsilon_{s2}N_I(V_B - V)/qN_A(N_A\varepsilon_{s1} + N_I\varepsilon_{s2}) \quad , \tag{3-11}$$

from Eqs. (3-3), (3-6), (3-8) and (3-9). As is clear from Eq. (3-11), the values of N_I and V_B can be graphically determined from the slope and the intercept on the abscissa, respectively, which is called a steady-state heterojunction-monitored capacitance (HMC) method.

Figure 3.9 shows the W_1^2-V characteristics of sample 7 (open circle), which was replotted from the data of Fig. 3.5. The data reveals quite a good linear relationship, indicating that the abrupt heterojunction model is applicable to the present system consisting of amorphous/crystalline heterolayer structure. The magnitudes of N_I and V_B are graphically determined from Eq. (3-11), which are listed in Table 3-1.

The thickness dependence of the W_1^2-V characteristics is investigated. The similar plot for sample 3 (solid triangle) is

also shown in Fig. 3.9, which is deviated from the straight line. This apparent invalidity of Eq. (3-11) simply originates from a thinner undoped a-Si:H layer (0.8 μm thick). The depletion layer spreads over the whole a-Si:H (i.e., W_2=L) when the reverse bias voltage exceeds some critical value, resulting in an upward break of the characteristic curve because much more fraction of reverse bias voltage is supported in p c-Si than that expected from Eq. (3-9). On other words, the slope of the W_1^2-V characteristics changes from $2\varepsilon_{s1}\varepsilon_{s2}N_I/qN_A(N_A\varepsilon_{s1}+N_I\varepsilon_{s2})$ to $2\varepsilon_{s1}/qN_A$ as the reverse bias voltage increases from the critical value to higher reverse bias. Using the value of N_I obtained from sample 7, the critical bias voltage, at which W_2 reaches to L (0.8 μm) for sample 3, was calculated as around -2 V, being in good agreement with the data in the figure.

The dependence of N_I on the p c-Si resistivity is studied. The undoped a-Si:H films of samples 5-8 were deposited simultaneously on four different p c-Si substrates. The capacitances of samples 5 and 6 (lower resistivities of p c-Si) were independent of the applied voltage, resulting from the formation of the wide depletion region only in the side of a-Si:H because N_A is much larger than N_I. On the other hand, the value of N_I obtained from sample 7 with the p c-Si resistivity of 1-2 Ω cm coincided with that of sample 8 with the resistivity of 5-10 Ω cm. And also the undoped a-Si:H films of samples 9 and 10 were deposited simultaneously by the inductively-coupled rf glow discharge on two different p c-Si substrates. Both of N_I were quite similar, as shown in Table 3-1.

From the studies of the thickness- and resistivity-dependencies, the steady-state HMC method is considered to be reasonable for the present heterojunctions. From the resistivity-dependence, one had better select p c-Si with N_A which is close to the value of N_I, indicating that several p c-Si substrates should be used in order to estimate N_I in the case that N_I is unknown at all.

3-2-3. Band discontinuity between a-Si:H and c-Si

Knowing band discontinuities at amorphous/crystalline

semiconductor heterojunctions is important in order to describe their electric properties as well as to design a heterojunction-bipolar transistor (HBT) with a wide-bandgap emitter.[1] As is clear from the energy-band diagram shown in Fig. 3.6, the energy difference between the conduction band in a-Si:H and the Fermi level at the interface is expressed as $qV_{B2}+\delta_2$ in the a-Si:H side and $\Delta E_C-qV_{B1}+E_{g1}-\delta_1$ in the c-Si side. Therefore, ΔE_C is expressed by

$$\Delta E_C = \delta_1 + \delta_2 - E_{g1} + qV_B \quad . \tag{3-12}$$

On the other hand, ΔE_C is defined as

$$\Delta E_C \equiv \chi_1 - \chi_2 \quad . \tag{3-13}$$

Experimentally, the value of δ_1 is estimated from N_A as shown in Table 3-1 and the value of δ_2 is the same as the activation energy of dark conductivity of a-Si:H. By substituting quantitative data on δ_1, δ_2, χ_1, E_{g1}, and V_B to Eqs. (3-12) and (3-13), the values of ΔE_C and χ_2 are determined as

$$\Delta E_C = 0.20 \pm 0.07 \text{ eV}$$

and

$$\chi_2 = 3.85 \pm 0.07 \text{ eV} \quad ,$$

using E_{g1}=1.12 eV and χ_1=4.05 eV.[9] Figure 3.10 shows the energy-band diagrams for the diodes (samples 5-8) with four different p c-Si resistivities, sketched on the basis of the above results.

3-3. Simulation of High-frequency C-V Characteristics

3-3-1. Modeling

Though only the undoped (i.e., slightly n-type) a-Si:H/p c-

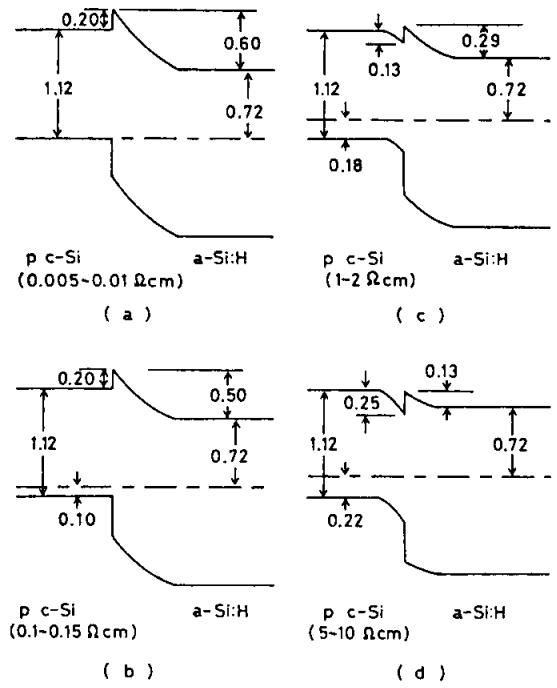

Fig.3.10. Energy-band diagrams in interface regions for heterojunctions using p c-Si with different resistivities. Resistivities of p c-Si are (a) 0.005-0.01 Ω cm, (b) 0.1-0.15 Ω cm, (c) 1-2 Ω cm, and (d) 5-10 Ω cm.

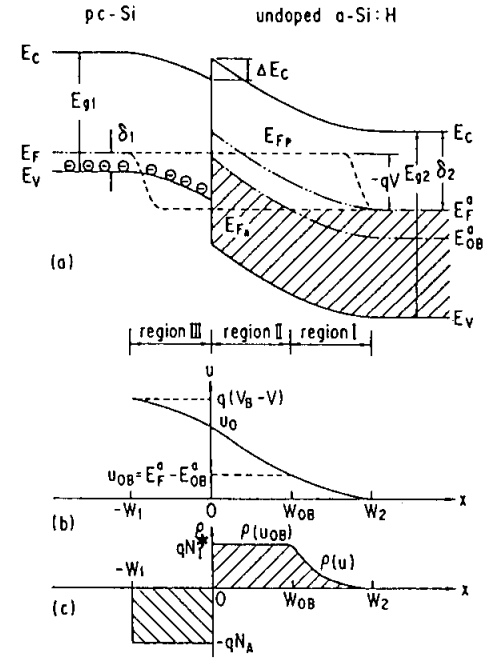

Fig.3.11. Schematic sketches of p c-Si/undoped a-Si heterojunction: (a) energy-band diagram, (b) energy variation for electron, and (c) space-charge density variation for dc reverse-bias voltage condition. Gap states indicated by hatched area of (a) are occupied by electrons.

Si heterojunction is considered in this section, it is easily able to expand this discussion into a general discussion about highly resistive amorphous/lowly resistive crystalline semiconductor heterojunctions. Although there are reports on the simulation of the zero-frequency C-V characteristics of those heterojunctions,[10-13] there is no report on that of the high-frequency C-V characteristics. Here, the following models for simulating the C-V characteristics of the heterojunction are adopted;

(1) one kind of g(E) in undoped a-Si:H, instead of two kinds of g(E) [i.e., donorlike g(E) and acceptorlike g(E)], because it is unnecessary to classify g(E) into two kinds of g(E) as is getting clear from the following discussion;

(2) a carrier occupation function for gap states in the depletion region, which is derived from emission rates for electrons and holes, instead of the Fermi-Dirac distribution function, because the heterojunctions exhibit good rectifying properties in current-voltage (I-V) characteristics, which is quite different from the MOS diodes.

Figure 3.11 shows an energy-band diagram, an energy variation [u(x)] for electrons, and space charges produced by the dc reverse bias (V) for such a heterojunction. When V is applied across the heterojunction, the depletion regions in both a-Si:H and c-Si are formed as shown in Fig. 3.11(a). Because a-Si:H has continuous distribution of the gap states, the spatial distribution of the space charge in the a-Si:H depletion region is not simple. The difference between the a-Si:H depletion region ($0 \leqq x \leqq W_2$) and the neutral region ($x \geqq W_2$) is based on:

1. Whether electrons exist at gap states between E_F and E_{OB};
2. Whether electrons exist in the conduction band as well as in the conduction-band tail.

These changes will result in the formation of the positive space charge in the depletion region of a-Si:H. In this analysis, therefore, charged states (e.g., shallow donors) in both neutral and depletion regions need not be explicitly considered.

In the neutral region, for instance, the electron concentration (n) in the conduction band of undoped a-Si:H is about 6×10^{9} cm^{-3}, which is calculated using the relation $\sigma_2=q\mu_2 n$, where the dark conductivity (σ_2) is 10^{-9} S/cm, the electron charge (q) is 1.6×10^{-19} C, and the drift mobility (μ_2) is 1 $cm^2V^{-1}s^{-1}$. Since this value is much smaller than the expected space-charge density ($\geq 10^{15}$ cm^{-3}, which is the experimentally obtained value of N_I) in the depletion region of undoped a-Si:H, the contribution of the electrons in the conduction band to the production of the space charge can be neglected.

The electron density (n_{BT}) in the conduction-band tail can be estimated as

$$n_{BT} = \int_{E_F^a}^{E_C} f(E)N(E_C)\exp[-(E_C - E)/E_{BT}]dE \quad , \qquad (3\text{-}14)$$

where f(E) is the Fermi-Dirac distribution function, $N(E_C)$ is the density at the bottom of the conduction band, E_F^a is the Fermi level in the neutral region of a-Si:H, and E_{BT} is the characteristic energy for the conduction-band tail of a-Si:H. The value of n_{BT} is 2×10^{13} cm^{-3} using $N(E_C)=10^{21}$ $cm^{-3}eV^{-1}$, $(E_C-E_F^a)=0.73$ eV, and $E_{BT}=50$ meV, suggesting that the contribution of the electrons in the conduction-band tail to the production of the space charge can be also neglected. Since E_{BT} of 50 meV is overestimated (i.e., E_{BT} is usually considered to be smaller than 40 meV),[14] other gap states above E_F must be hidden by the assumed conduction-band tail states. Therefore, the change of occupation at the gap states below the Fermi level mainly produces the positive space charge in the depletion region.

The electron occupation at gap states in the depletion region is governed by a balance between the thermal emission process and the capture process of electrons and holes between gap states and the extended states.[15,16] It is useful to consider one particular energy level (E_{OB}) at which the thermal-emission rate for electrons equals that for holes in the following discussion.

The quasi-Fermi level of electrons (E_{Fn}) is almost constant in the whole depletion region and rises toward the Fermi level near the edge of the depletion region in p c-Si, while the quasi-Fermi level of holes (E_{Fp}) falls near the edge of the depletion region in a-Si:H, as shown in Fig. 3.11(a). The concepts of E_{Fn} and E_{Fp} are important to calculate the carrier densities in the extended states. On the other hand, the concept of the occupation function is important to estimate the trapped carrier density at gap states especially between E_{Fn} and E_{Fp}. The value of E_{OB} in a-Si:H is given by (See Appendix)

$$E_{OB} = E_V + E_{g2}/2 + (kT/2)\ln(\nu_p/\nu_n) \quad , \qquad (3\text{-}2)$$

and the states above E_{OB} are approximately considered to be empty of electrons while the states below E_{OB} are approximately considered to be full of electrons, as long as $E_{OB}>E_{Fn}$. Here, k is the Boltzmann's constant, T is the absolute temperature, E_V is the top of the valence band of a-Si:H, E_{g2} is the energy bandgap of a-Si:H, and ν_n and ν_p are the pre-exponential factors of thermal-emission rates (i.e., attempt-to-escape frequencies) for electrons and holes at the gap states, respectively.

Now considered is the space charge in the two depletion regions (region Ⅰ and region Ⅱ) of a-Si:H which are divided by the cross point (W_{OB}) at $E_{Fn}=E_{OB}$. In region Ⅰ ($W_{OB} \leqq x \leqq W_2$), where E_{Fn} is above E_{OB}, the space-charge density (ρ_I) at the spatial position (x) is expressed as

$$\rho_I[u(x)] = \int_{E_F^a - u(x)}^{E_F^a} g(E)dE \quad , \qquad (3\text{-}15)$$

where u(x) is the energy variation shown in Fig. 3.11(b), E_F^a is the Fermi level in the neutral region, and g(E) is the density-of-state distribution in a-Si:H. Here, for simplicity, the Fermi-Dirac distribution function and the electron occupation function for gap states are approximated by step functions.

In region Ⅱ ($0 \leqq x \leqq W_{OB}$), where E_{Fn} is below E_{OB}, the space-charge density is kept constant and is expressed as

$$\rho_I(u_{OB}) = \int_{E_F^a - u_{OB}}^{E_F^a} g(E)dE \qquad (3\text{-}16)$$

and

$$qN_I^* = \rho_I(u_{OB}) \qquad (3\text{-}17)$$

with

$$u_{OB} = E_F^a - E_{OB}^a \quad , \qquad (3\text{-}18)$$

where u_{OB} is the energy variation at $x=W_{OB}$, N_I^* is the density of midgap states between E_F^a and E_{OB}^a in a-Si:H, E_{OB}^a is E_{OB} in the neutral region of a-Si:H. At thermal equilibrium (i.e., V=0 V), when the built-in potential for a-Si:H is larger than the value of $(E_F^a - E_{OB}^a)/q$, $\rho_I(x)$ near the interface exceeds qN_I^* because the Fermi level is below E_{OB} near the interface. This situation near the interface remains the same even when the reverse bias is applied. However, as will be discussed later, the contribution of the excess charges near the interface can be included in the effect of charged states in the near-interface region.

In the depletion region in p c-Si, which is region Ⅲ ($-W_1 \leq x \leq 0$) in Fig. 3.11, the space-charge density is given by $-qN_A$ under the reasonable assumption that the p c-Si has only shallow acceptors whose density is N_A. As a consequence, the space-charge density can be schematically shown in Fig. 3.11(c).

3-3-2. Simulation

Based on the energy-band diagram mentioned above, the C-V characteristics of the amorphous/crystalline semiconductor heterojunction is theoretically considered. Simulations of the C-V characteristics of the amorphous/crystalline semiconductor heterojunctions at 0 Hz were reported,[10-13] but it is experimentally difficult to measure their very low frequency C-V characteristics that would correspond to the simulation data. Moreover, the experimental low frequency C-V characteristics vary with the measuring frequency due to the dielectric relaxation and

trapping/detrapping processes in the amorphous film.

On the other hand, it is easy to measure their high-frequency C-V characteristics, and when the measuring frequency is high enough, the dielectric relaxation process as well as the trapping/detrapping process can be neglected in the amorphous film. So the change in width of the depletion region in the crystalline semiconductor, produced by the dc reverse bias, is only needed to calculate the capacitance. This leads to an accurate simulation of the high-frequency C-V characteristics of highly resistive amorphous/lowly resistive crystalline heterojunctions. The analytical approach here is that the contribution of a-Si:H to the measured capacitance is equal to the geometric capacitance of the a-Si:H film due to its longer dielectric relaxation time, whereas that of c-Si is associated with the depletion width of c-Si. The measured capacitance is essentially the result of two capacitances in series. In the following, discussed is the simulation condition for the high-frequency C-V characteristics of the amorphous/crystalline heterojunction.

The potential u(x)/q for electrons can be derived from the Poisson equation;

$$d^2[u(x)/q]/d^2x = \rho_I[u(x)]/\varepsilon_{s2} \quad , \tag{3-19}$$

where ε_{s2} is the semiconductor permittivity for a-Si:H. The space-charge Q_{rI} per unit area in region I ($W_{OB} \leqq x \leqq W_2$) is given by

$$Q_{rI} = [2\varepsilon_{s2} \int_0^{u_{OB}} \rho_I(u)du]^{1/2} \tag{3-20}$$

and the electric field (E_{rI}) at $x=W_{OB}$ is given by

$$E_{rI} = Q_{rI}/\varepsilon_{s2} \quad . \tag{3-21}$$

In region Ⅱ, Eq. (3-19) can be solved easily with the boundary conditions of $u(0)=u_0$, $-d[u(x)/q]/dx=E_{rI}$ at $x=W_{OB}$, and $u(W_{OB})=u_{OB}$, because $\rho_I=qN_I^*$, where N_I^* is constant in the region.

The value of W_{OB} is calculated as a function of u_0. Then, the width (W_1) of the depletion region in p c-Si is estimated from the charge neutrality;

$$qN_AW_1 = qN_I^*W_{OB} + Q_{rI} \tag{3-22}$$

and the reverse voltage is calculated from the relation

$$V_B^* - V = u_0/q + qN_AW_1^2/2\varepsilon_{s1} \quad , \tag{3-23}$$

where V_B^* is the built-in potential and ε_{s1} is the semiconductor permittivity for c-Si.

Finally, the high-frequency capacitance (C) is estimated as

$$C= S(\varepsilon_{s1}/W_1 + \varepsilon_{s2}/L) \quad , \tag{3-24}$$

because of the long dielectric relaxation time of undoped a-Si:H, where L is the thickness of a-Si:H and S is the electrode area.

To calculate N_I^* in Eq. (3-17) it is necessary to know the g(E) in a-Si:H. Because the main midgap states in the a-Si:H are reported to be the dangling bonds, which will be described in Chapter V, the g(E) is assumed to have a Gaussian distribution given by

$$g(E) = g_{max}\exp\{-[(E - E_p)^2/2E_W^2]\} \quad , \tag{3-25}$$

where g_{max} is the maximum value of the Gaussian distribution, E_p is the energy level of the maximum value, and E_W is the half-width of the distribution.

Next it is necessary to consider the interface states and the states located in the near-interface region that is qualitatively different from the bulk region. Here, one kind of positively charged layer with thickness d_s and density N_s^* are considered. This layer is located between c-Si and a-Si:H, and represents the interface and near-interface regions of the heterojunction. This layer is called an interface layer in this section, and the charge Q_{ss} per unit area is given by $N_s^*d_s$. If

the effect of the interface layer cannot be neglected, Eq. (3-22) becomes

$$qN_AW_1 = qN_I^*W_{OB} + Q_{rI} + Q_{ss} \quad (3\text{-}26)$$

$$= qN_I^*W_{OB} + Q_{rI} + N_s^*d_s \quad . \quad (3\text{-}27)$$

The parameters used in the present simulation are given in Table 3-2 and almost all the parameters are fixed, since the purpose in this section is to understand the physical background of the space-charge density (N_I) as well as the built-in potential (V_B) obtained from the steady-state HMC method which is described in the former section. The value of ε_{s1} is also assumed to be equal to the value of ε_{s2}.

3-3-3. Reliability of steady-state HMC method

Figure 3.12(a) shows the simulated high-frequency C-V characteristics of a highly resistive amorphous/lowly resistive crystalline heterojunction (with parameters of $g_{max}=10^{16}$ $cm^{-3}eV^{-1}$ and $N_A=10^{15}$ cm^{-3}), and Fig. 3.12(b) shows the W_1^2-V relation obtained from the C-V curve given in Fig. 3.12(a) by using Eq. (3-10). According to the steady-state HMC method [Eq. (3-11)], the values of N_I and V_B can be graphically obtained from the slope and the intercept on the abscissa, respectively. The value of N_I obtained in the reverse-bias region ($-6\ V \leqq V \leqq -1\ V$) is 2.5×10^{15} cm^{-3}. This value is close to N_I^* of 2.0×10^{15} cm^{-3} calculated from Eqs. (3-16) and (3-17) using the parameters given in Table 3-2 ($g_{max}=10^{16}$ $cm^{-3}eV^{-1}$). The value of V_B, which is obtained from the intercept of the straight line drawn in the reverse-bias region ($-6\ V \leqq V \leqq -1\ V$) on the abscissa, is 0.21 V. This value is a little lower than the given value of $V_B^*=0.30$ V, because the additional potential u_{OB}/q is necessary to make the space-charge density constant. Figure 3.13 depicts N_I and V_B as a function of N_I^*. Figure 3.14 shows the dependence of N_I and V_B on N_A. From both figures, N_I represents the midgap-state density well, although N_I is a little larger than the given value of N_I^*.

The simulated high-frequency C-V characteristics, in which

TABLE 3-2. Parameters used for simulating high-frequency C-V characteristics.[a,b]

Amorphous film			
Neutral region	Midgap states	Interface layer	Others
$E_C-E_F^a=0.73$ eV $E_C-E_{OB}^a=0.97$ eV	$E_C-E_p=0.85$ eV $E_W=0.10$ eV $g_{max}=10^{16}-10^{17}$ cm^{-3}eV^{-1}	$N_S^*=0-10^{18}$ cm^{-3} $d_S=0$ or 50 Å	$V_B^*=0.3$ V $L=1.2$ μm $S=0.785$ mm^2 $N_A=10^{15}-10^{17}$ cm^{-3}

[a] N_I^* is calculated from Eq. (3-16) using the given g_{max}.
[b] N_I and V_B obtained from the steady-state HMC method correspond to the parameters N_I^* and V_B^* for the simulation, respectively.

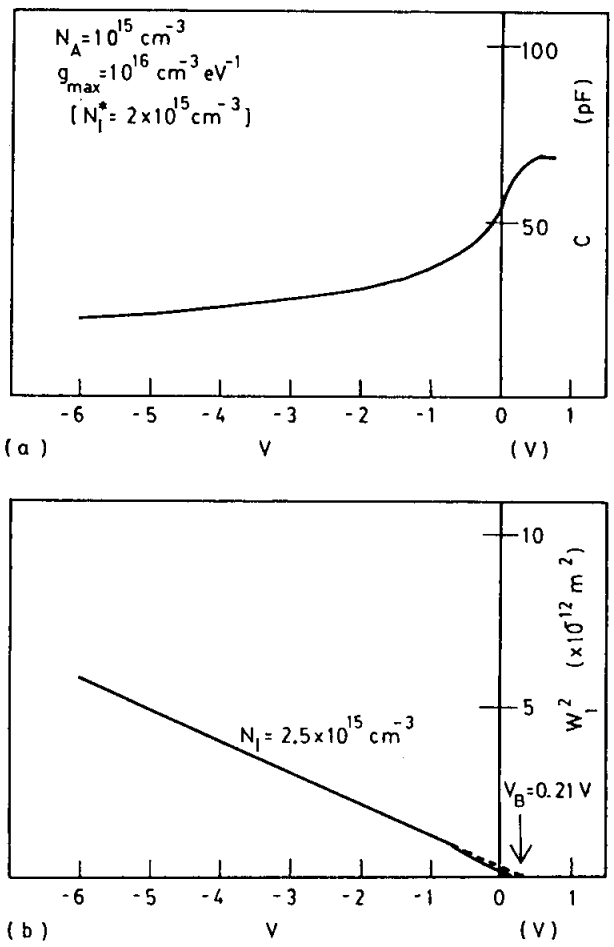

Fig.3.12. Calculated results without interface layer; (a) calculated C-V characteristics and (b) voltage dependence of square of depletion width in crystalline semiconductor. The values of N_I and V_B are obtained from the steady-state HMC method. The solid line is calculated data, and the dashed line is a line extrapolated from high reverse biases.

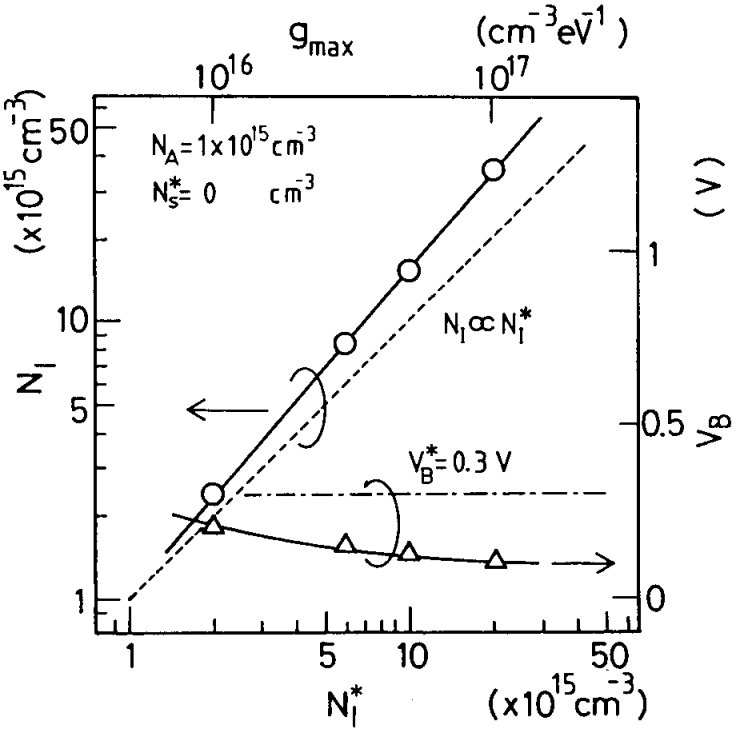

Fig.3.13. Dependencies of N_I and V_B obtained from steady-state HMC method on N_I^* without interface layer. The values of N_I^* and V_B^* are parameters for simulating the high-frequency C-V characteristics.

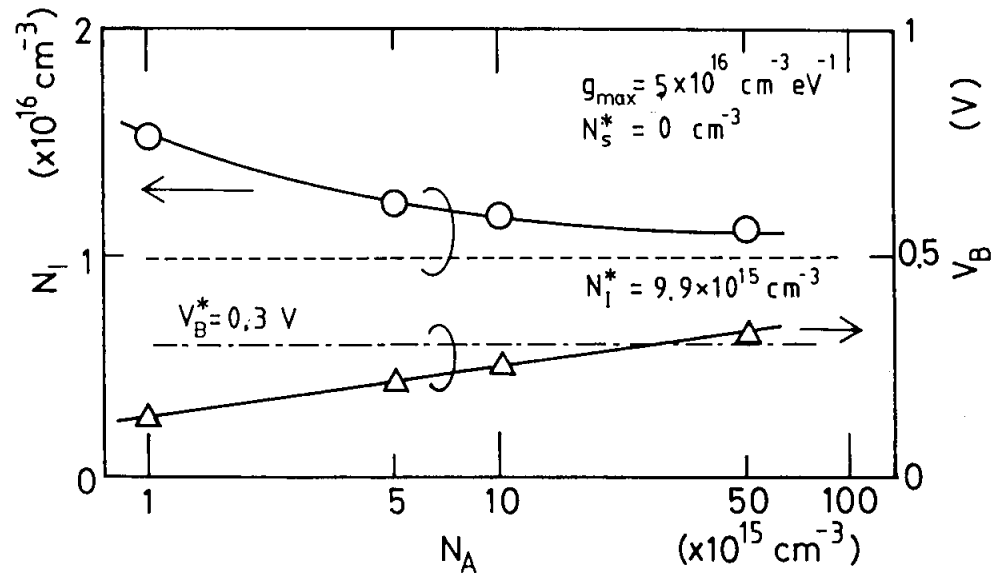

Fig.3.14. Dependencies of N_I and V_B obtained from steady-state HMC method on acceptor density in crystalline semiconductor without interface layer.

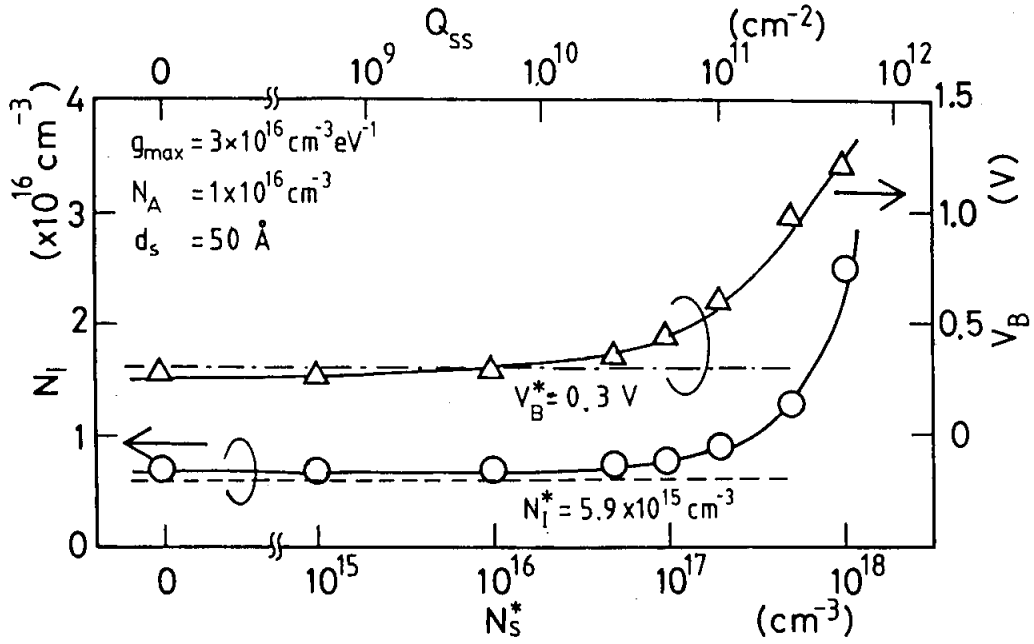

Fig.3.15. Dependencies of N_I and V_B on density of interface layer.

the interface layer was taken into account, were similar to those in Fig. 3.12, although the lowest reverse bias, where the discrepancy from the straight line starts to occur, is higher than the reverse bias (about 0.7 V) calculated without the effect of the interface layer. Figure 3.15 shows the dependence of N_I and V_B on the charge ($Q_{SS}=N_S^* d_S$) of the interface layer for $g_{max}=3\times10^{16}$ $cm^{-3}eV^{-1}$ and $N_A=10^{16}$ cm^{-3}. In the region of $N_S^* \leqq 2\times10^{17}$ cm^{-3} (i.e., the interface-state density Q_{SS} is less than 10^{11} cm^{-2}), the values of N_I and V_B are quite close to the values of N_I^* and V_B^*, respectively, then they increase rapidly with N_S^* in the case of $N_I^*=5.9\times10^{15}$ cm^{-3}. These increases result from Q_{SS}. This critical value of Q_{SS} (or N_S^*) increases with an increase of N_I^*.

It is clear from the above results that if Q_{SS} is low, the values of N_I and V_B obtained by the steady-state HMC method represent the real midgap-state density and the real built-in potential, respectively.

3-4. Summary

The high-frequency (e.g., 100-kHz) C-V characteristics of undoped (i.e., slightly n-type) a-Si:H/p c-Si heterojunctions have been studied experimentally as well as theoretically. These heterojunctions have been found to form depletion regions in both sides of a-Si:H and c-Si by dc bias voltages, and energy-band diagrams for those heterojunctions with four different resistivities of p c-Si have been presented. Since the measuring frequency is much higher than the reciprocal of the dielectric relaxation time of the high-resistivity undoped a-Si:H, the capacitance in the a-Si:H side is determined by the thickness of the a-Si:H film. That is why the measuring capacitance at the high frequency becomes a series of this capacitance in a-Si:H and the other capacitance which is determined by the width of the depletion region in c-Si. Moreover, the trapping/detrapping processes cannot respond to the high-frequency ac voltage, which easily enables us to analyze the C-V characteristics. The main

results are summarized as follows:

(1) The high-frequency C-V characteristics of the heterojunctions with high-resistivity a-Si:H have been successfully analyzed, from which it has been made clear that the abrupt heterojunction model is valid for a-Si:H/c-Si heterojunctions.

(2) A method for estimating the midgap-state density (N_I) of undoped a-Si:H has been developed, which is called a steady-state heterojunction-monitored capacitance (HMC) method. Those densities of the highly resistive films have been difficult to be estimated from the studies of Schottky barrier junctions and homogeneous p-n junctions.

(3) The conduction-band discontinuity between a-Si:H and c-Si has been estimated as 0.20 ± 0.07 eV, from which the electron affinity of a-Si:H is found to be 3.85 ± 0.07 eV.

(4) A model for simulating high-frequency C-V characteristics of those heterojunctions has been developed for the first time, and the physical background of the space-charge density (N_I) of the amorphous film, which is obtained from the steady-state HMC method, has been discussed.

(5) From the simulation of their high-frequency C-V characteristics, in the reasonable case that their interface-state density is less than 10^{11} cm^{-2}, the values of N_I and V_B obtained by the steady-state HMC method are found to represent the midgap-state density of the amorphous film and the built-in potential of the heterojunction, respectively.

References

1) H. Matsuura, IEEE Trans. **ED-36**(1989)2908.
2) H. Matsuura and H. Okushi, in Amorphous and Microcrystalline Semiconductor Devices Vol. Ⅱ : Materials and Device Physics, edited by J. Kanicki(Artech House, Boston, 1992), Chapter 11, p. 517.
3) G. Sasaki, S. Fujita, and A. Sasaki, J. Appl. Phys. **53**(1982)1013.
4) S. B. Iyer, V. Kumar, and K. S. Harshavardhan, Jpn. J. Appl. Phys. **28**(1989)L744.
5) S. B. Iyer, V. Kumar, and K. S. Harshavardhan, Solid-State Electron. **34**(1991)535.
6) H. Matsuura, T. Okuno, H. Okushi, and K. Tanaka, J. Appl. Phys. **55**(1984)1012.
7) D. K. Sharma and K. L. Narashimhan, Phil. Mag. **B63**(1991)543.
8) A. G. Melnes and D. L. Feucht, Heterojunctions and Metal-Semiconductor Junctions(Academic, New York, 1972), p. 34.
9) S. M. Sze, Physics of Semiconductor Devices, 2nd ed.(Wiley-Interscience, New York, 1981), p. 275.
10) F. Rubinelli, S. Albornoz, and R. Buitrago, Solid-State Electron. **28**(1985)741.
11) F. A. Rubinelli, M. R. Battioni, and R. H. Buitrago, J. Appl. Phys. **61**(1987)650.
12) F. A. Rubinelli, Solid-State Electron. **30**(1987)593.
13) Z. Y. Xu, W. Chen, B. F. Zhao, C. A. Wang, F. Q. Zhang, and J. Y. Wang, J. Non-Cryst. Solids **97&98**(1987)983.
14) S. Yamasaki, H. Oheda, A. Matsuda, H. Okushi, and K. Tanaka, Jpn. J. Appl. Phys. **21**(1982)L539.
15) C. H. Hyun, M. S. Shur, and A. Madan, J. Non-Cryst. Solids **46**(1981)221.
16) E. H. Rhoderick and R. H. Williams, Metal-Semiconductor Contacts, 2nd ed.(Clarendon, Oxford, 1988), p. 162.

CHAPTER Ⅳ CURRENT-VOLTAGE CHARACTERISTICS OF UNDOPED a-Si:H/p c-Si HETEROJUNCTIONS

4-1. Introduction

There are very few reports concerning amorphous/crystalline semiconductor heterojunctions after the first report of Grigorovici et al.[1] on amorphous germanium (a-Ge)/crystalline germanium (c-Ge) heterojunctions. Those a-Ge films had such a lot of gap states that p-n control in the films could not be made. According to Stourac,[2] for the case of chalcogenide materials as an amorphous material, the current-transport mechanism was based on space-charge-limited currents (SCLC) in the chalcogenide materials. Concerning hydrogenated amorphous silicon (a-Si:H)/crystalline semiconductor heterojunctions, almost no data had been published before this study started, where a-Si:H has been attractive for device applications because p-n control in a-Si:H has succeeded.[3]

This chapter presents a systematic study of undoped (i.e., slightly n-type) a-Si:H/p-type crystalline silicon (p c-Si) heterojunctions for the first time. The purpose in this chapter is to elucidate the current-transport mechanism of those heterojunctions.

4-2. I-V Characteristics

Figure 4.1 shows the typical I-V characteristics in (a) log-log and (b) semilog presentations for an undoped a-Si:H/p c-Si heterojunction with an acceptor density (N_A) in p c-Si of 1.0×10^{16} cm^{-3}. Two sorts of current-transport mechanisms have been proposed to explain these I-V characteristics;

(1) a bulk-limited (space-charge-limited) current-transport mechanism,[4]

(2) a junction-limited current-transport mechanism.[5]

The essential difference between (1) and (2) is whether the

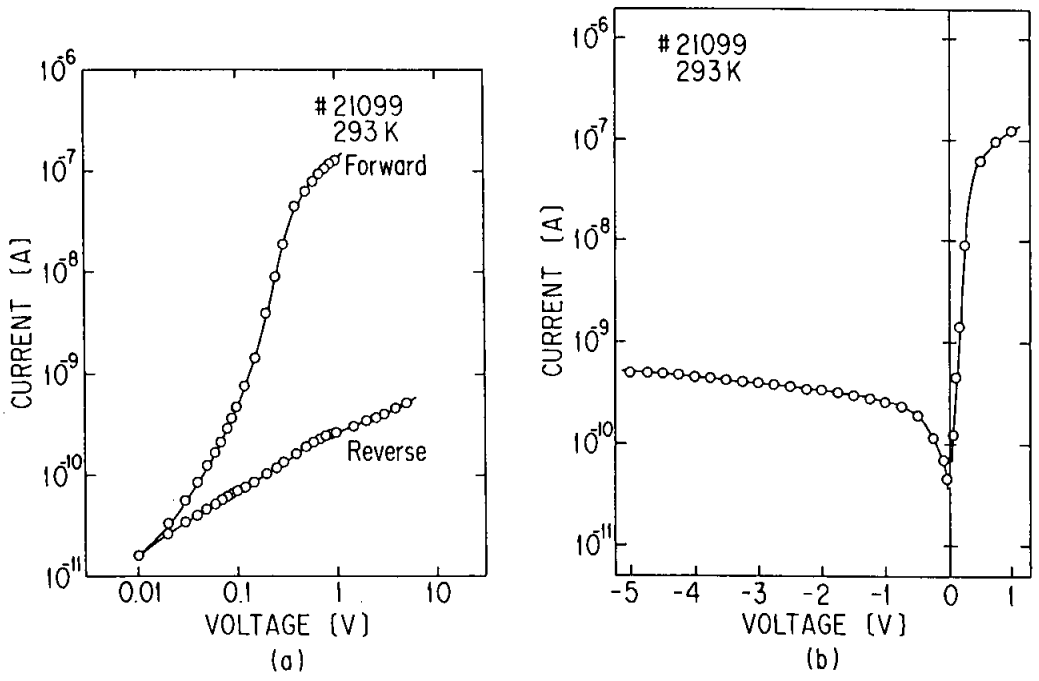

Fig.4.1. I-V characteristics of undoped a-Si:H/p c-Si (N_A=1.0x10^{16} cm^{-3}) heterojunction; (a) log I-log V plots and (b) log I-V plots.

resistance of the depletion region is higher or lower than the resistance of the amorphous film. On other words, in the bulk-limited case the applied bias drop is mainly across the whole amorphous layer, while in the junction-limited case the applied bias drop is across the depletion regions. Because the resistivity and thickness of the a-Si:H film were about 10^9 Ω cm and 1.2 μm, respectively, the expected current in the bulk-limited case should be equal to or larger than 3.3×10^{-9} A at 0.05 V for an electrode area of 0.785 mm^2. The current at bias voltages lower than 0.05 V seems to be Ohmic in nature, as Smid pointed out,[4] because the value of I seems to be proportional to V in this voltage region. The observed current, however, is much smaller than 3.3×10^{-9} A. Judging from the magnitude of the current, the current for $V \leq 0.4$ V (close to the built-in potential, V_B) is thought to be limited by the a-Si:H/c-Si heterojunction. The voltage dependence of the junction-limited current can generally be expressed by

$$I = I_0[\exp(AV) - 1] \quad , \tag{4-1}$$

where A is voltage-independent and I_0 is the prefacter independent of the voltage. The forward current seems to be proportional to V in the voltage range lower than 0.05 V because exp(AV) can be approximately expanded in Talyor's series of 1+AV. Therefore, the I-V characteristics should be discussed on the basis of the junction-limited current-transport mechanism in the voltage region. There is another evidence that the current flowing through this heterojunction is not an SCLC. According to the SCLC model,[6] the relationship between I/L and V/L^2 should be independent of the thickness (L) of the a-Si:H film. However, I/L-V/L^2 characteristics in this study strongly depended on the thickness, indicating that the SCLC model cannot apply to this heterojunction.

4-3. Forward I-V Characteristics

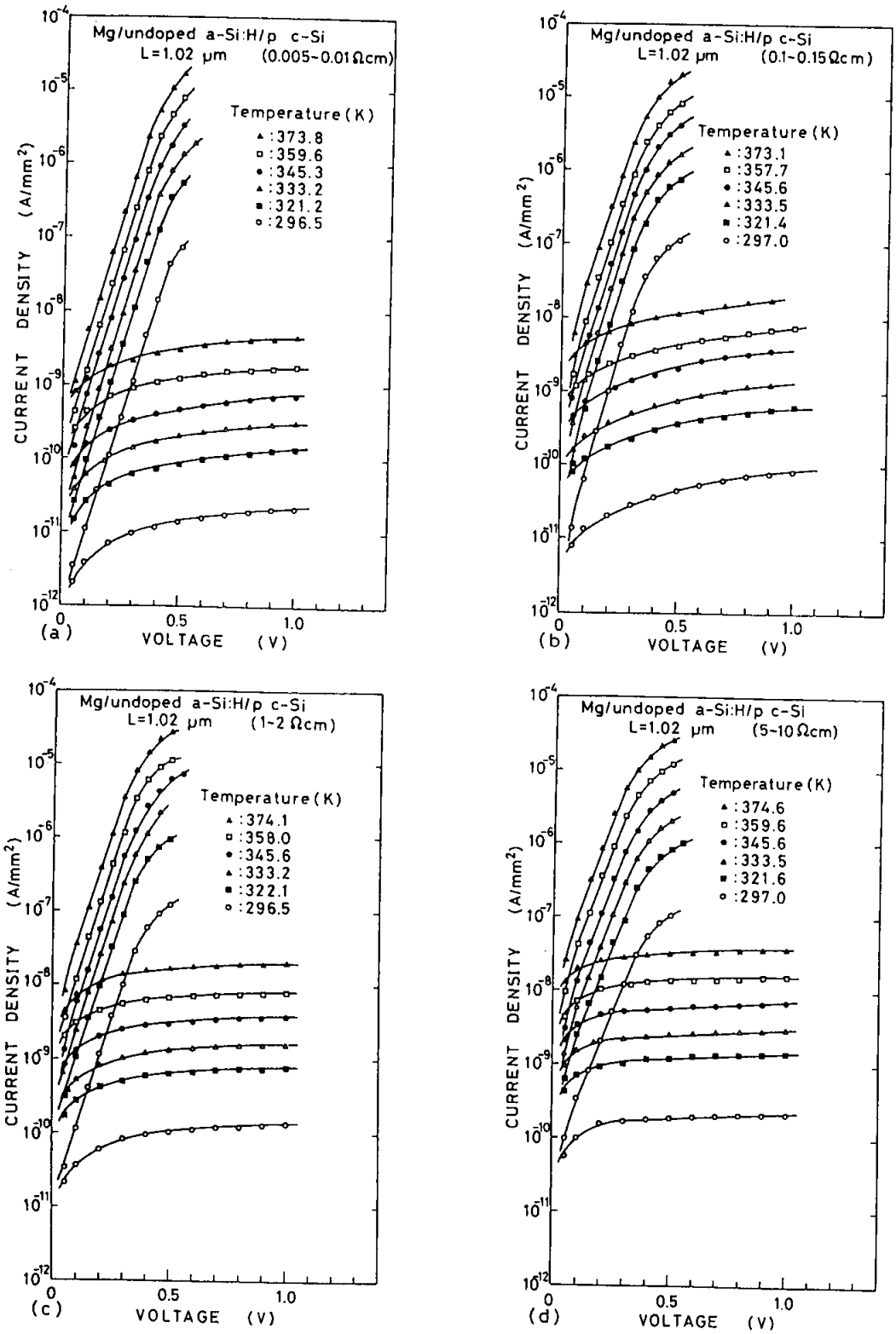

Fig.4.2. I-V characteristics of samples [(a) sample 5, (b) sample 6, (c) sample 7, (d) sample 8] measured at six different temperatures.

CHAPTER Ⅳ I-V CHARACTERISTICS

Three kinds of models for explaining the current of heterojunctions, which can be expressed in Eq. (4-1), are discussed:

(1) A is independent of the measuring temperature (T) for a tunneling model;

(2) A=q/kT for a diffusion model;

(3) A=q/2kT for a recombination model.

Samples 5-8 shown in Table 3-1 in Chapter Ⅲ have been used for studying the I-V characteristics, since the a-Si:H films of 1.02 μm in thickness were deposited simultaneously on p c-Si with four different resistivities; sample 5 (0.005-0.01 Ω cm), sample 6 (0.1-0.15 Ω cm), sample 7 (1-2 Ω cm), and sample 8 (5-10 Ω cm). Their I-V characteristics have been measured as a function of temperature in the range of 297-374 K, but the temperature range scanned in the present work is rather limited. Not only the band-like conduction but also hopping conduction like a variable-range hopping might prevail in the transport of a-Si:H at low temperatures as LeComber et al.[7] reported that the nearest-neighbor hopping predominated below 240 K. Furthermore, their current below 297 K decreases down to as low as 10^{-12} A, causing another difficulty for measuring accurate currents.

Figure 4.2 shows temperature dependencies of the I-V characteristics of Mg/undoped a-Si:H/p c-Si diodes for samples 5-8, respectively. It is clear from the experimental results that the slope (A) of the forward characteristics is constant for different temperatures; therefore, the current in this voltage region can be described by

$$I = I_0 \exp(AV) \tag{4-2}$$

and

$$I_0 = B_0 \exp(-\Delta E_{af}/kT) \quad , \tag{4-3}$$

where A, ΔE_{af}, and B_0 are temperature- and voltage-independent constants. From Eq. (4-3) the values of ΔE_{af} were estimated to be 0.72, 0.80, 0.65, and 0.63 eV for samples 5-8, respectively,

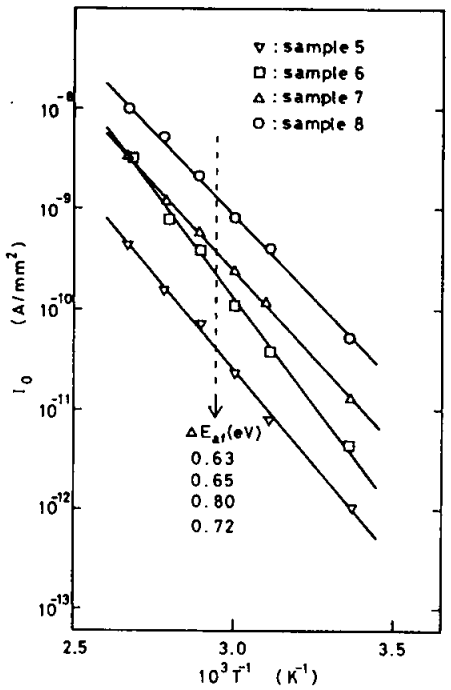

Fig.4.3. Temperature dependence of I_0 of samples 5-8.

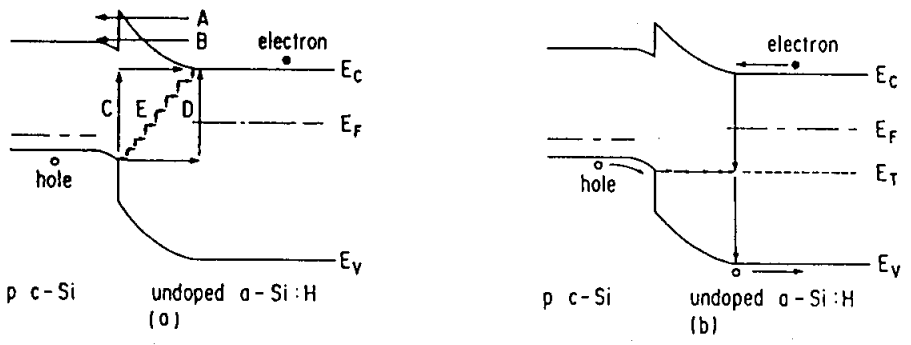

Fig.4.4. Tunneling models for heterojunctions; (a) reported tunneling models and (b) a multistep-tunneling capture-emission (MTCE) model.

as shown in Fig. 4.3. Since the value of A in Eq. (4-2) is independent of temperature, the forward current must be limited by tunneling.

Models for junction transport based on tunneling processes have been proposed by several groups,[8,9] and these are schematically shown in Fig. 4.4(a). To explain the present experimental results, each model is examined separately.

The simplest model consists of the tunneling of carriers through the spike-shaped barrier in the conduction band shown in Fig. 4.4(a). According to Riben,[9] predominant tunnel flux takes place at an energy close to the peak of the barrier within an energy difference of about 0.1 eV for crystalline heterojunctions, which is indicated by path A in the figure. In the present heterojunction, however, a tunneling process at an energy range far below the barrier peak, indicated by path B in the figure, is quite possible because the gap states are quasi-continuously distributed within the gap of a-Si:H, spatially as well as energetically. The magnitude of ΔE_{af} is expected to be larger than 1.12 eV for sample 5, because at V=0 V the difference between the conduction-band edge in p c-Si and the Fermi level in a-Si:H is 1.12 eV, as is clear from Fig. 3.10(a). This requirement contradicts the actual data, i.e., the value of ΔE_{af} for sample 5 was obtained experimentally to be 0.72 eV.

A second model based on the tunneling of carriers was originally presented as the reason for the excess current in tunnel diodes.[10] As was discussed by Riben,[9,11] one-step tunneling [C or D in Fig. 4.4(a)] is always smaller than multistep tunneling [E in Fig. 4.4(a)]. The multistep-tunneling process should predominate in the present system because gap states are quasi-continuously distributed in the mobility gap. According to this multistep-tunneling process, I_0 should change exponentially with T due to the temperature dependence of the bandgap.[9,11] The value of I_0 obtained in this study, however, varies exponentially with -1/T, as shown in Fig. 4.3.

In order to solve this disagreement, a multistep-tunneling capture-emission (MTCE) process has been proposed as the most probable model for the present system, shown in Fig. 4.4(b). A

hole in the valence band of p c-Si flows from a gap state to another in a-Si:H located in an energy range of kT by a multistep-tunneling process and keeps flowing until the tunneling rate becomes smaller than the rate for hole release from the gap state to the valence band of a-Si:H or the rate for recombination of the hole with an electron in the conduction band of a-Si:H. An ending point of tunneling must be close to the edge of the depletion layer in a-Si:H, since the tunneling rate decreases due to a decrease of the electric field.

Thus, a current flowing from p c-Si to undoped a-Si:H is given by

$$I = B(e_p + \sigma_n v_{th} n)\exp(AV) \quad , \tag{4-4}$$

where B is a constant almost independent of the applied voltage and temperature, σ_n is the capture cross section of electrons, v_{th} is the thermal velocity of electrons, n is the electron density in the conduction band of a-Si:H given by

$$n = N_C \exp[-(E_C - E_F)/kT] \quad , \tag{4-5}$$

e_p is the hole emission rate given as

$$e_p = \sigma_p v_{th} N_V \exp[-(E_T - E_V)/kT] \quad , \tag{4-6}$$

σ_p is the capture cross section of holes, N_V and N_C are the effective densities of states in the valence band and the conduction band of a-Si:H, respectively, and E_F, E_V, E_C, and E_T are the energies of the Fermi level, the top of the valence band, the bottom of the conduction band, and the gap state where the hole combines with an electron or emits into the valence band, respectively. Therefore, the current is described by

$$I = I_0 \exp(AV) \tag{4-2}$$

with

$$I_0 = B\{\sigma_p v_{th} N_V \exp[-(E_T - E_V)/kT] + \sigma_n v_{th} N_C \exp[-(E_C - E_F)/kT]\} \quad . \qquad (4\text{-}7)$$

By comparing Eqs. (4-3) and (4-7) with the experimental data, several possibilities can be deduced. For the junction property using p c-Si with the lowest resistivity (sample 5), the value of ΔE_{af}=0.72 eV was obtained. This coincides with the activation energy δ_2 (=E_C-E_F) of the dark conductivity of undoped a-Si:H. Therefore, considering the energy-band diagram shown in Fig. 4.4(b), the electron-capture rate is larger than the hole-emission rate, that is, the second term predominates in the right-hand side of Eq. (4-7). For samples 6-8, on the other hand, the obtained values of ΔE_{af} were 0.80, 0.65, and 0.63 eV, respectively, which correlates with an increase in the substrate resistivity. As is clear from Fig. 3.10(b)-(d), the magnitude of E_T-E_V decreases with an increase in the substrate resistivity. This suggests that the hole emission dominates for these samples, namely, the first term in the right-hand side of Eq. (4-7) determines the magnitude of I_0. It is in progress that the transition from the electron-capture process to the hole-emission process is discussed in detail.

4-4. Reverse I-V Characteristics

The a-Si:H/c-Si heterojunctions can keep a small dark current even at higher reversed bias range, as shown in Figs. 4.1 and 4.2. From Eq. (4-1), the saturated value of the reverse current is expected to be I_0. However, the reverse current exceeds the value of I_0, indicating that the reverse current should be limited by another transport mechanism.

Figure 4.5 shows the reverse current as a function of $(V_B\text{-}V)^{1/2}$ for samples 5 and 6 with lower-resistivity p c-Si substrates, which is replotted from the data given in Fig. 4.2(a) and (b), respectively. Figure 4.6 shows the reverse current as a function of $(V_B\text{-}V)^{1/2}$ in the larger range of -5 V$\leqq$ V $\leqq$ -0.5 V,

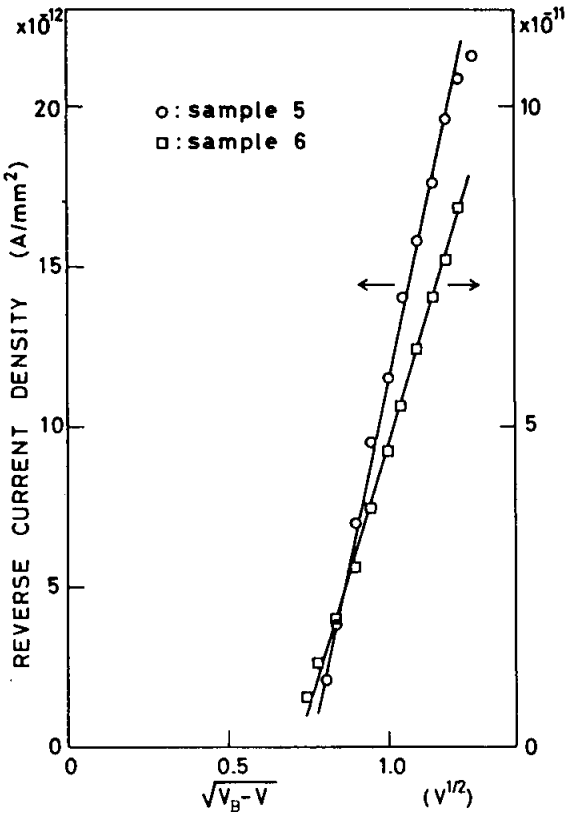

Fig.4.5. Reverse I-V characteristics of samples 5 and 6. The values of V_B are 0.60 and 0.50 V for samples 5 and 6, respectively. The resistivities for samples 5 and 6 are 0.005-0.01 and 0.1-0.15 Ω cm, respectively.

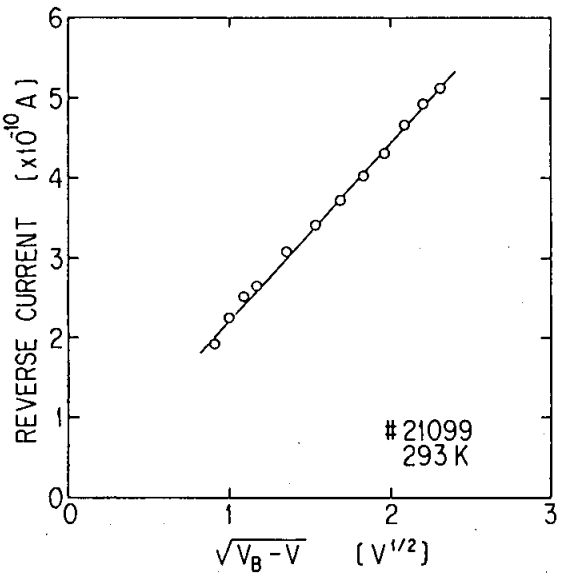

Fig.4.6. Reverse I-V characteristics of sample 21099. The value of V_B is 0.35 V and N_A is 1.0×10^{16} cm^{-3}.

which is replotted from the data given in Fig. 4.1. When a generation current is taken into account in the depletion region,[12] this current should be proportional to the width of the depletion region that varies with $(V_B-V)^{1/2}$. The data show a good linearity, indicating that their reverse currents should be limited by the generation process in the depletion region. This proportionality between reverse current and $(V_B-V)^{1/2}$ is held throughout the temperature range studied here. In sample 5, the depletion region exists only on the a-Si:H side because the p c-Si is heavily B-doped, indicating that its generation current is produced in the depletion region of a-Si:H under reverse bias conditions.

The reverse current is an increasing function of the p c-Si resistivity, as shown in Fig. 4.2. Because the width of the depletion region in c-Si increases with an increase of the p c-Si resistivity as shown in Fig. 3.10, the contribution of the generation current in p c-Si to the reverse current increases with an increase of the c-Si resistivity. Those suggest that the generation current per unit volume in the depletion region of c-Si is greater than that in the depletion region of a-Si:H. This may be because the bandgap (1.12 eV) of c-Si is narrower than that (about 1.7 eV) of a-Si:H.

4-5. Summary

The current-transport mechanism of the undoped a-Si:H/p c-Si heterojunctions has been discussed from their I-V characteristics and their temperature dependence. The main results are summarized as follows.

(1) The forward current, described as $\exp(-\Delta E_{af}/kT) \times \exp(AV)$, can be explained by a multistep-tunneling capture-emission (MTCE) model, where a hole in the valence band of p c-Si keeps flowing from one gap state to another in a-Si:H by the multistep-tunneling process until its tunneling rate becomes smaller than a rate either for hole releasing from the state to the valence band or for its recombination with an electron in the

conduction band of a-Si:H.

(2) The reverse current, which is proportional to $(V_B-V)^{1/2}$, is reasonably ascribed to a generation process in both depletion regions of a-Si:H and c-Si. The generation current per unit volume in the depletion region of c-Si is considered to be greater than that in the depletion region of a-Si:H.

References

1) R. Grigorovici, N. Croitoru, A. Devenyi, and E. Teleman, Proc. Int. Conf. Semiconductors, Paris 1964(Academic Press, New York, 1964), p. 423.
2) L. Stourac, Proc. Int. Conf. Amorphous Semiconductors, edited by R. Grigorovici and M. Ciurea, Bucharest 1982(Central Institute of Physics, Bucharest, 1982), p. 104.
3) W. E. Spear and P. G. LeComber, Solid State Commun. **17**(1975)1193.
4) V. Smid, J. J. Mares, L. Stourac, and J. Kristofik, in Tetrahedrally-Bonded Amorphous Semiconductors, edited by D. Adler and H. Fritzsche(Plenum, New York, 1985), p. 483.
5) H. Matsuura. T. Okuno. H. Okushi, and K. Tanaka, J. Appl. Phys. **55**(1984)1012.
6) M. A. Lampert and P. Mark, Current Injection in Solids (Academic Press, New York, 1970), Chapter 4.
7) P. G. LeComber and W. E. Spear, Phys. Rev. Lett. **25**(1970)509.
8) A. G. Chynoweth, W. L. Feldmann, and R. A. Logan, Phys. Rev. **121**(1961)684.
9) A. R. Riben and D. L. Feucht, Solid-State Electron. **9**(1966)1055.
10) S. M. Sze, Physics of Semiconductor Devices(Wiley-Interscience, New York, 1969), p. 169.
11) A. R. Riben and D. L. Feucht, Int. J. Electron. **20**(1966)1468.
12) S. M. Sze, Physics of Semiconductor Devices(Wiley-Interscience, New York, 1969), p. 103.

CHAPTER V MIDGAP-STATE PROFILES DETERMINED BY TRANSIENT HMC METHOD

5-1. Introduction

The optoelectronic properties of hydrogenated amorphous silicon (a-Si:H) films are critically linked with the density and distribution of gap states in a-Si:H. In order to enhance the performance of a-Si:H-based devices, such as solar cells and thin-film transistors, a low density-of-state (DOS) distribution [g(E)] in the mobility gap is essential. Measurements of the g(E) and understanding of the nature of the gap states are, therefore, very important. The problem has received considerable attention, and many techniques have been developed to determine the g(E). These include both optical and electrical methods as mentioned in Chapter I.

This chapter has tried to determine the g(E) below the Fermi level in highly resistive amorphous semiconductor, such as undoped a-Si:H films and undoped hydrogenated amorphous silicon germanium alloy ($a\text{-}Si_{1-x}Ge_x:H$) films, the importance of the latter arising from the low band-gap component in tandem-type amorphous solar cells.

Prior to this, from the study of the capacitance-voltage (C-V) characteristics of undoped (i.e., slightly n-type) a-Si:H/p-type crystalline silicon (p c-Si) heterojunctions under high frequency ($\geq$ 100 kHz), a midgap-state density (N_I) of a-Si:H and its electron affinity (χ_2) were obtained, as discussed in Chapter III. The analytical approach there has been that at a high-frequency small ac voltage the capacitance of a-Si:H becomes equal to geometric capacitance of the a-Si:H film due to its longer dielectric relaxation time, while that of c-Si is associated with the depletion width of c-Si which reflects the space charge of the depletion region in a-Si:H by a dc reverse bias. This method is called a steady-state heterojunction-monitored capacitance (HMC) method.

In this chapter, it has been demonstrated that the g(E)

below the Fermi level in highly resistive amorphous films can be determined from the experimental results involving measurements of transient capacitance as well as its temperature-dependence of those heterojunctions.

5-2. Transient Capacitance

Figure 5.1 shows the change in the capacitance after a reverse-bias voltage (-4 V) is applied to an undoped a-Si:H/p c-Si (N_A=1.0x10^{16} cm^{-3}) heterojunction which was under the zero-bias condition for a certain time. In almost of the whole a-Si:H, the gap states between E_F and E_{OB} are full of electrons under the zero-bias condition. After applying the reverse-bias voltage, the electrons trapped at the gap states between E_F and E_{OB} are going to be re-emitted to the conduction band, which results in the change of the positive space-charge density in the depletion region of undoped a-Si:H. Because a-Si:H possesses deep gap states whose emission rates are small, the capacitance gradually decreases with time (t). Since the steady-state HMC method has made it possible to get the midgap-state density, this transient HMC must include information on the g(E) of the midgap states. From the transient behavior of the capacitance, the g(E) in undoped a-Si:H can be determined as discussed in the following sections. This method is a powerful technique for determining the g(E) below the Fermi level in undoped a-Si:H because it has been difficult to obtain the g(E) in such a highly resistive semiconductor by the conventional transient capacitance methods, such as deep-level transient spectroscopy (DLTS)[1] and isothermal capacitance transient spectroscopy (ICTS)[2] using Schottky barrier diodes and homogeneous p-n diodes, as mentioned in Chapter I .

5-3. Theory of Transient HMC Method

In order to estimate the g(E) below the Fermi level, the

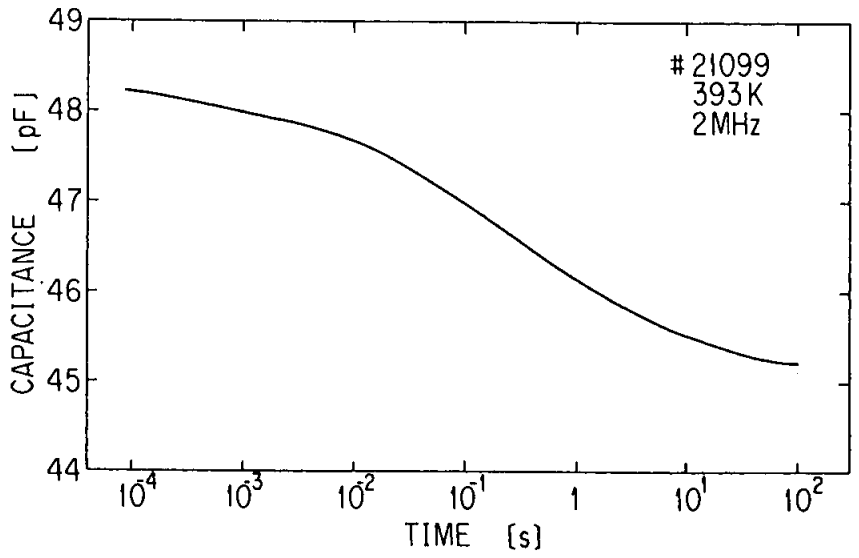

Fig.5.1. Transient capacitance of undoped a-Si:H/p c-Si (N_A=1.0x10^{16} cm^{-3}) heterojunction.

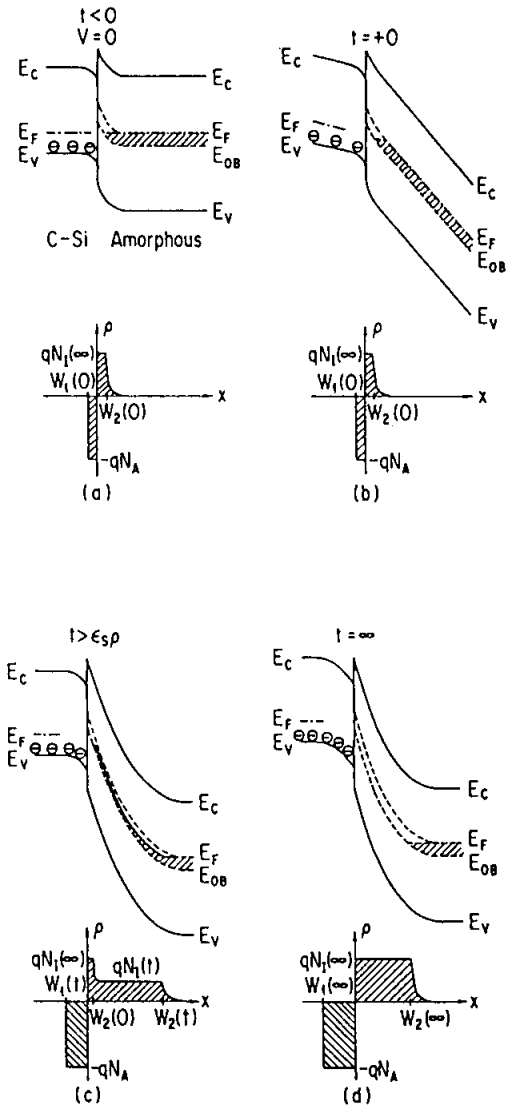

Fig.5.2. Schematic representation of energy-band diagram and space-charge density of heterojunction at four different times: (a) t<0, (b) t=+0 , (c) $t>\varepsilon_s\rho$, and (d) t=∞. In energy-band diagrams, gap states as indicated by hatched areas are occupied by electrons, so are neutral. In the depletion region, therefore, empty gap states between E_F and E_{OB} behave as positively charged states. Gap states below E_{OB} are always occupied by electrons. The symbol of ⊖ represents a negatively charged acceptor.

transient HMC is considered after a reverse-bias voltage (V_R) is applied to the sample for a certain period of time. The zero-bias condition is kept for t<0 s in order to fill electrons at gap states below the Fermi level, as shown in Fig. 5.2(a). At t=+0 s, the voltage V_R is applied across the whole regions of a-Si:H and c-Si as shown in Fig. 5.2(b). Electrons trapped at shallower states are thermally emitted into the conduction band. After the applied bias has been on the dielectric relaxation time of the amorphous film, the space charge in the vicinity of the heterojunction will redistribute itself in response to the applied potential [Fig. 5.2(c)]. Here, the dielectric relaxation time of c-Si is much shorter than that of the amorphous film.

The HMC data after the dielectric relaxation time can be analyzed using Eq. (3-11), where W_1 and N_I are a function of time (t), thus,

$$W_1^2(t) = 2\varepsilon_{s1}\varepsilon_{s2}N_I(t)(V_B - V_R)/qN_A[N_I(t)\varepsilon_{s2} + N_A\varepsilon_{s1}]. \quad (5\text{-}1)$$

Since

$$V_1(t) = qN_AW_1^2(t)/2\varepsilon_{s1} \quad , \quad (5\text{-}2)$$

Eq. (5-1) can be written as

$$V_1(t)[N_I(t)\varepsilon_{s2} + N_A\varepsilon_{s1}] = \varepsilon_{s2}N_I(t)(V_B - V_R) \quad . \quad (5\text{-}3)$$

By solving $N_I(t)$ from Eq. (5-3), we obtain

$$N_I(t) = \varepsilon_{s1}V_1(t)N_A/\varepsilon_{s2}[V_B - V_R - V_1(t)] \quad , \quad (5\text{-}4)$$

where $W_1(t)$ is the depletion width in c-Si at time t and $V_1(t)$ is the voltage at t across the depletion region of c-Si. From Eq. (3-10), on the other hand, we can also obtain experimentally

$$W_1(t) = \varepsilon_{s1}[1/C(t) - 1/C_2] \quad , \quad (5\text{-}5)$$

where C(t) is the measured capacitance (HMC) at t, as shown in

Fig. 5.1. To make the above analysis feasible, the absolute value of V_R must be high enough for $N_I(t)W_2(t)$ to become much larger than $N_I(\infty)W_2(0)$, indicating that the average value of N_I over the depletion region at t becomes close to $N_I(t)$. This condition also suggests that its interface states do not affect the measurement of HMC.

The function H(t) is defined as

$$H(t) \equiv td[\Delta N_I(t)]/dt \quad , \tag{5-6}$$

with

$$\Delta N_I(t) \equiv N_I(t) - N_I(\infty) \quad . \tag{5-7}$$

Since $N_I(\infty)$, which represents N_I at t=∞ s, is constant, Eq. (5-6) can be rewritten as

$$H(t) = tdN_I(t)/dt \quad . \tag{5-8}$$

Therefore, the HMC signal of H(t) is experimentally obtained from Eqs. (5-2), (5-4), (5-5) and (5-8).

On the other hand, the signal of H(t) is theoretically considered. The value of $\Delta N_I(t)$ is determined by the change in the electron occupation of the g(E), thus:(See Appendix)

$$\Delta N_I(t) = -\int_{E_V}^{E_C} [f(E) - F_\infty(E)]g(E)\exp\{-[e_n(E) + e_p(E)]t\}dE, \tag{5-9}$$

where E_C and E_V are the conduction-band edge and valence-band edge, respectively, f(E) is the Fermi-Dirac distribution function which coincides with the occupation function at t=0 s, $F_\infty(E)$ is the occupation function at t=∞ s, and $e_n(E)$ and $e_p(E)$ are thermal emission rates of electrons and holes, respectively. The function f(E) is expressed as

$$f(E) = 1/\{1 + \exp[(E - E_F)/kT]\} \quad , \tag{5-10}$$

and $F_\infty(E)$ is given by the thermal-emission process:(See Appendix)

$$F_\infty(E) = e_p(E)/[e_n(E) + e_p(E)] \quad . \tag{5-11}$$

The values of $e_n(E)$ and $e_p(E)$ are described as

$$e_n(E) = \nu_n \exp[(E - E_C)/kT] \tag{5-12}$$

and

$$e_p(E) = \nu_p \exp[(E_V - E)/kT] \quad . \tag{5-13}$$

Then from Eqs. (5-6) and (5-9), we obtain

$$H(t) = \int_{E_V}^{E_C} [f(E) - F_\infty(E)]g(E)[e_n(E) + e_p(E)]t \times \exp\{-[e_n(E) + e_p(E)]t\}dE \quad . \tag{5-14}$$

The determination of g(E), by which H(t) of Eq. (5-14) can be obtained to fit the measured H(t) using Eqs. (5-10)-(5-13), is described in the next section.

In the case that $e_n(E)$ is much larger than $e_p(E)$, on the other hand, the following relation between g(E) and H(t) is obtained. Equation (5-14) can be rewritten as

$$H(t) = \int_{E_V}^{E_C} [f(E) - F_\infty(E)]g(E)D(E,t)dE \quad , \tag{5-15}$$

where

$$D(E,t) = e_n(E)t \exp[-e_n(E)t] \quad . \tag{5-16}$$

The function D(E,t) is maximum at $e_n(E)t=1$. If this function is assumed to be a delta function, the following relation could be obtained approximately:

$$H(t_m) \fallingdotseq [f(E_m) - F_\infty(E_m)]g(E_m) \int_{E_V}^{E_C} D(E,t_m)dE$$

$$\fallingdotseq [f(E_m) - F_\infty(E_m)]g(E_m) \int_{0}^{\infty} D(E,t_m)dE$$

$$= [f(E_m) - F_\infty(E_m)]g(E_m)kT \quad , \qquad (5\text{-}17)$$

where E_m is the energy at which D(E,t) has a maximum value when

$$e_n(E_m)t_m = 1 \quad . \qquad (5\text{-}18)$$

Therefore, the relation between E_m and t_m is derived from Eqs. (5-12) and (5-18):

$$E_C - E_m = kT\ln(\nu_n t_m) \quad . \qquad (5\text{-}19)$$

In a more general form, this equation can be expressed as

$$E_C - E(t) = kT\ln(\nu_n t) \quad . \qquad (5\text{-}20)$$

Under the conditions that $e_n(E)$ is much higher than $e_p(E)$ [i.e., $F_\infty(E)=0$] as well as that f(E) is close to unity for the gap states between E_F and E_{OB}, the relation between H(t) and g(E) is generally obtained from Eq. (5-17) as

$$g(E) = H(t)/kT \quad . \qquad (5\text{-}21)$$

Therefore, the g(E) around the middle of the energies between E_F and E_{OB} can be easily estimated from the measured H(t) using Eqs. (5-20) and (5-21).

5-4. Transient HMC Measurements

Undoped a-Si:H films were deposited by the rf glow-discharge decomposition of pure SiH_4, and undoped a-$Si_{1-x}Ge_x$:H films were prepared by the rf glow-discharge decomposition of

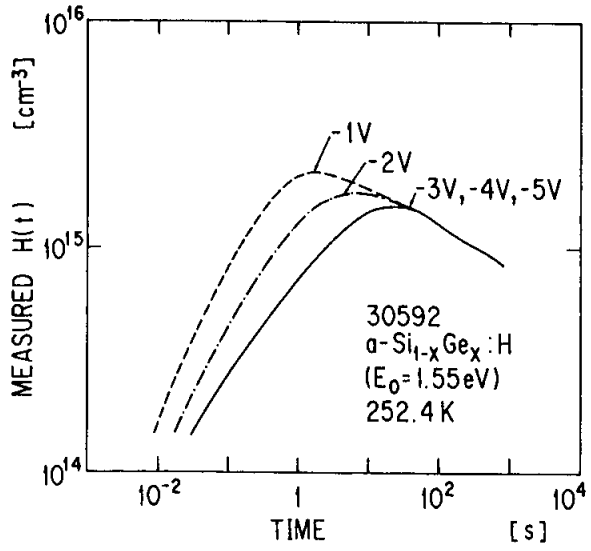

Fig.5.3. Reverse-bias dependence of measured H(t).

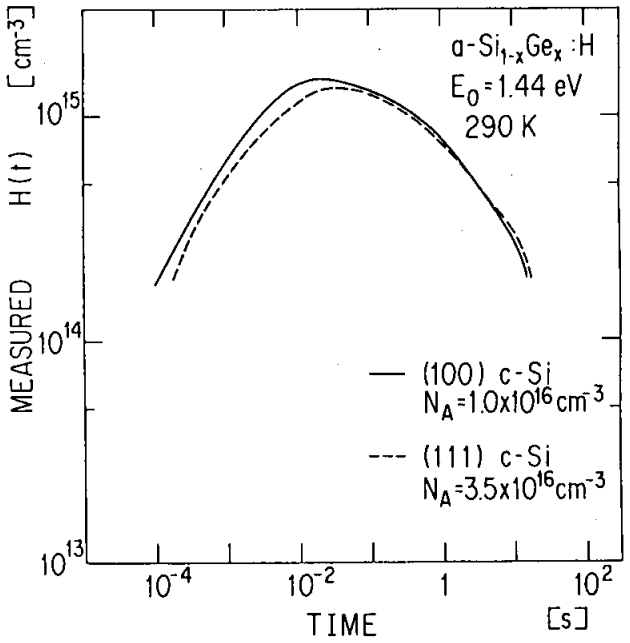

Fig.5.4. Set of two measured H(t) corresponding to (111) and (100) surfaces of p c-Si for undoped a-Si_{1-x} Ge_x:H (E_0=1.44 eV).

$GeH_4/SiH_4/H_2$ gas mixture. Good quality films could be obtained by those techniques. The optical gap (E_0) was determined by the Tauc plots of $(\alpha h\nu)^{1/2}=B_1(h\nu-E_0)$, where α is the optical absorption coefficient, $h\nu$ is the photon energy, and B_1 is a constant. The heterojunctions were fabricated by depositing the amorphous films onto p c-Si substrates (N_A=1.0x10^{16} or 3.5x10^{16} cm^{-3}) heated to 250 ℃ and then evaporating Mg on an area (0.785 mm^2) of those films at room temperature in a vacuum of 7x10^{-7} Torr. Thicknesses of amorphous films were kept between 0.8 and 1.2 μm. Mg formed a good Ohmic contact with those amorphous films. All the heterojunctions exhibited good rectifying properties.

Transient HMC measurements were carried out at 2 MHz for various temperatures. Only signals of H(t) at time longer than the dielectric relaxation time are valid as mentioned in Section 5-3. The signals of H(t) get saturated at a filling time τ_f (under the zero-bias condition) longer than 1 s. In the following measurements, H(t) has been measured at τ_f=50 s under the zero-bias condition.

Figure 5.3 shows the reverse-bias dependence of H(t) for an $a\text{-}Si_{1-x}Ge_x$:H(E_0=1.55 eV)/p c-Si heterojunction. The signals of H(t) for -5 V$\leqq V_R \leqq$-3 V are found to be independent of the reverse bias V_R, while the signals for V_R of -1 V and -2 V depend on V_R, indicating that the relation, that $N_I(t)W_2(t)$ is much larger than $N_I(\infty)W_2(0)$, is invalid for the reverse biases of -1 V and -2 V. As described in Section 5-3, these H(t) include information not only on the bulk but also on the interface. Since the g(E) in the bulk is necessary, H(t) has been measured at V_R=-4 V.

In order to check to what extent the interface states can affect the signal of H(t), the signals of H(t) with different surfaces of c-Si are compared, as shown in Fig. 5.4. The (111) surface of c-Si has the largest number of available bonds per cm^2, and the (100) surface has the smallest. According to the experimental results from Si/SiO_2 systems,[3,4] the interface-state density for the (100) surface is reported to be lower by a factor of 10 compared to that for the (111) surface. In the

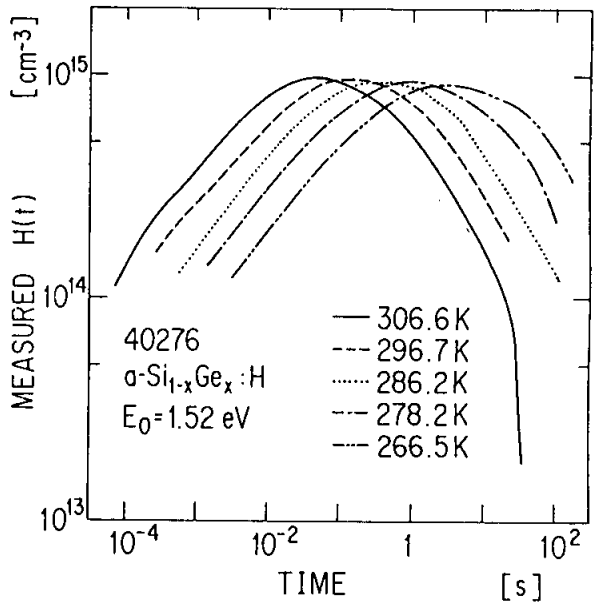

Fig.5.5. Set of five measured H(t) corresponding to five different measuring temperatures for undoped a-$Si_{1-x}Ge_x$:H/p c-Si:H (N_A=1.0x10^{16} cm^{-3}) heterojunction.

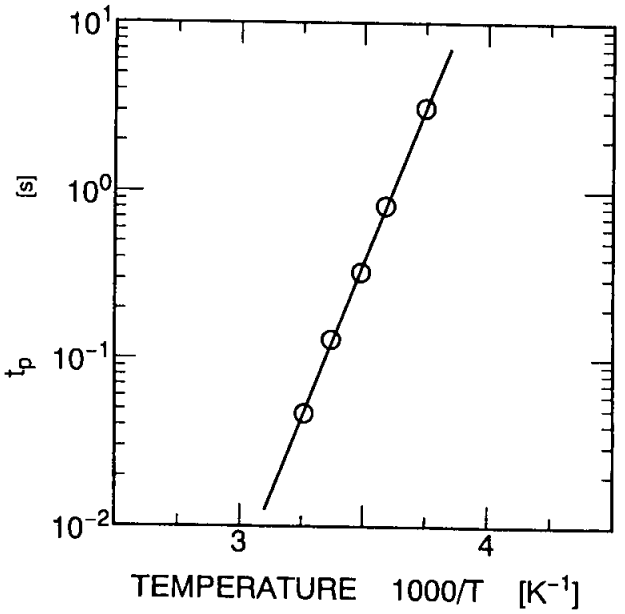

Fig.5.6. Temperature dependence of time (t_p) at which H(t) becomes maximum for undoped a-$Si_{1-x}Ge_x$:H/p c-Si (N_A=1.0x10^{16} cm^{-3}) heterojunction.

present work, however, H(t) has not shown any significant variation with surface orientation, as is clear from Fig. 5.4. Thus, H(t) is considered to be unaffected by the interface states in the present heterojunctions. From the figure, moreover, H(t) is considered to be independent of the resistivity of p c-Si, which is considered to be natural since N_I obtained from the steady-state HMC method is independent of the p c-Si resistivity as discussed in Chapter Ⅲ.

In order to calculate H(t) using Eq. (5-14), only ν_n and ν_p are necessary. Here, an undoped a-$Si_{1-x}Ge_x$:H/p c-Si heterojunction with $N_A=1.0\times10^{16}$ cm^{-3}, as shown in Fig. 5.5, is considered in order to estimate the values of ν_p and ν_n. The electron thermal-emission rate [$e_n(E)$] for a particular gap state at a depth (E_C-E) from the conduction band is given by Eq. (5-12), and the time , which is required for a trapped electron to be thermally re-emitted, is $1/e_n(E)$. Under the assumption that the gap states corresponding to the peak of H(t) is located between E_F and E_{OB}, the $g(E_p)$ is obtained as $H(t_p)/kT$ from Eq. (5-21). Therefore, the value of ν_n can be approximately estimated from the temperature dependence of the time (t_p) at the peak of H(t). Then,

$$t_p = 1/e_n(E_p)$$

$$= (1/\nu_n)\exp[(E_C - E_p)/kT] \quad , \qquad (5\text{-}22)$$

if ν_n is independent of temperature and energy. Figure 5.6 shows the temperature dependence of t_p, and from the intercept on the vertical axis in the figure using Eq. (5-22) the value of ν_n is found to be 2×10^{13} s^{-1}. Next, a maximum value of ν_p/ν_n is estimated as follows. Figure 5.7 shows the calculated H(t) for different ν_p with $g(E)=1\times10^{17}$ $cm^{-3}eV^{-1}$ and $\nu_n=2\times10^{13}$ s^{-1}. The measured H(t) at 1.4 s (T=306.6 K) is about 5×10^{14} cm^{-3} from Fig. 5.5, while in the case of $\nu_p/\nu_n=1$ using $E_{g2}=E_0=1.52$ eV the calculated one is about 10^8 cm^{-3} from Fig. 5.7, suggesting that the value of g(E) corresponding to 1.4 s should attain an unreasonable value of 5×10^{23} $cm^{-3}eV^{-1}$ simply because

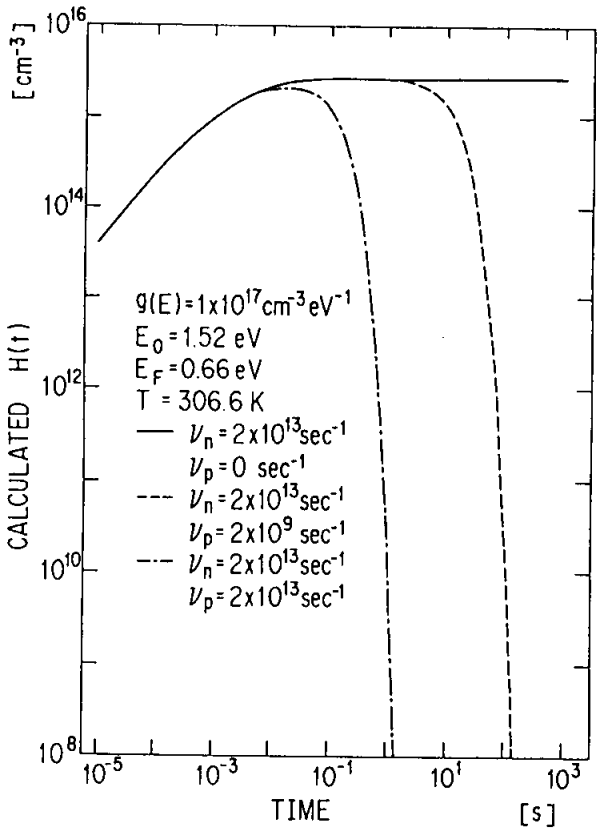

Fig.5.7. Set of three calculated H(t) corresponding to three different attempt-to-escape frequencies for holes with $g(E)=1x10^{17}$ $cm^{-3}eV^{-1}$ and $\nu_n=2x10^{13}$ s^{-1} for $E_{g2}=E_0=1.52$ eV.

$$g(E) : 1x10^{17} = 5x10^{14} : 10^{8} \quad .$$

From the above consideration, the value of ν_n and the maximum value of ν_p are taken as $2x10^{13}$ and $2x10^{9}$ s^{-1}, respectively. The calculated H(t) was approached to the measured H(t) by changing g(E), and then the g(E) shown in Fig. 5.8 made the calculated H(t) fit in with the measured H(t) very well, as shown in Fig. 5.9. Here, it is assumed that the mobility gap coincides with E_0. Figure 5.10 shows the temperature dependence of the calculated H(t) which fits in with the measured H(t) at each temperature.

The g(E) for undoped a-Si:H, estimated from the measured H(t) in Fig. 5.11, is shown in Fig. 5.12 using ν_n=$1x10^{11}$ s^{-1}, ν_p=$1x10^{8}$ s^{-1}, and E_{g2}=E_0=1.70 eV. Density-of-state distributions for other amorphous silicon-based alloys will be discussed in Chapter VI.

The distribution g(E) obtained here is found to be the bulk DOS distribution unaffected by interface states. This appears to be the first systematic effort to electrically estimate the g(E) below the Fermi level for undoped amorphous materials. Therefore, the following part of this section considers the validity of this transient HMC method in more detail. The following pertinent questions could arise, viz.,

(1) Is the assumption that ν_n and ν_p are independent of temperature and energy correct?

(2) Are the values obtained for ν_n and ν_p reasonable?

(3) To what degree does tunneling affect g(E)?

There has been a controversy in opinion regarding the answers to (1) and (2) mainly on the basis of results obtained from DLTS[1,5,6] and ICTS.[2,7] These techniques have mainly been applied to P-doped a-Si:H, but no data exist for undoped a-Si:H and undoped a-$Si_{1-x}Ge_x$:H.

If ν_n has a temperature dependence of the form

$$\nu_n = \nu_{n0} T^2 \exp(-\Delta E_\nu / kT) \quad , \qquad (5\text{-}23)$$

where ν_{n0} and ΔE_ν are constants independent of T, Eq. (5-22)

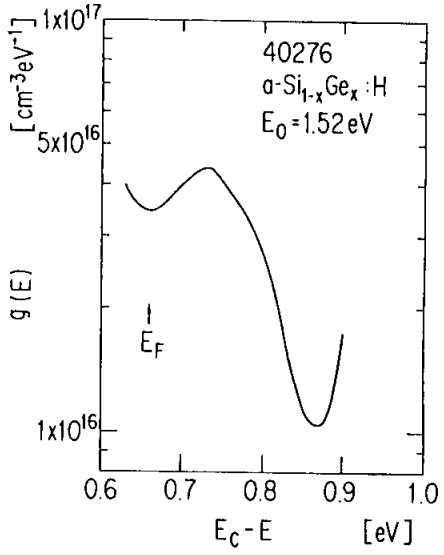

Fig.5.8. Density-of-state distribution for a-$Si_{1-x}Ge_x$:H (E_0=1.52 eV).

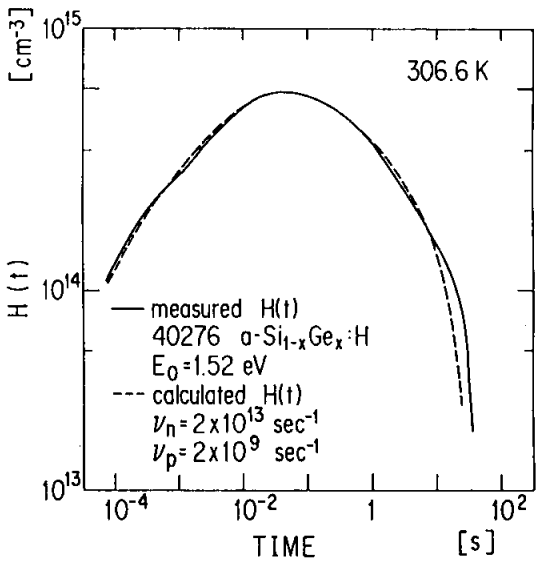

Fig.5.9. Comparison between measured H(t) for a-$Si_{1-x}Ge_x$:H (E_0=1.52 eV) and calculated H(t) with E_{g2}=1.52 eV, ν_n=2x10^{13} s^{-1} and ν_p=2x10^9 s^{-1}.

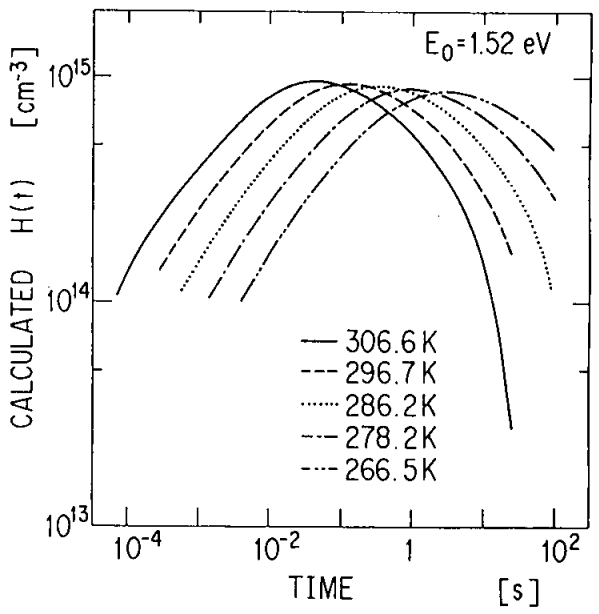

Fig.5.10. Set of five calculated H(t) corresponding to five different temperatures for E_{g2}=1.52 eV with ν_n=2x10^{13} s^{-1} and ν_p=2x10^{9} s^{-1}.

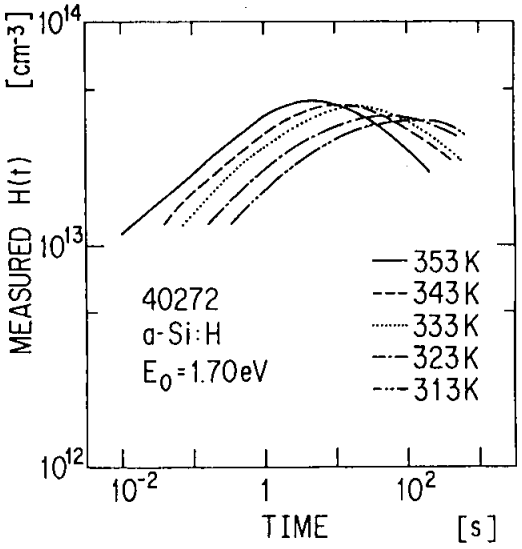

Fig.5.11. Set of five measured H(t) corresponding to five different measuring temperatures for undoped a-Si:H/p c-Si (N_A=1.0x10^{16} cm^{-3}) heterojunction.

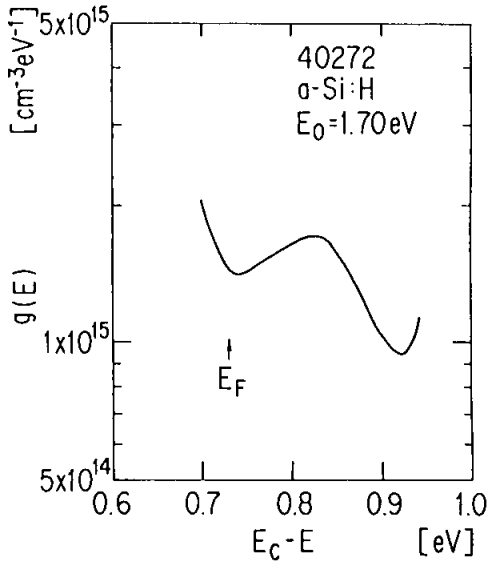

Fig.5.12. Density-of-state distribution for a-Si:H (E_0=1.70 eV) which can fit measured H(t) with calculated H(t) using E_{g2}=1.70 eV, ν_n=1x10^{11} s^{-1}, and ν_p=1x10^8 s^{-1}.

changes into

$$t_p = (1/\nu_{n0}T^2)\exp[(E_C - E_p + \Delta E_\nu)/kT] , \qquad (5\text{-}24)$$

indicating that the energies shown in Figs. 5.8 and 5.12 are overestimated because of the assumption that $\Delta E_\nu = 0$. The situation is the same as that reported by Lang and Cohen.[1] Therefore, it is important to investigate the temperature dependence of ν_n. Furthermore, Lang and Cohen[1] assumed that ν_n was independent of energy locations of gap states which were ascribed to the same origin, while Okushi[2] reported that ν_n has an energy dependence. In the above discussion, the energy-independence of ν_n is adopted. We has tried to investigate the temperature- and energy-dependencies of ν_n by means of the trap filling method like ICTS which investigates the dependence of H(t) on the filling time (τ_f),[2] but difficulty has been encountered owing to the long dielectric relaxation time of amorphous films. However, the energy locations of the peak of DOS for undoped materials are found to be close to those reported by Tsutsumi et al.,[8] and Kocka, Vanecek and Schaver.[9]

Since the values of ν_n are reported to be between 10^9 and 10^{13} s^{-1} for Si dangling bonds,[1-2] the values obtained here are considered to be reasonable. On the other hand, there is no experimental data on the values of ν_p. The value of ν_p estimated from the fitting procedure depends strongly on the mobility gap (E_{g2}) because $e_p(E)$ is a function of $(E_C-E)-E_{g2}$. The g(E) estimated with $\nu_n=\nu_p=1\times10^{11}$ s^{-1} and E_{g2}=1.91 eV is the same as the g(E) shown in Fig. 5.12 with $\nu_n=1\times10^{11}$ s^{-1}, $\nu_p=1\times10^{8}$ s^{-1}, and E_{g2}=1.70 eV because E_{OB} is the same in both cases. The value of the mobility gap poses an open question. Vanecek et al.[10] concluded that the mobility gap of a-Si:H was quite close to E_0 ($\sim$1.7 eV). On the other hand, Lang and co-workers[6] used the values between 1.9 and 2.1 eV for the mobility gap of a-Si:H based on the assumption of $\nu_n=\nu_p=10^{13}$ s^{-1}. Jackson et al.[11] reported it as 1.93 ± 0.2 eV. However, the estimated g(E) does not change at all when the best fit is obtained using the maximum of ν_p/ν_n which is determined by the

value of E_{g2}.

Regarding the third question, it seems like tunneling does not affect the g(E) in the range of the measuring temperatures from the consideration similar to the ICTS analysis of P-doped a-$Si_{1-x}Ge_x$:H.[12] The value of t_p , when the tunneling process affects H(t), is not on the linear relation between t_p and 1/T expected from the range of higher temperature. In the present study, the linear relations between them are obtained in the whole temperature range studied here for all the samples. This transient HMC method will be applied not only to determining the g(E) in other undoped amorphous silicon alloys but also to investigating the changes of g(E) by light-soaking, rapid cooling, and thermal annealing in the following chapter.

5-5. Summary

A novel technique for determining the magnitude as well as energy location of midgap states in highly resistive amorphous materials has been developed from the study of the transient capacitance in the highly resistive amorphous/lowly resistive crystalline semiconductor heterojunctions. This transient HMC method has been tested and applied on undoped a-Si:H and undoped a-$Si_{1-x}Ge_x$:H. The g(E) obtained by the transient HMC method is found to be representative of a homogeneous bulk property of the amorphous material, unaffected by their interface states.

References

1) J. D. Cohen and D. V. Lang, Phys. Rev. **B25**(1982)5321.
2) H. Okushi, Phil. Mag. **B52**(1985)33.
3) P. V. Gray and D. M. Brown, Appl. Phys. Lett. **8**(1966)31.
4) M. H. White and J. R. Cricchi, IEEE Trans. **ED-19**(1972)1280.
5) J. D. Cohen, D. V. Lang, and J. P. Harbison, Phys. Rev. Lett. **45**(1980)197.
6) D. V. Lang, J. D. Cohen, and J. P. Harbison, Phys. Rev. **B25**(1982)5285.
7) H. Okushi, Y. Tokumaru, S. Yamasaki, H. Oheda, and K. Tanaka, Jpn. J. Appl. Phys. **20**(1981)L549.
8) Y. Tsutsumi, S. Sakata, K. Abe, Y. Nitta, H. Okamoto, and Y. Hamakawa, J. Non-Cryst. Solids **97&98**(1987)1063.
9) J. Kocka, M. Vanecek, and F. Schaver, J. Non-Cryst. Solids **97&98**(1987)715.
10) M. Vanecek, J. Stuchlik, J. Kocka, and A. Triska, J. Non-Cryst. Solids **77&78**(1985)299.
11) W. B. Jackson, S. M. Kelso, C. C. Tsai, J. W. Allen, and S. J. Oh, Phys. Rev. **B31**(1985)5187.
12) H. Matsuura, H. Okushi, and K. Tanaka, J. Non-Cryst. Solids **97&98**(1987)963.

CHAPTER VI CHANGES OF MIDGAP STATES

6-1. Introduction

Many techniques, summarized by LeComber and Spear,[1] have been developed to determine a density-of-states distribution [g(E)] in hydrogenated amorphous silicon (a-Si:H), silicon-germanium alloy (a-$Si_{1-x}Ge_x$:H) and silicon-carbon alloy (a-$Si_{1-x}C_x$:H) films, because the electric properties of these films are critically linked with their g(E). All these techniques have some limitations in their application. It is especially difficult to determine the g(E) in highly resistive (e.g., undoped) amorphous semiconductors, but the properties of undoped films usually limit the performance of amorphous devices, such as solar cells and thin-film transistors. Chapters III and V have developed techniques for determining a midgap-state density (N_I) and the g(E) below the Fermi level (E_F) in highly resistive amorphous semiconductors from the high-frequency capacitance of highly resistive amorphous/lowly resistive crystalline semiconductor heterojunction structures, referred to as the heterojunction-monitored capacitance (HMC) method.

Once the g(E) in undoped a-Si:H has been determined, the change of g(E) due to incorporation of Ge or C into undoped a-Si:H is interesting. Furthermore, the changes of g(E) in undoped a-Si:H by light soaking, rapid cooling and thermal annealing are anxious to be surveyed in order to understand the nature of metastable midgap states which has been interesting to researchers both studying the physics of amorphous semiconductors and designing a-Si:H-based devices.

The existence of the light-induced reversible changes in a-Si:H has attracted considerable attention, mostly because of the degradation of the efficiency of a-Si:H solar cells. This effect, which is known as the Staebler-Wronski (S-W) effect,[2] arises from the creation of metastable gap states by light soaking, and it is recovered by the thermal annealing at 150-200 ℃. Stutzmann et al.[3] have proposed the following mechanism;

the rate of increase in dangling bond density (N_s) determined by electron spin resonance (ESR) measurements is given by the relationship that dN_s/dt is proportional to $\Delta n \Delta p$, where Δn and Δp are the free electron and hole concentrations, respectively under light exposure. Each concentration is proportional to G/N_s, where G is the carrier generation rate by light exposure. They have concluded that $N_s(t)$ is proportional to $G^{2/3}t^{1/3}$.

Once N_s has been increased by light exposure, the kinetics of its thermal annealing can be explored. Stutzmann et al.[4] have proposed a monomolecular annealing process with a distribution of activation energies (E_a), while Lee et al.[5] have proposed a bimolecular annealing process with one E_a. Smith and Wagner[6] have expanded the Stutzmann's models for creation and annealing of midgap states into a more general model which can explain the reason why N_s cannot be reduced to the value below 10^{15} cm^{-3} for undoped a-Si:H.

Han and Fritzsche,[7] and Qiu et al.[8] have reported that two kinds of light-induced states are produced by light soaking; one is detected by photoconductivity measurements, and the other is observed by constant photocurrent measurements (CPM). Kumeda et al.[9] have pointed out from the results of ESR that singly-occupied dangling bonds (D^0) created by short-time (3-h) light soaking are easily annealed out, while D^0 created by long-time (53-h) light soaking are resistant to the annealing.

Section 6-2 has applied the HMC method to undoped a-Si:H, undoped a-$Si_{1-x}Ge_x$:H and undoped a-$Si_{1-x}C_x$:H, and discusses the behavior of these midgap states when Ge atoms (or C atoms) are incorporated into undoped a-Si:H. In Section 6-3, the thermal annealing kinetics of midgap states in undoped a-Si:H are investigated, and E_a at each energy position of midgap states (i.e., D^0) is directly determined from the transient HMC method. Since the transient HMC method can obtain the g(E) in a short time (e.g., several seconds), it enables us to carry out the real-time measurements of g(E) in the process of a 150-℃ annealing. In Section 6-4, changes of g(E) in undoped a-Si:H are investigated before and after light soaking, rapid cooling, and thermal annealing by means of the HMC method.

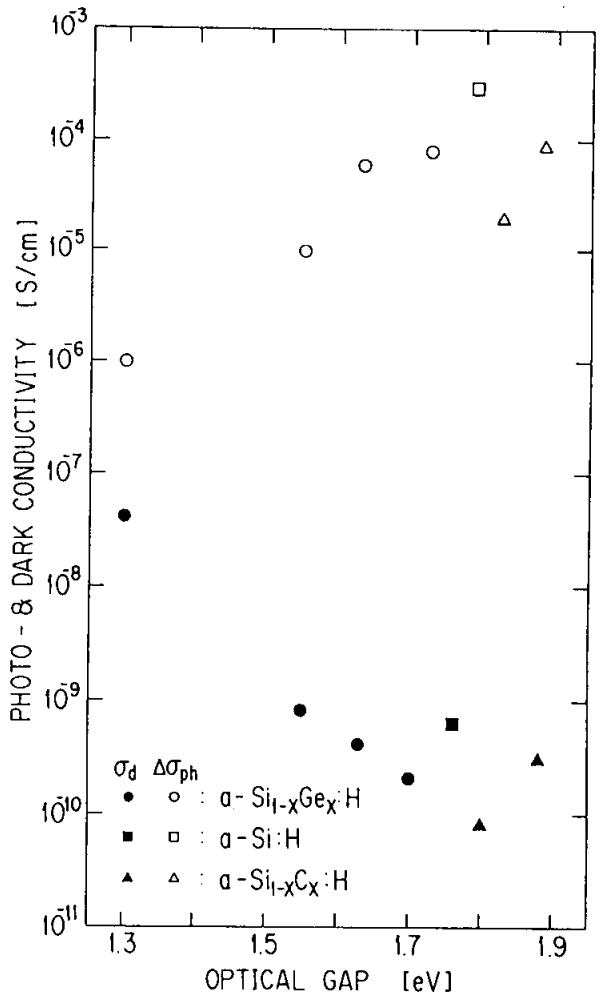

Fig.6.1. Dark conductivity(●, a-Si_{1-x} Ge_x:H; ■, a-Si:H; and ▲, a-Si_{1-x} C_x:H) and photoconductivity (○, a-Si_{1-x} Ge_x:H; □, a-Si:H; and △, a-Si_{1-x} C_x:H) under AM1 (100 mW/cm^2) of undoped films with various optical gaps.

6-2. Midgap-state Profiles in Undoped Hydrogenated Amorphous Silicon-based Alloys

Undoped a-Si:H films and undoped a-$Si_{1-x}C_x$:H films were deposited using a diode-type rf glow-discharge reactor from pure SiH_4 gas and $H_2/SiH_4/CH_4$ gas mixture, respectively. Undoped a-$Si_{1-x}Ge_x$:H films with an optical gap (E_0) of 1.30 and 1.44 eV were deposited using a diode-type rf glow-discharge reactor from $H_2/GeH_4/SiH_4$ gas mixture, and undoped a-$Si_{1-x}Ge_x$:H (1.55 eV$\leqq E_0 \leqq$ 1.70 eV) films were prepared using a triode-type rf glow-discharge reactor from GeH_4/SiH_4 gas mixture. The thicknesses were between 0.5 and 1.2 μm.

The heterojunctions were fabricated by depositing the amorphous films onto p-type crystalline silicon (p c-Si) substrates with an acceptor density (N_A) of 1.0×10^{16} cm^{-3}, heated to 250 ℃, and then evaporating Mg on an area (0.785 mm^2) of those films at room temperature. Mg formed a good Ohmic contact with those amorphous films. All the heterojunctions exhibited good rectifying properties. The samples for measurements of optical gap, conductivity, photothermal defection spectroscopy (PDS) and ESR were fabricated by depositing the amorphous films onto fused silica substrates heated to 250 ℃.

The capacitance was measured using a Sanwa MI-415 capacitance meter (2 MHz). The transient HMC was measured as a function of temperature in the range between 213 and 413 K.

Figure 6.1 shows the dark conductivity and photoconductivity of films used in this study, indicating that the quality of the films was good. The Ge contents (x) determined from electron probe microanalysis (EPMA) in a-$Si_{1-x}Ge_x$:H were 0.80, 0.48, 0.44, and 0.27 for E_0=1.30, 1.55, 1.63, and 1.70 eV, respectively. The C contents (x) determined from Auger electron spectroscopy (AES) in a-$Si_{1-x}C_x$:H were 0.11 and 0.15 for E_0=1.80 and 1.88 eV, respectively. The Urbach energies obtained from PDS were 73, 58, 52, 62, 50, 84, and 87 meV for E_0=1.30, 1.55, 1.63, 1.70, 1.76, 1.80, and 1.88 eV, respectively. The Urbach energy is considered to be related with the slope in the valence-band tail.

Figure 6.2 shows the relation between the optical gap (E_0)

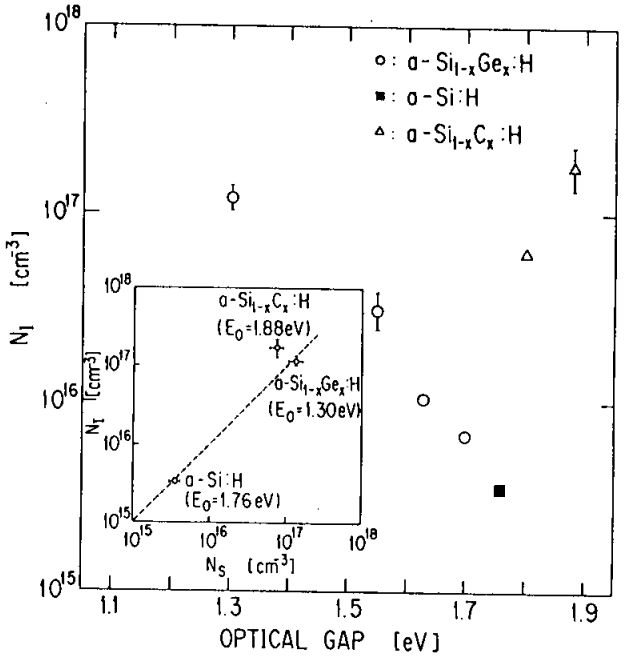

Fig.6.2. Densities (N_I) of midgap states of undoped films with various optical gaps. The relation between N_I and bulk spin density (N_S) obtained from ESR is inserted.

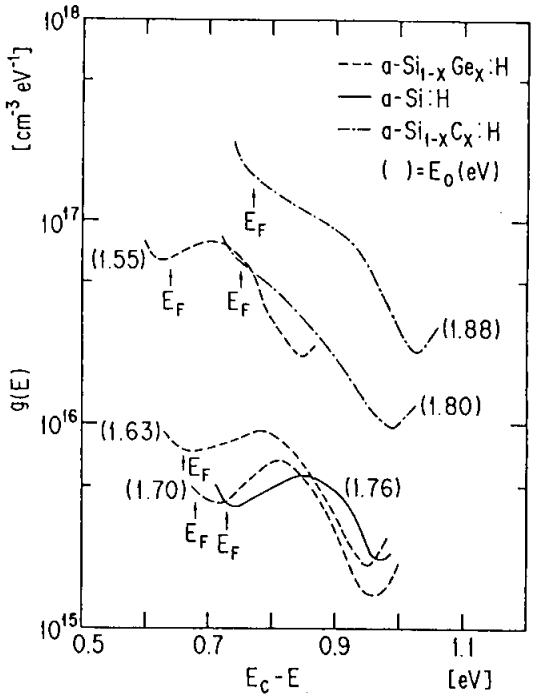

Fig.6.3. Density-of-state distributions in undoped films with various optical gaps.

and the density of midgap states (N_I) obtained from the steady-state HMC method, and the relationship between N_I and the bulk spin densities (N_S) from ESR which represent the density of D^0 is inserted. The density of midgap states increases slowly with the Ge content, while it increases rapidly with the C content. This optical-gap dependence of the midgap-state density coincides with the result obtained from PDS, where the midgap-state density obtained from PDS is reported to be proportional to N_S. As is clear from the inserted figure, furthermore, the value of N_I is close to the corresponding bulk ESR spin density where surface state contributions were estimated by results from a series of films over a range of thicknesses, indicating N_I represents the density of D^0 in the bulk.

The g values obtained from ESR were 2.018, 2.006, and 2.005 for a-$Si_{1-x}Ge_x$:H (E_0=1.30 eV), a-Si:H (E_0=1.76 eV), and a-$Si_{1-x}C_x$:H (E_0=1.88 eV), respectively. Shimizu et al.[10] have reported that the g values for dangling bonds of Ge, Si, and C are 2.019, 2.005, and 2.003, respectively. Morimoto et al.[11] have reported that the ratio of Ge dangling bonds to Ge atoms is higher by a factor of four to fifteen than the ratio of Si dangling bonds to Si atoms in a-$Si_{1-x}Ge_x$:H films. According to their experimental results, N_I in a-$Si_{1-x}Ge_x$:H with $E_0 \leqq 1.63$ eV represents the D^0 density of Ge. In a-$Si_{1-x}C_x$:H ($E_0 \leqq 1.88$ eV) and a-Si:H, N_I represents the D^0 density of Si. The value of N_I for the C content of 0.15 was 1.7×10^{17} cm^{-3} although N_I for the Ge content of 0.27 was 6.5×10^{15} cm^{-3}, indicating that the ratio of Si dangling bonds to Si atoms in a-$Si_{1-x}C_x$:H should be much higher than that in a-$Si_{1-x}Ge_x$:H. This indication seems reasonable in the light of bonding energies (Ge-H<Si-H<C-H), in other words, preferential attachment of H to Ge, Si, and C. Thus, incorporating a small amount of C into a-Si:H causes C atoms to take H atoms from Si-H bonds near the surface of the film during the deposition, resulting in formation of excess Si dangling bonds.

Figure 6.3 shows six g(E) corresponding to E_0, which are estimated from the transient HMC method. Here, the attempt-to-escape frequencies (ν_n) for electrons which were experimentally

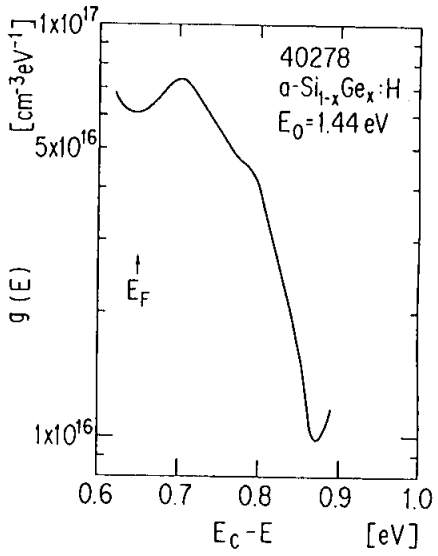

Fig.6.4. Density-of-state distribution for a-$Si_{1-x}Ge_x$:H (E_0=1.44 eV).

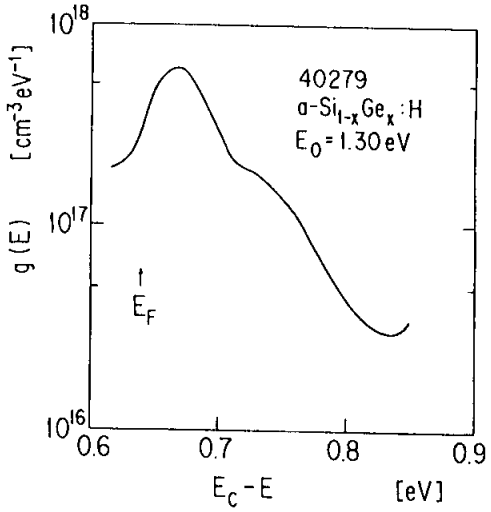

Fig.6.5. Density-of-state distribution for a-$Si_{1-x}Ge_x$:H (E_0=1.30 eV).

obtained were $4x10^{12}$, $1x10^{12}$, $8x10^{11}$, $4x10^{11}$, $4x10^{11}$, and $8x10^{11}$ s^{-1} for E_0=1.55, 1.63, 1.70, 1.76, 1.80, and 1.88 eV, respectively, and they were used to estimate the g(E), as described in Chapter V. As the Ge content increases in the film, the energy location of the peak of g(E) is shifted slowly toward the conduction band. In the figure, however, the two peaks of dangling bonds of Si and Ge cannot be seen. Figure 6.4 shows the g(E) for a-$Si_{1-x}Ge_x$:H (E_0=1.44 eV) with ν_n=$1x10^{14}$ s^{-1}, which is obtained from Fig. 5.4. Figure 6.5 depicts the g(E) for a-$Si_{1-x}Ge_x$:H (E_0=1.30 eV) with ν_n=$3x10^{14}$ s^{-1}. Both the films were deposited using an inductively-coupled rf glow-discharge reactor from $H_2/GeH_4/SiH_4$ gas mixture on p c-Si substrates heated to 200 ℃. As is clear from the study of ESR, both the main midgap states are D^0 of Ge. In the figures, therefore, both the main peaks of their g(E) should arise from D^0 of Ge, and the shoulders, which appear in the right-hand side, must result from D^0 of Si.

In the case of a-$Si_{1-x}C_x$:H ($E_0 \leq$ 1.88 eV), as is clear from ESR, the main midgap states originate from D^0 of Si, indicating that the g(E) shown in Fig. 6.3 should represent the distribution of singly-occupied Si dangling bonds. From the fact that the peak of g(E) does not appear clearly in a-$Si_{1-x}C_x$:H, however, the singly-occupied Si dangling bonds are considered to be distributed in energy wider than them in a-Si:H. Since the ratio of Si dangling bonds to Si atoms in a-$Si_{1-x}C_x$:H becomes higher than that in a-Si:H, the limitation on formation of Si dangling bonds in a-$Si_{1-x}C_x$:H should get looser than that in a-Si:H, and the energy location of the Si dangling bonds in a-$Si_{1-x}C_x$:H are allowed to broaden, coinciding with the broaden of their g(E) shown in Fig. 6.3.

As indicated in Fig. 6.3, the energy location of D^0 in a-Si:H is around 0.85 eV below the conduction band edge, which belongs to group B classified by LeComber and Spear,[1)] whereas group A has insisted that the energy location of D^0 of Si is around 1.1 eV. These results for the peak energy location of D^0 in a-$Si_{1-x}Ge_x$:H coincides with the results obtained by Tsutsumi et al.[12)] who could not, however, determine the g(E) of D^0.

CHAPTER VI CHANGES OF MIDGAP STATES

Since there are only a few data concerned with the peak energy location of D^0 in a-$Si_{1-x}Ge_x$:H and there is no data concerned with that in a-$Si_{1-x}C_x$:H, a lot of researches determining their energy location should be performed by means of different techniques.

6-3. Thermal Recovery Process of Midgap-state Profile of Light-soaked Undoped a-Si:H

Undoped a-Si:H films (about 1.2 μm thickness) were deposited by the rf glow-discharge decomposition of pure SiH_4. In order to measure dark conductivity (σ_2), photoconductivity ($\Delta\sigma_{ph}$), and the activation energy ($\delta_2 = E_C - E_F$) of dark conductivity in a-Si:H films, samples with coplanar electrodes were fabricated by depositing a-Si:H onto Corning 7059 glass substrates heated to 250 ℃ for sample 21099 and heated to 310 ℃ for sample AK362, and subsequently by evaporating Al at room temperature. Thus-determined properties are shown in Table 6-1. Oxygen, carbon, and nitrogen concentrations estimated using secondary-ion mass spectrometry (SIMS) were $7x10^{19}$, $1x10^{19}$, and $3x10^{18}$ cm^{-3} in sample 21099, respectively, and they were $5x10^{19}$, $2x10^{19}$, and $8x10^{17}$ cm^{-3} in sample AK362, respectively.

The heterojunctions were fabricated by depositing the films onto p c-Si substrates heated to 250 ℃ for sample 21099 and heated to 310 ℃ for sample AK362. The acceptor density (N_A) of p c-Si was $1.0x10^{16}$ cm^{-3}. Since Mg has been known to form a good Ohmic contact with undoped a-Si:H, Mg was then evaporated on an area (0.785 mm^2) of as-deposited a-Si:H films at room temperature. For other heterojunctions, Mg was evaporated after a-Si:H films were exposed to the AM1 light with 100 mW/cm^2 at room temperature. As soon as the sample 21099 heated to 150 ℃ in a vacuum, the transient HMC was measured using the Sanwa MI-415 capacitance meter (2 MHz). It was also measured 30-min later, 1-h later, and 2-h later. However, the transient HMC of sample AK362 could not be measured at 150 ℃ because of low resistivity of its a-Si:H film. Therefore, after the sample was

TABLE 6-1. Film properties of samples 21099 and AK362.

Sample	As-deposited	Light exposure	Anneal[c]	Anneal[d]
21099[a]				
σ_2 ($\times 10^{-8}$ S/cm)	0.1	0.01	0.09	0.2
$\Delta\sigma_{ph}$ ($\times 10^{-4}$ S/cm)	2	0.2	1	2
E_C-E_F (eV)	0.71	0.78	0.76	0.69
AK362[b]				
σ_2 ($\times 10^{-8}$ S/cm)	1	0.02	0.6	2
$\Delta\sigma_{ph}$ ($\times 10^{-4}$ S/cm)	3	0.2	2	3
E_C-E_F (eV)	0.63	0.70	0.66	0.62

[a] AM1, 100 mW/cm^2 for 3.3 h.
[b] AM1, 100 mW/cm^2 for 4 h.
[c] 150 ℃ for 3 h.
[d] 200 ℃ for 1.5 h.

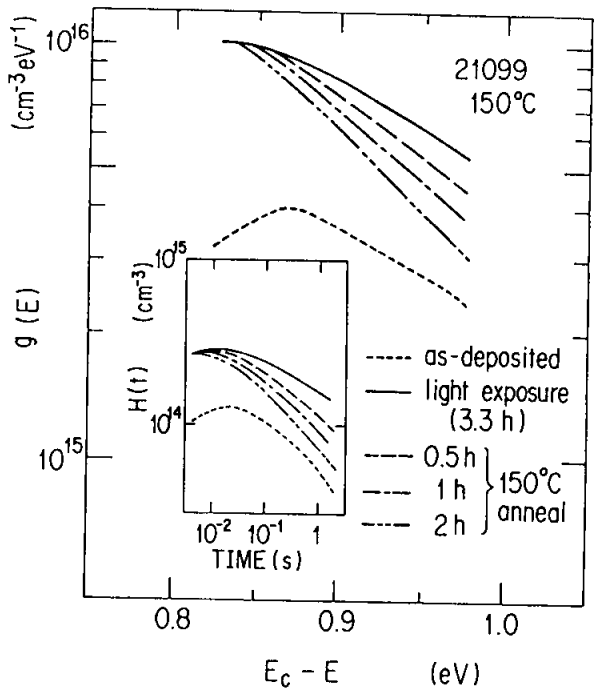

Fig.6.6. Changes of g(E) at measuring temperature of 150 °C. The signal H(t) of transient HMC, from which the g(E) was calculated, is inserted.

annealed at 150 ℃ for 3 h, the sample was cooled down, and then the transient HMC was measured at 80, 100, and 120 ℃. After this, the sample was annealed at 200 ℃ for 1.5 h, and then the transient HMC was measured at 80, 100, 120 ℃. The signal H(t) of transient HMC for as-deposited films did not change before and after the heterojunctions were annealed even at 200 ℃ for 1.5 h in a vacuum. Figure 6.6 shows the time-resolved g(E) and the corresponding signals H(t) of the transient HMC in the inset. These g(E) were calculated from these H(t) using the attempt-to-escape frequency for electrons (ν_n) of 10^{12} s^{-1}. The signal of H(t) for the as-deposited film did not change at all during the thermal annealing process at 150 ℃, indicating that contact properties were not affected by this thermal treatment. Therefore, changes of H(t) in the light-soaked film should be ascribed to the changes of the bulk g(E) in a-Si:H.

Two sorts of models have been proposed for explaining the thermal annealing kinetics;

(1) monomolecular kinetics,[4)]

(2) bimolecular kinetics.[5)]

Lee et al.[5)] have proposed a bimolecular annealing process with constant E_a;

$$d[\Delta N_s(t)]/dt = -\gamma_a \exp(-E_a/kT)\Delta N_s(t)^2 \quad , \qquad (6\text{-}1)$$

while Stutzmann et al.[4)] have proposed a monomolecular annealing process with a distribution of E_a;

$$d[\Delta N_s(E_a,t)]/dt = -\nu_a \exp(-E_a/kT)\Delta N_s(E_a,t) \quad . \qquad (6\text{-}2)$$

Though they discussed the change (ΔN_s) of the total density estimated from ESR, the transient HMC method enables us to investigate the annealing behavior of midgap states at each energy position (E_C-E). Let us consider the bimolecular annealing process at each energy position;

$$d[\Delta g(E,t)]/dt = -\gamma_a \exp(-E_a/kT)\Delta g(E,t)^2 \qquad (6\text{-}3)$$

and

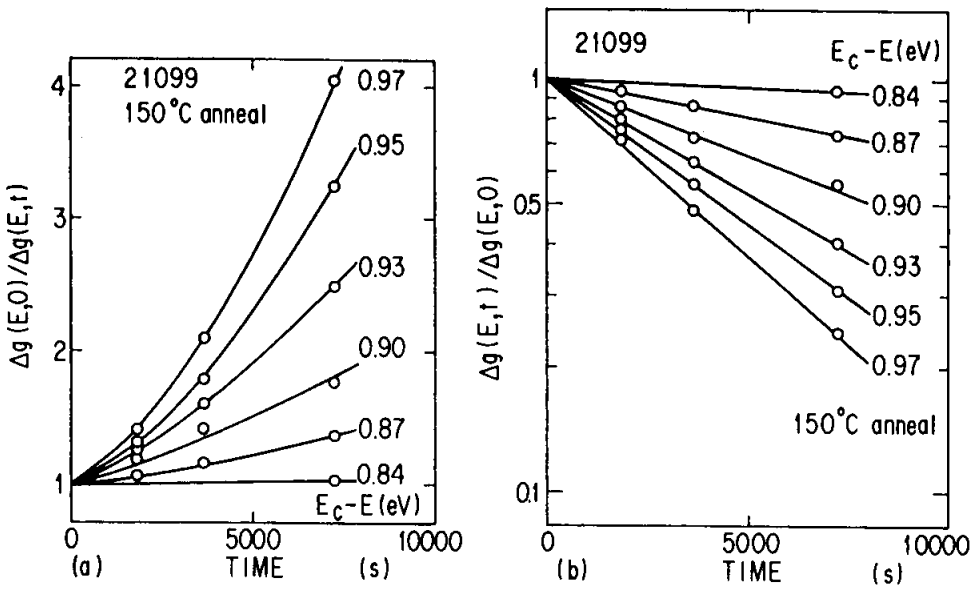

Fig.6.7. Annealing behavior of light-induced midgap states plotted assuming (a) bimolecular kinetics and (b) monomolecular kinetics.

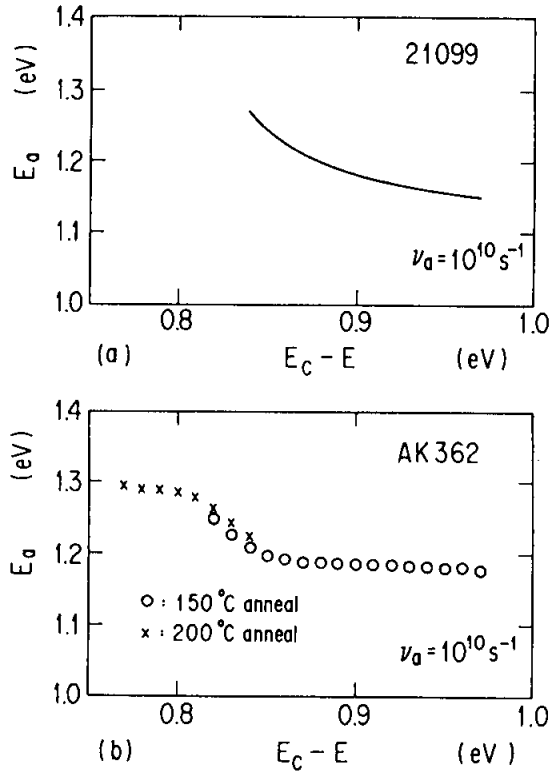

Fig.6.8. Activation energy for thermal annealing; (a)obtained from slopes in Fig.6.7(b), and (b)estimated from films annealed at 150 and 200 °C.

$$\Delta g(E,t) = g(E,t) - g_0(E) \quad , \qquad (6\text{-}4)$$

where $g(E,0)$ and $g_0(E)$ are the midgap-state profiles for the light-soaked film and the as-deposited film, respectively, t is the annealing time, and γ_a is the pre-exponential factor of the bimolecular decay rate. The integral of Eq. (6-3) implies that

$$\Delta g(E,0)/\Delta g(E,t) = 1 + \gamma_a \exp(-E_a/kT)\,\Delta g(E,0)t. \qquad (6\text{-}5)$$

Although this equation predicts a linear relation between $\Delta g(E,0)/\Delta g(E,t)$ and t, the experimental data did not produce the straight lines, as shown in Fig. 6.7(a).

The monomolecular annealing process is given by

$$d[\Delta g(E,t)]/dt = -\nu_a \exp(-E_a/kT)\,\Delta g(E,t) \quad , \qquad (6\text{-}6)$$

and the integral of this equation implies that

$$\ln[\Delta g(E,t)/\Delta g(E,0)] = -\nu_a \exp(-E_a/kT)t \quad , \qquad (6\text{-}7)$$

where ν_a is the pre-exponential factor of the monomolecular decay rate. As is shown in Fig. 6.7(b), the data produce a straight line for each value of $(E_C\text{-}E)$, indicating that the experimental results can be predicted by Eq. (6-7). Values of E_a obtained from the slope of the curves of Fig. 6.7(b) are plotted as a function of $(E_C\text{-}E)$ in Fig. 6.8(a). Here, the value of ν_a is tentatively assumed to be 10^{10} s^{-1}, which Stutzmann et al.[4] reported. The value of E_a decreases monotonously with an increase in $(E_C\text{-}E)$.

From the above results, at least phenomenologically, the monomolecular annealing kinetics with a distribution of E_a are more suitable for explaining these experimental data.

The behavior of E_a for states closer to the conduction band has been investigated. Although the real-time measurement of $g(E)$ in sample AK362 could not be carried out at 150 ℃ due to its low resistivity, E_a could roughly be estimated using Eq. (6-7) from low-temperature (80-120 ℃) measurements in the films

annealed at 150 and 200 ℃. The g(E) after light exposure increased by a factor of about 1.7 compared with the g(E) for the as-deposited film, but the energy position of the peak of midgap states did not change by light exposure. After annealing at 150 ℃ for 3 h, the g(E) for (E_C-E) in the range higher than 0.8 eV decreased. In the film annealed at 200 ℃ for 1.5 h, the g(E) for (E_C-E) in the range higher than 0.85 eV approached to the g(E) for the as-deposited film, while for (E_C-E) in the range lower than 0.85 eV it was still larger than the g(E) for the as-deposited film. The value of E_a which was roughly estimated from this experiment is shown in Fig. 6.8(b), and E_a seems to get saturated in lower (E_C-E).

This is the first report which elucidates the relation between E_a and (E_C-E). Although Stutzmann et al.[4] and Smith et al.[6] predicted that midgap states should have a distribution of E_a, they did not discuss the relation between E_a and (E_C-E). The values of E_a are similar to those reported by Qiu et al.,[8] while they are rather larger than those reported by Stutzmann et al..[4] Shepard et al.[13] have predicted from photoconductivity measurements that the g(E) above the Fermi level (maybe doubly-occupied dangling bonds, D^-) closest to the midgap is annealing first, with which the present results coincide if the correlation energies between D^0 and D^- are kept constant.

6-4. Optically and Thermally Induced Reversible Changes of Midgap States in Undoped a-Si:H

Undoped a-Si:H/p c-Si heterojunctions were fabricated as follows. Undoped a-Si:H films (1.2-1.5 μm thickness) were deposited by the rf glow-discharge decomposition of pure SiH_4 gas onto p c-Si substrates heated to T_s=200-300 ℃. After turning off the plasma, the substrate temperature was kept as it was for 10 min. Then the specimen was cooling down slowly. The acceptor density (N_A) in p c-Si was 1.0×10^{16} cm^{-3}. Since Mg is known to form a good Ohmic contact with undoped a-Si:H, Mg was evaporated on an area (0.785 mm^2) of as-deposited films at room temperature

(as-deposited films). For other heterojunctions, Mg was evaporated at room temperature after the a-Si:H films were exposed to AM1 light with 100 mW/cm^2 at room temperature (light-soaked films), or after those films, which had been kept at a given high temperature (T_{RC}) in H_2 atmosphere for 10 min, were immediately dropped into liquid nitrogen (rapidly-cooled films).

The midgap-states density (N_I) of undoped a-Si:H was estimated from the high-frequency (1-MHz) capacitance-voltage (C-V) characteristics at room temperature using the steady-state HMC method, as mentioned in Chapter III. The HMC signals of H(t), which are obtained from the transient capacitances of their heterojunctions measured at 2 MHz, approximately correspond to their density-of-states distributions [g(E)] through (See Chapter IV)

$$g(E) = H(t)/kT \quad , \tag{6-8}$$

and the energy location below the conduction band edge (E_C) is expressed by

$$E_C - E = kT\ln(\nu_n t) \quad , \tag{6-9}$$

where k is the Boltzmann's constant, T is the measuring absolute temperature, t is the time after the reverse bias is applied to the junction, ν_n is the attempt-to-escape frequency for electrons which can be estimated from the temperature dependence (353-393 K) of the time (t_p) at the peak of H(t).

First, the illumination-time dependence is considered. The value of N_I increased with about one-third powers of the illumination time (t_{IL}), whose behavior was quite similar to the results obtained from the ESR measurements, as described in Section 6-1. The value of the activation energy (δ_2) of dark conductivity of the film was independent of t_{IL} as long as t_{IL} was longer than 3 h. The value of δ_2 of light-soaked films, however, was larger than that of as-deposited films, as is similar to the data in Table 6-1. The H(t) signals did not change before and after the as-deposited film was annealed at 200

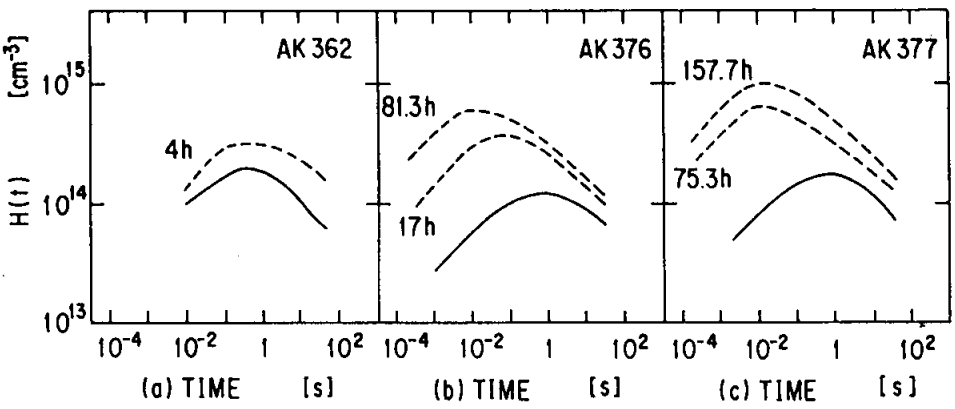

Fig.6.9. Dependence of H(t) signals on illumination time: (a) 4-h illumination on sample Ak362; (b) 17 h and 81.3 h on AK376; and (c) 75.3 h and 157.7 h on AK377. The solid curves represent H(t) for as-deposited films.

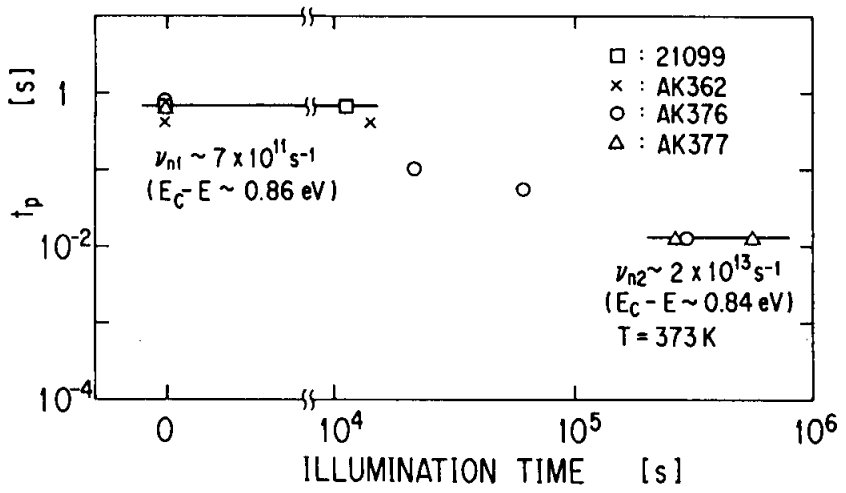

Fig.6.10. Dependence of time(t_p) on illumination time(t_{IL}). The solid lines are guides to eye.

℃ for 2 h in a vacuum, and the H(t) signals for the films annealed at 200 ℃ for 2 h after the light soaking were quite similar to those for as-deposited films.

Figure 6.9 shows the dependence of H(t) signals on t_{IL}. After short-time ($\leq$ 4-h) light soaking, the magnitude of H(t) increased without any shift of t_p, while after long-time ($\geq$ 75-h) light soaking t_p was shifted toward shorter time and kept constant, as is clearly shown in Fig. 6.10. From the temperature dependence of t_p, ν_n and the energy position (E_C-E_p) corresponding to the peak of H(t) were estimated; ν_{n1} and (E_C-E_{p1}) for the as-deposited and the short-time light-soaked films were about 7×10^{11} s^{-1} and 0.86 eV, respectively, and ν_{n2} and (E_C-E_{p2}) for the long-time light-soaked films were about 2×10^{13} s^{-1} and 0.84 eV, respectively. Although the change of t_p could, as one possibility, be thought to arise from the change of the free electron concentration in the depletion region of a-Si:H which leads to the change in the reverse current of the heterojunction,[14] the reverse current for the long-time light-soaked film was the same as that for the as-deposited film, indicating that the change of t_p must originate from the change of ν_n. Figure 6.11 schematically summarizes the above results. The solid curve A represents the g(E) in the as-deposited film. After the short-time light-soaking, both midgap states increased. However, the midgap states with ν_{n2} (the dashed curve B1) are still hidden by those with ν_{n1} (the solid curve B1). Subsequent light-soaking makes the midgap states with ν_{n2} (the dashed curve B2) larger than those with ν_{n1} (the solid curve B2). Therefore, the rate of increase of midgap states with ν_{n2} must be larger than that with ν_{n1}.

Second, the change of light-soaked films by thermal annealing is discussed. Figure 6.12(a) shows the changes of H(t) for the long-time light-soaked films by a 150-℃ annealing for 2 h, and Fig. 6.12(b) shows those by a 200-℃ annealing. Since the H(t) signals include information on two kinds of midgap states, two sorts of energy scales corresponding to ν_{n1} and ν_{n2} are shown in the abscissa below the time scale. Section 6-3 has studied the thermal annealing kinetics using the short-time

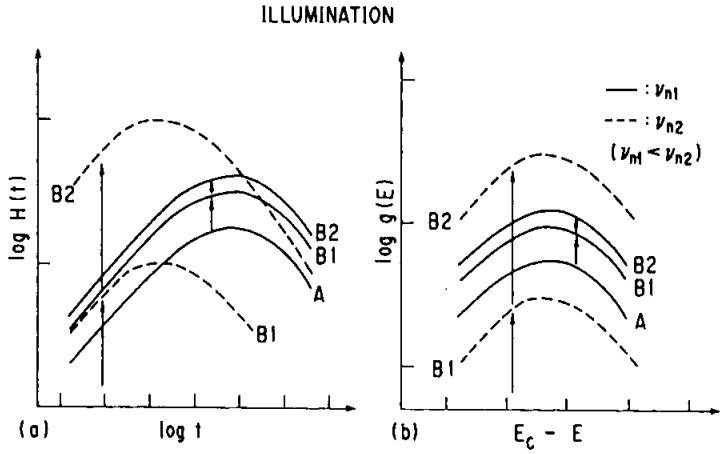

Fig.6.11. Schematic changes of midgap states by light soaking. The solid and dashed lines represent the states with small and large ν_n, respectively. A, B1, and B2 correspond to the as-deposited (or completely annealed), the short-time light-soaked, and the long-time light-soaked films, respectively. (b) is estimated from (a) using the relations of $g(E)=H(t)/kT$ and $E_C-E=kT\ln(\nu_n t)$.

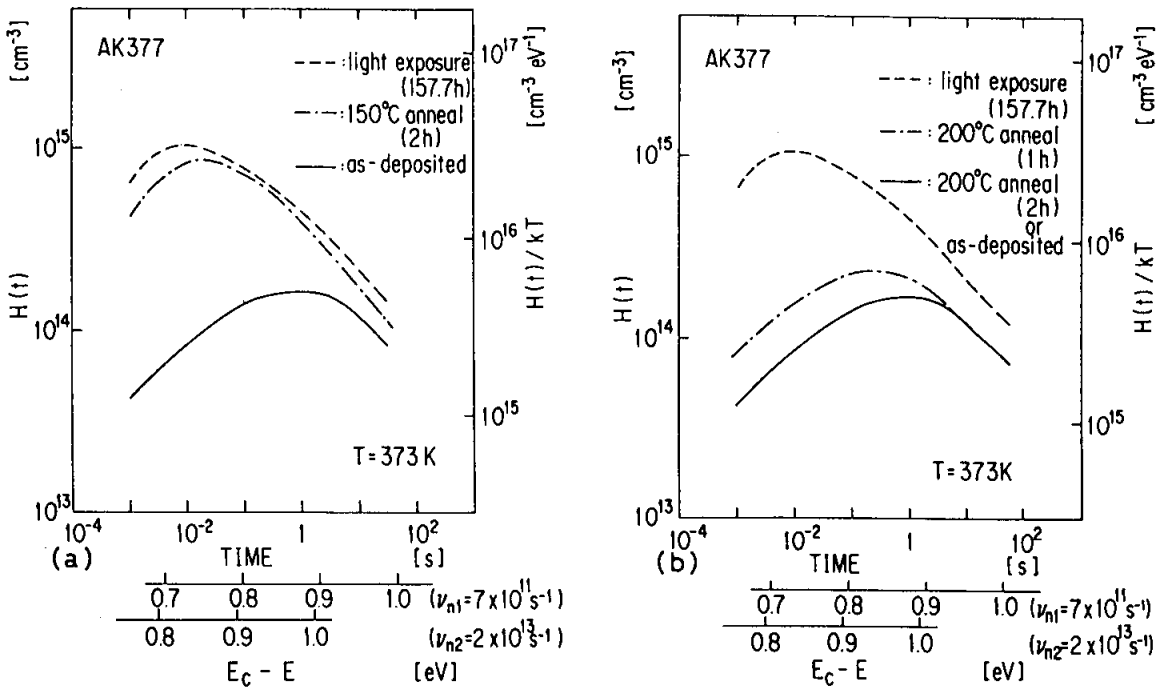

Fig.6.12. Changes of measured H(t) by (a) 150-℃ annealing and (b) 200-℃ annealing for long-time light-soaked film.

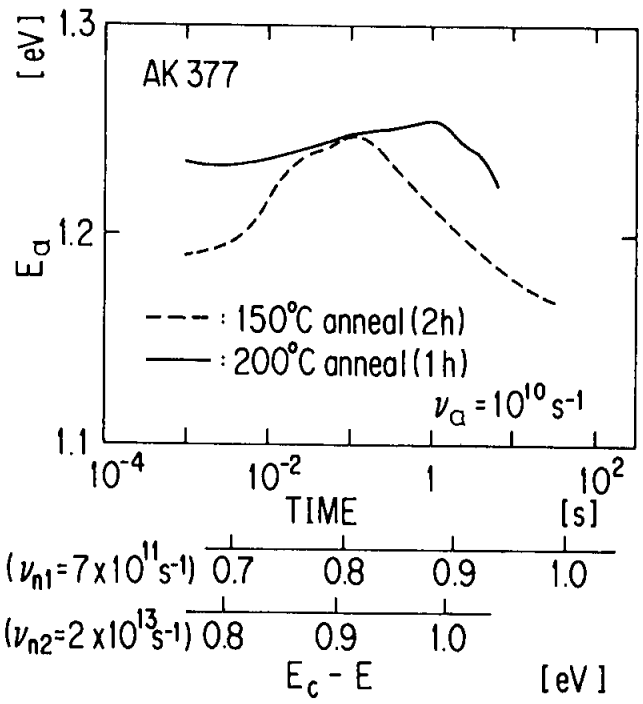

Fig.6.13. Activation energies estimated from studies of annealing at 150 °C for 2 h and subsequent annealing at 200 °C for 1 h.

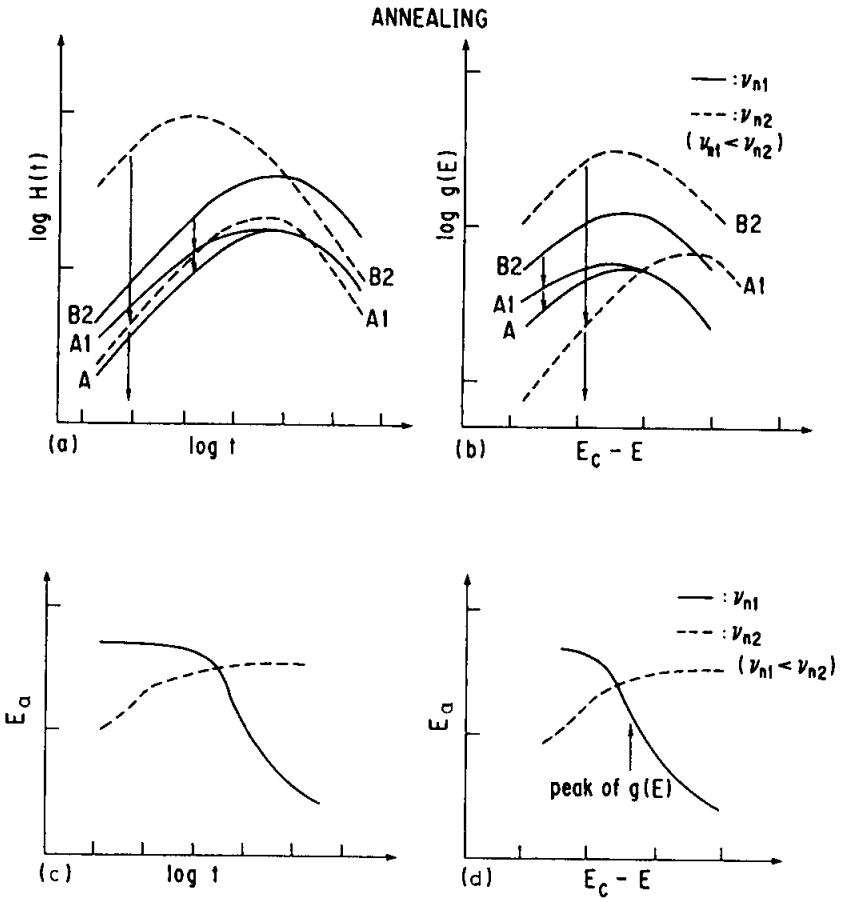

Fig.6.14. Schematic changes [(a) and (b)] of midgap states by thermal annealing and activation energies [(c) and (d)] for thermal annealing. The relation between (E_C-E) and t is given by $E_C-E=kT\ln(\nu_n t)$. The relation between H(t) and g(E) is expressed as $g(E)=H(t)/kT$. The solid and dashed lines represent the states with small and large ν_n, respectively. B2, A1, and A correspond to the long-time light-soaked, the short-time annealed, and the completely annealed films, respectively.

light-soaked films, from which the monomolecular annealing kinetics are found to be suitable for explaining those results. Figure 6.13 shows the activation energies for the 150-℃ annealing (2 h) and the 200-℃ annealing (1 h) from Fig. 6.12, assuming a monomolecular annealing process. In Fig. 6.13, the dashed curve at $t>10^{-1}$ s and the solid curve at $t<10^{-1}$ s are quite similar to the curve shown in Fig. 6.8, and those curves represent the activation energies for midgap states with ν_{n1}. So, the dashed curve at $t<10^{-1}$ s and the solid curve at $t>10^{-1}$ s must be affected by the activation energies for the midgap states with ν_{n2}. Since the energy dependence of E_a for the short-time light-soaked films is already known as shown in Fig. 6.8, changes in E_a and H(t) for the annealing process in the long-time light-soaked films can be schematically described as shown in Fig. 6.14. After the long-time light-soaking, there are the midgap states with ν_{n1} (the solid curve B2) and those with ν_{n2} (the dashed curve B2). The annealing at 150 ℃ for 1 h makes the midgap states decrease a little. Those decreases of midgap states correspond to that of the midgap states with ν_{n2} at $t<10^{-1}$ s and that of those with ν_{n1} at $t>10^{-1}$ s. Midgap states with ν_{n2} still dominate at $t<10^{-1}$ s and those states with ν_{n1} are still dominant at $t>10^{-1}$ s. The annealing at 200 ℃ for 1 h makes the midgap states decrease to the curve of A1. The value of E_a at $t<10^{-1}$ s is close to that with ν_{n1}, and E_a at 10^{-1} s$<t<$1 s must be close to that with ν_{n2}. In final, the subsequent 200-℃ annealing for more 1 h gets the midgap states with ν_{n2} hidden by those with ν_{n1} (the solid curve A).

Third, the effect of rapid cooling is mentioned using Fig. 6.15. Smith and Wagner[6] have combined the creation process with the annealing process, where both have been proposed by Stutzmann et al.[3,4];

$$dN_s/dt = c_{sw}np - \nu_a \exp(-E_a/kT)N_s \qquad (6\text{-}10)$$

and the product of n and p in the dark is expressed by

$$np = N_C N_V \exp(-E_{g2}/kT) \quad , \qquad (6\text{-}11)$$

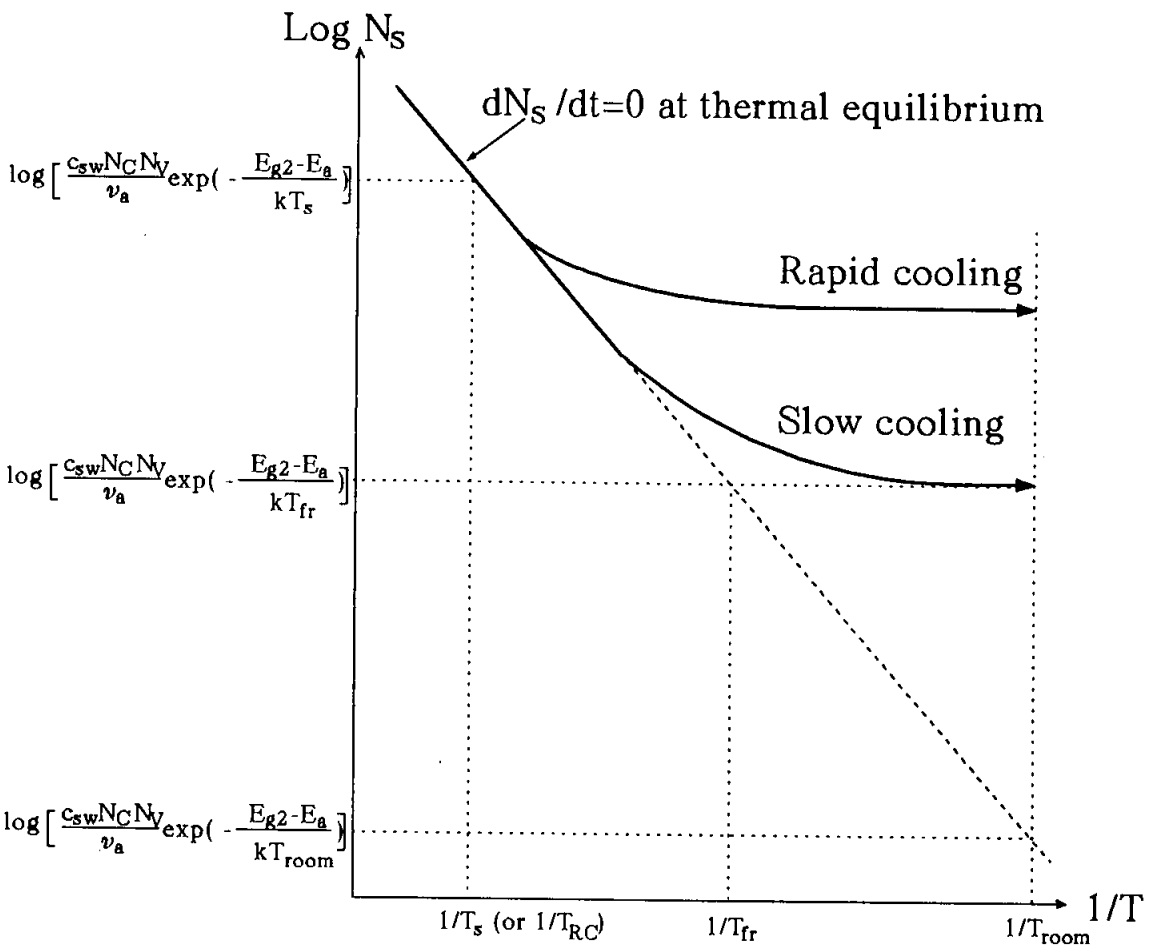

Fig.6.15. Schematic sketch of temperature-dependent midgap-state density.

where N_S is the total density of midgap states and c_{SW} is the constant related with the Staebler-Wronski effect, n and p are the free carrier densities in the conduction band and the valence band, respectively, and N_C and N_V are the effective densities of states in the conduction band and the valence band, respectively. During the deposition at a substrate temperature (T_s) or keeping the film at a given temperature (T_{RC}), the equilibrium condition ($dN_S/dt=0$) is assumed to be held. In this case, the total density of midgap states is expressed as

$$N_S = (c_{SW}N_CN_V/\nu_a)\exp[-(E_{g2} - E_a)/kT] \quad , \qquad (6\text{-}12)$$

where T represents T_s or T_{RC}. If the substrate was cooled very slowly from the high temperature to room temperature (T_{room}), the total density observed from ESR would be expressed as

$$N_S = (c_{SW}N_CN_V/\nu_a)\exp[-(E_{g2} - E_a)/kT_{room}] \quad , \qquad (6\text{-}13)$$

which means that N_S should be lower than 10^{15} cm^{-3}. However, it is impossible to cool down so slowly. Therefore, N_S is frozen in at some temperature (T_{fr}) which strongly depends on the cooling rate and it is expressed as Eq. (6-13) where T_{fr} replaces T_{room}. The actual cooling rate causes the value of N_S to become of the order of 10^{15} cm^{-3}.

In the case of the film deposited at 200 ℃, N_I in the rapidly-cooled film for T_{RC}=200 ℃ was equal to that (about 10^{16} cm^{-3}) in the as-deposited film. The value of N_I for T_{RC}=250 ℃ decreased as low as N_I (about $5x10^{15}$ cm^{-3}) in a good quality film. And then N_I increased with an increase of T_{RC}. In the case of the good quality films deposited at 250 ℃ and 300 ℃, on the other hand, N_I (about $5x10^{15}$ cm^{-3}) did not change in the range of $T_{RC} \leqq 250$ ℃, and then N_I increased with a further increase of T_{RC}. The midgap states may equilibrate during the deposition at 250-300 ℃, and the midgap states are frozen in at the temperature lower than 250 ℃ during the real slow cooling because the value of N_I at T_s=300 ℃ was close to that at T_s=250 ℃. From the result of rapid cooling from T_{RC}=250 ℃, the value

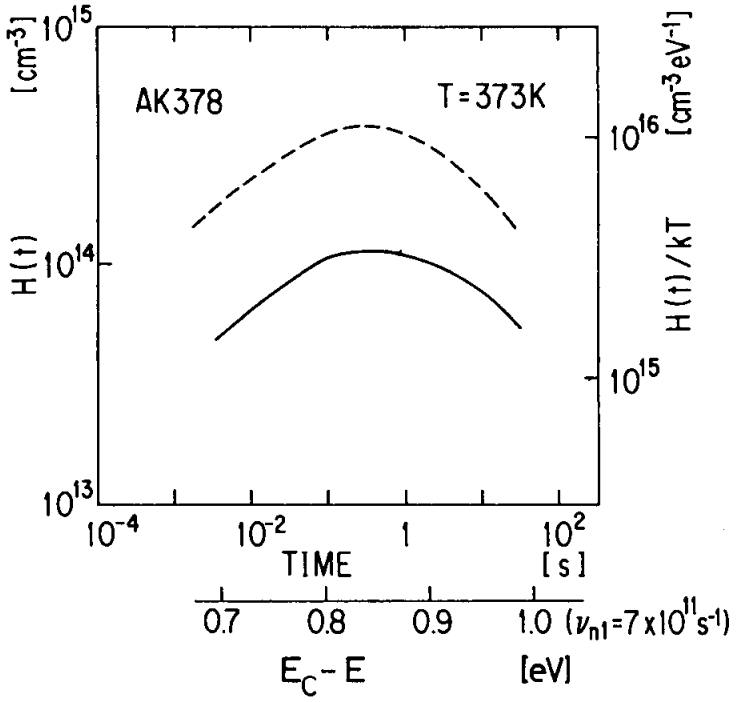

Fig.6.16. Change of measured H(t) by rapid cooling from 300 ℃. The solid and broken curves represent H(t) of as-deposited and rapidly-cooled films, respectively.

of $5x10^{15}$ cm^{-3} is considered to correspond to N_S at equilibrium near 250 ℃. Then, when the films are heated up to 300 ℃, the midgap states equilibrate at 300 ℃, which means that N_S at equilibrium becomes larger than $5x10^{15}$ cm^{-3}. By the rapid cooling, N_S becomes close to N_S at equilibrium near 300 ℃, resulting in the increase of N_S. The deposition condition of T_S=200 ℃, which is considered not to obey Eq. (6-12), is not good. So, this film has a lot of midgap states even if the substrate is cooled down slowly. When this film is heated to 250 ℃, the midgap states equilibrate at 250 ℃ according to Eq. (6-12). The rapid cooling makes the value of N_S keep at the condition near 250 ℃.

From the transient HMC method, the states increased by rapid cooling from 300 ℃ were the states having ν_{n1}, since t_p in the rapid cooling film was the same as t_p in the as-deposited film, as shown in Fig. 6.16. Therefore, the metastable states induced by rapid cooling are assigned to the midgap states in as-deposited films.

Finally, these results obtained by the HMC methods are discussed and compared with other results. Both states produced by the light soaking, which are distinguished by the difference in ν_n, must originate from electron-spin centers because the behavior of N_I by light soaking is quite similar to that obtained from ESR. From the study of as-deposited films, the states with ν_{n1} are found to be D^0 of Si, and those states could also be thermally created because they exist in the as-deposited and the rapidly-cooled films. On the other hand, the other states with ν_{n2}, which will be noted as D_L^0, can be created only by light soaking.

Han and Fritzsche,[7] and Qiu et al.[8] reported that two kinds of metastable states could be produced by light soaking. The first light-induced reversible states had a small capture-cross section (σ_{n1}) for electrons, and were detected by a constant photocurrent measurement (CPM). The second states had a large capture-cross section (σ_{n2}) for electrons, and were detected by an increment ($\Delta\sigma_p$) of conductivity using a small incident light flux with a 2-eV photon energy. The value of σ_{n1}

was smaller by about one order of magnitude than σ_{n2}, and both states were located in the midgap. The value of $\Delta\sigma_p$ decreased by the short-time (3-4 h) light soaking at 100 K, while an absorption coefficient (α_1) at 1.0 eV obtained from CPM did not change. By the same light soaking at 300 K, however, $\Delta\sigma_p$ decreased and α_1 increased. The values of $\Delta\sigma_p$ and α_1 are expressed as

$$\Delta\sigma_p = B_2/(\sigma_{n1}N_1 + \sigma_{n2}N_2) \qquad (6\text{-}14)$$

and

$$\alpha_1 = B_3(N_1 + N_2) \quad , \qquad (6\text{-}15)$$

respectively, and

$$\sigma_{n2} \fallingdotseq 10\sigma_{n1} \quad , \qquad (6\text{-}16)$$

where B_2 and B_3 are constants, N_1 is the density of the first states, and N_2 is the density of the second states. If the value of N_2 were smaller by the order of 10 than the value of N_1, the increment of N_2 could hardly be detected by the increment of α_1 according to Eq. (6-15), but it could easily be detected by the change of $\Delta\sigma_p$ according to Eq. (6-14) because of Eq. (6-16). Therefore, these indicate that the density of the first states increases only at high temperature, while the density of the second states increases at any temperature and that the value of N_2 is still smaller than that of N_1 in the short-time light-soaking. In the light of our results, the first states correspond to D^0 just as they concluded, and the second states should correspond to D_L^0 because ν_n is proportional to σ_n. Indeed, in the case of deuterated amorphous silicon (a-Si:D), only the midgap states with ν_{n1} were reported to increase by light-soaking.[15] That is why the rate of conductivity decrease in a-Si:D is reported to be smaller than that in a-Si:H. The origin of D_L^0 is still an open question, although Okushi et al.[16] have insisted a model in which the dangling-bond-like centers are

produced by a spatially intimated coupling of pairs between dangling bonds and positively ionized impurities.

6-5. Summary

(1) The steady-state and transient HMC methods have been applied to determining densities and profiles of midgap states in undoped a-$Si_{1-x}Ge_x$:H, undoped a-Si:H and undoped a-$Si_{1-x}C_x$:H. The midgap states are correlated with D^0; the density in a-$Si_{1-x}Ge_x$:H ($E_0 \leqq 1.63$ eV) represents the D^0 density of Ge, and in a-Si:H and a-$Si_{1-x}C_x$:H ($E_0 \leqq 1.88$ eV) it represents the D^0 density of Si. The density of midgap states increases slowly with the Ge content in the film, while it increases rapidly with the C content. The peak of the midgap-state profile appears clearly in a-Si:H and a-$Si_{1-x}Ge_x$:H, but it does not appear clearly in a-$Si_{1-x}C_x$:H.

(2) Thermal annealing kinetics of metastable gap states in short-time light-soaked a-Si:H have been investigated. Monomolecular kinetics are suitable for explaining the experimental data. The thermal activation energy (E_a) for annealing decreases monotonously with an increase in (E_C-E). This is the first report which elucidates the relation between E_a and (E_C-E).

(3) The midgap states having a small ν_n are created both optically and thermally, while the midgap states having a large ν_n are created only by light soaking. Both states are located around 0.85 eV below the conduction band edge.

References

1) P. G. LeComber and W. E. Spear, Phil. Mag. **B53**(1986)L1.
2) D. Staebler and C. R. Wronski, Appl. Phys. Lett. **31**(1977)292.
3) M. Stutzmann, W. B. Jackson, and C. C. Tsai, Appl. Phys. Lett. **45**(1984)1075.
4) M. Stutzmann, W. B. Jackson, and C. C. Tsai, Phys. Rev. **B34**(1986)63.
5) C. Lee, W. D. Ohlsen, P. C. Taylor, H. S. Ullal, and G. P. Ceasar, Phys. Rev. **B31**(1985)100.
6) Z E. Smith and S. Wagner, Phys. Rev. **B32**(1985)5510.
7) D. Han and J. Fritzsche, J. Non-Cryst. Solids **59&60**(1983)397.
8) C. Qiu, W. Li, D. Han, and J. Pankove, J. Appl. Phys. **64**(1988)713.
9) M. Kumeda, H. Yokomichi, A. Morimoto, and T. Shimizu, Jpn. J. Appl. Phys. **25**(1986)L654.
10) T. Shimizu, M. Kumeda, and Y. Kiriyama, Solid-State Commun. **37**(1981)699.
11) A. Morimoto, T. Miura, M. Kumeda, and T. Shimizu, Jpn. J. Appl. Phys. **20**(1981)L833.
12) Y. Tsutsumi, S. Sakata, K. Abe, Y. Nitta, H. Okamoto, and Y. Hamakawa, J. Non-Cryst. Solids **97&98**(1987)1063.
13) K. Shepard, Z E. Smith, S. Aljishi, and S. Wagner, Mater. Res. Soc. Symp. Proc., edited by A. Madan, M. J. Thompson, P. C. Taylor, P. G. LeComber, and Y. Hamakawa(Materials Research Society, Pittsburgh, 1988), Vol. 118, p. 147.
14) D. V. Lang, J. D. Cohen, J. P. Harbison, M. C. Chen, and A. M. Sergent, J. Non-Cryst. Solids **66**(1984)217.
15) G. Ganguly, S. Yamasaki, and A. Matsuda, Phil. Mag. **B63**(1991)281.
16) H. Okushi, R. Banerjee, and K. Tanaka, in Advances in Disordered Semiconductors, edited by H. Fritzsche(World Scientific, Singapore, 1989), Vol. 1, p. 657.

CHAPTER Ⅶ CONCLUSION

This thesis has mainly investigated and discussed

(1) the electrical properties of undoped hydrogenated amorphous silicon (a-Si:H)/p-type crystalline silicon (p c-Si) heterojunctions;

(2) new methods for determining a density (N_I) and a profile [g(E)] of midgap states in highly resistive amorphous semiconductors using the property of those amorphous/crystalline semiconductor heterojunctions; and

(3) the nature of midgap states in undoped a-Si:H, undoped hydrogenated amorphous silicon germanium alloys (a-Si_{1-x} Ge_x:H), and undoped hydrogenated amorphous silicon carbon alloys (a-$Si_{1-x}C_x$:H).

Prior to investigation of undoped (i.e., slightly n-type) a-Si:H/p c-Si heterojunctions in diodes with metal/a-Si:H/c-Si structures, each contact in those diodes has been studied in order to know whether each contact behaves like an Ohmic contact or like a rectifying contact. From this study, Mg was found to form a good Ohmic contact with undoped a-Si:H, instead of Al, and the undoped a-Si:H/p c-Si heterojunctions exhibited good rectifying properties. Additional results from the study were that the conduction type of a-Si:H was classified into three categories such as n-type for P-doped and undoped a-Si:H, intrinsic for B-doped a-Si:H with $B_2H_6/SiH_4 \sim 10^{-6}$, and p-type for B-doped a-Si:H with $B_2H_6/SiH_4 > 10^{-5}$, which has been difficult by means of Hall measurements due to their high resistivity.

The study of high-frequency ($\geqq$ 100-kHz) capacitance-voltage (C-V) characteristics of the undoped a-Si:H/p c-Si heterojunctions has made it possible to obtain the density (N_I) of midgap states in highly resistive amorphous semiconductors such as undoped a-Si:H, whose value was checked with that obtained from simulation of high-frequency C-V characteristics of a highly resistive amorphous/lowly resistive crystalline semiconductor heterojunction. In the reasonable case that its interface-state density was less than 10^{11} cm^{-2}, the density

experimentally obtained from the C-V measurement represented a bulk density of midgap states in undoped a-Si:H. This method is referred to as a steady-state heterojunction-monitored capacitance (HMC) method.

The forward currents in undoped a-Si:H/p c-Si heterojunctions were expressed as $\exp(-\Delta E_{af}/kT)\exp(AV)$, which could be explained by a multistep-tunneling capture-emission (MTCE) model proposed here, where A is a constant independent of the applied voltage (V), ΔE_{af} is a constant independent of the measuring temperature (T), and k is the Boltzmann's constant. The reverse currents were proportional to $(V_B-V)^{1/2}$, resulting from a generation process in both sides of a-Si:H and c-Si, where V_B is the built-in potential.

The investigation of transient capacitance of the undoped a-Si:H/p c-Si heterojunctions has made it possible to estimate the density-of-state distribution [g(E)] between the Fermi level and the midgap in highly resistive amorphous semiconductors. The distribution obtained from this method was considered to be unaffected by their interface states. This method is called a transient HMC method.

From the study of ESR, N_I represented the density of singly-occupied Si dangling bonds for undoped a-Si:H and undoped a-$Si_{1-x}C_x$:H [an optical gap (E_0) $\leq$ 1.88 eV], while N_I mainly was assigned to the density of singly-occupied Ge dangling bonds for undoped a-$Si_{1-x}Ge_x$:H ($E_0 \leq$ 1.63 eV). The peak of g(E) appeared clearly in a-Si:H and a-$Si_{1-x}Ge_x$:H, but it did not appear clearly in a-$Si_{1-x}C_x$:H. In a-$Si_{1-x}Ge_x$:H with E_0=1.30 and 1.44 eV, furthermore, not only a peak of g(E) originating from singly-occupied Ge dangling bonds but also a shoulder arising from singly-occupied Si dangling bonds were clearly observed.

Light soaking produced two sorts of metastable states which were annealed out completely up to 200 ℃ for 2 h; (1) one, which was dominant in short-time ($\leq$ 4-h) light soaking, had a small attempt-to-escape frequency (ν_n) for electrons and coincided with the midgap states in as-deposited films, and (2) the other, which became dominant in long-time ($\geq$ 75-h) light soaking, had a large ν_n. Both the metastable states were located in around

0.85 eV and they originated from singly-occupied Si dangling bonds, but the behavior by thermal annealing was quite different each other. The midgap states produced by rapid cooling from 300 ℃ were similar to those induced by the short-time light soaking.

From the fundamental research on capacitance in undoped hydrogenated amorphous silicon-based alloy/p c-Si heterojunctions, the steady-state and transient HMC methods have been developed in this thesis. The HMC methods have great potential for determining N_I and g(E) in highly resistive semiconductors with gap states.

APPENDIX

At thermal equilibrium (i.e., in the neutral region of an amorphous semiconductor film), the densities [$n_T(E)$ and $p_T(E)$] of traps [$g(E)$] occupied by electrons and holes (which mean vacancies of electrons), respectively, are expressed as

$$n_T(E)/g(E) = f(E) \tag{A-1}$$

and

$$g(E) = n_T(E) + p_T(E) \quad , \tag{A-2}$$

according to the Fermi-Dirac statistics, where f(E) is the Fermi-Dirac distribution function.

A rate equation for capture and emission processes of electrons and holes at gap states, which are located in an energy of E, is given by

$$\begin{aligned} dn_T(E)/dt = {} & n\sigma_n(E)v_{th}p_T(E) - e_n(E)n_T(E) \\ & - p\sigma_p(E)v_{th}n_T(E) + e_p(E)p_T(E) \quad , \end{aligned} \tag{A-3}$$

where n and p are concentrations for free electrons and free holes in the extended states, respectively, $\sigma_n(E)$ and $\sigma_p(E)$ are capture cross sections for electrons and holes at E, respectively, $e_n(E)$ and $e_p(E)$ are thermal emission rates of electrons and holes into the extended states, respectively, and v_{th} is the thermal velocity of electrons.

At the steady state and in the depletion region, Eq. (A-3) is considered. The condition [$dn_T(E)/dt=0$] holds for the steady state, and free electrons and free holes are swept out (i.e., the product of p and n is much smaller than n_i^2) in the depletion region, indicating that the first and third terms in the right-hand sides of Eq. (A-3) can be neglected, where n_i is the intrinsic carrier density. Therefore, Eq. (5-11) in Chapter V

$$F_\infty(E) \equiv n_T(E)/g(E) \qquad (A\text{-}4)$$

$$= e_p(E)/[e_n(E) + e_p(E)] \qquad (5\text{-}11)$$

is obtained from Eqs. (A-2) and (A-3).

In the depletion region, Eq. (A-3) can be rewritten as

$$dn_T(E)/dt = e_p(E)g(E) - [e_n(E) + e_p(E)]n_T(E) \quad , \qquad (A\text{-}5)$$

using Eq. (A-2), and this solution is

$$n_T(E;t) = [f(E) - F_\infty(E)]g(E)\exp\{-[e_n(E) + e_p(E)]t\} + e_p(E)g(E)/[e_n(E) + e_p(E)] \quad , \qquad (A\text{-}6)$$

using the relations of $n_T(E;0)=f(E)g(E)$ obtained from Eq. (A-1) and $n_T(E;\infty)=F_\infty(E)g(E)$ obtained from (A-4). Therefore,

$$\Delta N_I(t) = \int_{E_V}^{E_C} [n_T(E;\infty) - n_T(E;t)]dE$$

$$= -\int_{E_V}^{E_C} [f(E) - F_\infty(E)]g(E) \times \exp\{-[e_n(E) + e_p(E)]t\}dE \quad , \qquad (A\text{-}7)$$

is obtained, and then Eq. (5-14) in Chapter V

$$H(t) = \int_{E_V}^{E_C} [f(E) - F_\infty(E)]g(E)[e_n(E) + e_p(E)]t \times \exp\{-[e_n(E) + e_p(E)]t\}dE \qquad (5\text{-}14)$$

is derived from Eq. (A-7) easily.

On the other hand, the energy E_{OB} is derived from the condition of $F_\infty(E_{OB})=0.5$. Since

$$e_p(E)/[e_n(E) + e_p(E)] = 0.5 \quad , \qquad (A\text{-}8)$$

the following equation is obtained;

APPENDIX

$$e_p(E) = e_n(E) \quad . \tag{A-9}$$

Therefore, the equation appeared in Chapter Ⅲ

$$E_{OB} = E_V + E_{g2}/2 + (kT/2)\ln(\nu_p/\nu_n) \tag{3-2}$$

is obtained from the following equations in Chapter Ⅴ;

$$e_n(E) = \nu_n \exp[(E - E_C)/kT] \tag{5-12}$$

and

$$e_p(E) = \nu_p \exp[(E_V - E)/kT] \quad . \tag{5-13}$$

In the case of a metal-oxide-semiconductor (MOS) diode, a current does not flow across the junction, which means that the Fermi level can be defined even in the depletion region because the quasi-Fermi level for electrons coincides with the quasi-Fermi level for holes. Thus a relation ($np=n_i^2$) in the depletion region is valid and $n_T(E)/g(E)$ coincides with $f(E)$ as described by Eq. (A-1) instead of $F_\infty(E)$ as described by Eq. (A-4), indicating that the energy of E_{OB} and the occupation function of $F_\infty(E)$ cannot be defined even in the depletion region. Therefore, Eq. (3-2) in Chapter Ⅲ and Eq. (5-11) in Chapter Ⅴ are valid only when a current flows across the junction, i.e., the quasi-Fermi level for electrons does not coincide with the quasi-fermi level for holes in the depletion region.

LIST OF SYMBOLS

Symbol	Unit	Description
α	1/cm	Optical absorption coefficient
α_1	1/cm	Optical absorption coefficient at 1.0 eV obtained from CPM
C	pF/cm^2	Capacitance of heterojunction
C_2	pF/cm^2	Saturated capacitance at higher forward biases
c_{sw}	cm^3/s	Constant of the Staebler-Wronski effect
γ_a	cm^3/s	Pre-exponential factor of bimolecular decay rate
dV/dt	V/s	Voltage sweep rate
D(E,t)		Function which takes a maximum at $e_n(E)t=1$
d_s	cm	Thickness of interface layer
δ_1	eV	E_F-E_V in p c-Si
δ_2	eV	E_C-E_F in a-Si:H
E_a	eV	Activation energy of thermal annealing
ΔE_{af}	eV	Activation energy of a pre-exponential factor (I_0) for forward currents
E_{BT}	eV	Characteristic energy for conduction-band tail
E_F	eV	Fermi level
E_F^a	eV	Fermi level in a neutral region of a-Si:H
E_{Fn}	eV	Quasi-Fermi level of electron in the depletion region
E_{Fp}	eV	Quasi-Fermi level of holes in the depletion region
E_{g1}	eV	Energy bandgap of c-Si
E_{g2}	eV	Energy bandgap of a-Si:H
E_0	eV	Optical gap determined by Tauc plot
E_{OB}	eV	Energy level at which a thermal emission rate for electrons equals to one for holes
E_{OB}^a	eV	E_{OB} in a neutral region of a-Si:H
E_p	eV	Energy level of a peak value of g(E)
E_{p1}	eV	Energy level of a peak value of g(E) with

		a small ν_n
E_{p2}	eV	Energy level of a peak value of g(E) with a large ν_n
E_T	eV	Energy level of the gap state where a tunneling hole combines with an electron or emits into the valence band in a-Si:H
E_w	eV	Half width of Gaussian distribution
E_{rI}	V/cm	Electric field at $x=W_{OB}$
E_m	eV	Energy at which D(E,t) takes a maximum value
E_C	eV	Conduction-band edge
ΔE_C	eV	Conduction-band discontinuity
E_V	eV	Valence-band edge
ΔE_V	eV	Valence-band discontinuity
ΔE_ν	eV	Activation energy for ν_n
$e_n(E)$	1/s	Thermal emission rate of electrons
$e_p(E)$	1/s	Thermal emission rate of holes
ε_0	pF/cm	Free space permittivity
ε_{s1}	pF/cm	Semiconductor permittivity for c-Si
ε_{s2}	pF/cm	Semiconductor permittivity for a-Si:H
$F_\infty(E)$		Occupation function at $t=\infty$ s
f(E)		Occupation function at t=0 s (i.e., Fermi-Dirac distribution function)
G	$1/cm^3s$	Carrier generation rate by light exposure
g(E)	$1/cm^3eV$	Density-of-state distribution in a-Si:H
g(E,0)	$1/cm^3eV$	Midgap-state profile in light-soaked film
$g_0(E)$	$1/cm^3eV$	Midgap-state profile in as-deposited film
g(E,t)	$1/cm^3eV$	Midgap-state profile at thermal annealing time t
$\Delta g(E,t)$	$1/cm^3eV$	$g(E,t)-g_0(E)$ at thermal annealing time t
g_{max}	$1/cm^3eV$	Maximum value of g(E) with Gaussian distribution
H(t)	$1/cm^3$	Transient HMC (heterojunction-monitored capacitance) signal
$h\nu$	eV	Photon energy
I	A	Current
k	eV/K	Boltzmann constant
L	cm	Thickness of a-Si:H

μ_2	cm^2/Vs	Mobility in a-Si:H
μ_n	cm^2/Vs	Mobility of electrons
μ_p	cm^2/Vs	Mobility of holes
ν_a	1/s	Pre-exponential factor of monomolecular decay rate
ν_n	1/s	Pre-exponential factor of thermal emission rate (attempt-to-escape frequency) for electrons
ν_{n0}	$1/sK^2$	Pre-exponential factor of ν_n with temperature dependence
ν_{n1}	1/s	Small attempt-to-escape frequency for electrons
ν_{n2}	1/s	Large attempt-to-escape frequency for electrons
ν_p	1/s	Pre-exponential factor of thermal emission rate (attempt-to-escape frequency) for holes
N_A	$1/cm^3$	Density of acceptors in p c-Si
N_C	$1/cm^3$	Effective density of states in the conduction band
$N(E_C)$	$1/cm^3eV$	Density-of-state distribution at a bottom of the conduction band
N_I	$1/cm^3$	Midgap-state density (i.e., space-charge density) graphically estimated from the steady-state HMC method
N_I^*	$1/cm^3$	Density of midgap states between E_F and E_{OB} in a-Si:H
$N_I(t)$	$1/cm^3$	Midgap-state density (space-charge density) at time t
$\Delta N_I(t)$	$1/cm^3$	Change in space-charge density at time t
$N_I(\infty)$	$1/cm^3$	Space-charge density at $t=\infty$ s
N_S	$1/cm^3$	Bulk spin density obtained from electron spin resonance (ESR) measurements
$N_S(t)$	$1/cm^3$	Bulk spin density from ESR at light-soaking time t
N_S^*	$1/cm^3$	Density of defects between p c-Si and a-Si:H in plate of interface layer (i.e.,

		interface and the near-interface regions)
N_V	$1/cm^3$	Effective density of states in the valence band
N_1	$1/cm^3$	Density of first states
N_2	$1/cm^3$	Density of second states
n	$1/cm^3$	Electron density in the conduction band of a-Si:H
n_{BT}	$1/cm^3$	Electron density in conduction-band tail
n_i	$1/cm^3$	Intrinsic carrier density in a-Si:H
$n_T(E)$	$1/cm^3$	Density of traps occupied by electrons
$n_T(E;t)$	$1/cm^3$	Density of traps occupied by electrons at time t
Δn	$1/cm^3$	Electron density under light exposure
p	$1/cm^3$	Hole density in the valence band of a-Si:H
$p_T(E)$	$1/cm^3$	Density of traps occupied by holes (i.e., density of empty traps)
Δp	$1/cm^3$	Hole density under light exposure
Q_{rI}	C/cm^2	Space charge in region I ($W_{OB} \leqq x \leqq W_2$) in a-Si:H
Q_{ss}	C/cm^2	Space charge in interface layer
ρ_I	C/cm^3	Space-charge density in region I
ρ_2	Ω cm	Dark resistivity of a-Si:H
q	C	Magnitude of electronic charge
σ_2	S/cm	Dark conductivity of a-Si:H
σ_n	cm^2	Capture-cross section of electrons
σ_{n1}	cm^2	Small capture-cross section of electrons
σ_{n2}	cm^2	Large capture-cross section of electrons
σ_p	cm^2	Capture-cross section of holes
$\Delta\sigma_p$	S/cm	Increment of conductivity using a small incident light flux with a 2-eV photon energy
$\Delta\sigma_{ph}$	S/cm	Photoconductivity with AM1 light
S	cm^2	Electrode area
T	K	Measuring absolute temperature
T_{fr}	℃ (or K)	Freeze-in temperature
T_{RC}	℃ (or K)	Temperature from which a film is rapidly cooled by liquid N_2

T_{room}	℃ (or K)	Room temperature
T_s	℃ (or K)	Substrate temperature during deposition
t_{IL}	s	Illumination time
τ_f	s	Filling time
u(x)	eV	Energy at position x
u_{OB}	eV	Energy at $x=W_{OB}$
ϕ_m	eV	Work function of metal
ϕ_s	eV	Work function of a-Si:H
V	V	Applied bias voltage ($V=V_1+V_2$)
V_B	V	Built-in potential graphically estimated from steady-state HMC method
V_{B1}	V	Built-in potential at heterojunction for c-Si
V_{B2}	V	Built-in potential at heterojunction for a-Si:H
V_B^*	V	Built-in potential at heterojunction
V_R	V	Reverse bias voltage under transient HMC measurement
V_1	V	dc applied-bias voltage for c-Si
$V_1(t)$	V	Voltage at time t across the depletion region in c-Si
V_2	V	dc applied-bias voltage for a-Si:H
v_{th}	cm/s	Thermal velocity of electrons
χ_1	eV	Electron affinity of c-Si
χ_2	eV	Electron affinity of a-Si:H
$\chi(SiO_2)$	eV	Electron affinity of SiO_2
W_1	cm	Width of the depletion region in c-Si
W_2	cm	Width of the depletion region in a-Si:H
$W_1(t)$	cm	Depletion width in c-Si at time t
$W_2(t)$	cm	Depletion width in a-Si:H at time t
W_{OB}	cm	Cross point at $E_{Fn}=E_{OB}$ in a-Si:H

LIST OF ACRONYMS

AES	Auger electron spectroscopy
AM1	Air Mass 1
a-Ge	Amorphous germanium
a-Si:D	Deuterated amorphous silicon
a-Si:H	Hydrogenated amorphous silicon
$a\text{-}Si_{1-x}C_x:H$	Hydrogenated amorphous silicon carbon alloy
$a\text{-}Si_{1-x}Ge_x:H$	Hydrogenated amorphous silicon germanium alloy
c-GaAs	Crystalline gallium arsenide
c-Ge	Crystalline germanium
CPM	Constant photocurrent measurement
c-Si	Crystalline silicon
C-V	Capacitance-voltage
DLTS	Deep-level transient spectroscopy
DOS	Density-of-state distribution
D^0	Singly-occupied dangling bond
D_L^0	D^0 with ν_{n2}
D^-	Doubly-occupied dangling bonds
EPMA	Electron probe microanalysis
ESR	Electron spin resonance
HBT	Heterojunction bipolar transistor
HMC	Heterojunction-monitored capacitance
I-V	Current-voltage
ICTS	Isothermal capacitance transient spectroscopy
MOS	Metal-oxide-semiconductor
MPC	Modulated photocurrent
MTCE	Multistep-tunneling capture-emission
PAS	Photoacoustic spectroscopy
PDS	Photothermal deflection spectroscopy
p c-Si	p-type c-Si
p^+ c-Si	p-type c-Si with resistivity lower than 0.01 Ω cm
rf	Radio frequency
SCLC	Space-charge-limited current
SIMS	Secondary ion mass spectroscopy
S-W	Staebler-Wronski effect

CONSTANTS

q	$= 1.60210 \times 10^{-19}$	C		
k	$= 1.38054 \times 10^{-23}$	J/K	$= 8.61707 \times 10^{-5}$	eV/K
ε_0	$= 8.854 \times 10^{-12}$	F/m	$= 8.854 \times 10^{-2}$	pF/cm
h	$= 6.6256 \times 10^{-34}$	Js	$= 4.1356 \times 10^{-15}$	eVs
m	$= 9.1091 \times 10^{-31}$	kg		

LIST OF PUBLICATIONS

I . Full Papers

(1) **Electrical properties of n-amorphous/p-crystalline silicon heterojunctions**
Hideharu Matsuura, Tetsuhiro Okuno, Hideyo Okushi, and Kazunobu Tanaka: J. Appl. Phys. **55**(1984)1012-1019.

(2) **Dark current transport mechanism of p-i-n hydrogenated amorphous silicon diodes**
Hideharu Matsuura, Akihisa Matsuda, Hideyo Okushi, and Kazunobu Tanaka: J. Appl. Phys. **58**(1985)1578-1583.

(3) **Schottky barrier junctions of hydrogenated amorphous silicon-germanium alloys**
Hideharu Matsuura and Hideyo Okushi: J. Appl. Phys. **62**(1987)2871-2879.

(4) **A novel method for determining the gap-state profile and its application to amorphous $Si_{1-x}Ge_x$:H films**
Hideharu Matsuura: J. Appl. Phys. **64**(1988)1964-1973.

(5) **Hydrogenated amorphous-silicon/crystalline-silicon heterojunctions: Properties and applications**
Hideharu Matsuura: IEEE Trans. **ED-36**(1989)2908-2914.

(6) **Simulation of high-frequency capacitance-voltage characteristics of amorphous/crystalline heterojunctions**
Hideharu Matsuura: J. Appl. Phys. **68**(1990)1138-1142.

II . Letters

(1) **Ohmic contact properties of magnesium evaporated onto undoped and P-doped a-Si:H**
Hideharu Matsuura, Tetsuhiro Okuno, Hideyo Okushi, Satoshi

Yamasaki, Akihisa Matsuda, Nobuhiro Hata, Hidetoshi Oheda, and Kazunobu Tanaka: Jpn. J. Appl. Phys. **22**(1983)L197-L199.

(2) **Metal-semiconductor junctions and amorphous-crystalline heterojunctions using B-doped hydrogenated amorphous silicon**
Hideharu Matsuura, Akihisa Matsuda, Hideyo Okushi, Tetsuhiro Okuno, and Kazunobu Tanaka: Appl. Phys. Lett. **45**(1984)433-435.

(3) **Density of mid-gap states for undoped a-$Si_{1-x}Ge_x$:H and a-Si:H determined by steady-state heterojunction-monitored capacitance method**
Hideharu Matsuura: Jpn. J. Appl. Phys. **27**(1988)L513-L515.

(4) **Density-of-state distribution for undoped a-Si:H and a-$Si_{1-x}Ge_x$:H determined by transient heterojunction-monitored capacitance method**
Hideharu Matsuura: Jpn. J. Appl. Phys. **27**(1988)L516-L518.

(5) **Thermal recovery process of the midgap-state profile of light-soaked undoped hydrogenated amorphous silicon**
Hideharu Matsuura: Appl. Phys. Lett. **54**(1989)344-346.

(6) **Midgap-state profiles in undoped amorphous-silicon-based alloys**
Hideharu Matsuura, Z E. Smith, Akihisa Matsuda, Seiichiro Yokoyama, Mitsuhiro Tanaka, Masashi Ueda, and Kazunobu Tanaka: Phil. Mag. Lett. **59**(1989)109-114.

Ⅲ. International Conferences

(1) **Electrical properties of n^--p amorphous-crystalline silicon heterojunctions**
Hideharu Matsuura, Tetsuhiro Okuno, Hideyo Okushi, Nobuhiro Hata, Satoshi Yamasaki, Hidetoshi Oheda, Akihisa Matsuda, and Kazunobu Tanaka: Ext. Abs. 15th Conf. Solid State

Devices & Materials, Tokyo, 1983(Bus. Center Acad. Soc. Japan, Tokyo, 1983), pp. 185-188.

(2) **Schottky barrier junctions of hydrogenated amorphous silicon-germanium alloys**
Hideharu Matsuura, Hideyo Okushi, and Kazunobu Tanaka: 12th Int. Conf. Amorphous & Liquid Semiconductors, Prague, 1987; J. Non-Cryst. Solids **97&98**(1987)963-966.

(3) **The density-of-state distribution in undoped a-Si:H and a-SiGe:H determined by heterojunctions with c-Si**
Hideharu Matsuura and Kazunobu Tanaka: Mater. Res. Soc. Symp., Reno Nev., 1988; Mater. Res. Soc. Symp. Proc. **118**(1987)647-652.

(4) **Properties of amorphous silicon/crystalline silicon heterojunctions (Invited)**
Hideharu Matsuura: Int. Topical Conf. Hydrogenated Amorphous Silicon Devices and Technology, Yorktown Heights N.Y., 1988, pp. 151-154.

(5) **Optically and thermally induced reversible changes of midgap states in undoped a-Si:H**
Hideharu Matsuura: 13th Int. Conf. Amorphous & Liquid Semiconductors, Asheville N.C., 1989; J. Non-Cryst. Solids **114**(1989)609-611.

Ⅳ. Books

(1) **Junction properties of amorphous semiconductors**
Hideharu Matsuura: in Glow-Discharge Hydrogenated Amorphous Silicon, edited by K. Tanaka(KTK Scientific Publishers, Tokyo, 1989), Chapter 10, pp. 227-249.

(2) **Electrical properties of amorphous/crystalline-semiconductor heterojunctions**

Hideharu Matsuura and Hideyo Okushi: in Amorphous and Microcrystalline Semiconductor Devices: Vol. II Materials and Device Physics, edited by J. Kanicki(Artech House, Boston, 1992), Chapter 11, pp. 517-561.